Functional MRI using pseudo-continuous arterial spin labeling

by

Hesamoddin Jahanian

A dissertation submitted in partial fulfillment
of the requirements for the degree of
Doctor of Philosophy
(Biomedical Engineering)
in The University of Michigan
2012

Doctoral Committee:

Professor Douglas C. Noll, Co-Chair
Research Associate Professor Luis Hernandez-Garcia, Co-Chair
Professor J. Brian Fowlks
Professor Jon-Kar Zubieta

To My Family

Acknowledgements

I am deeply indebted to my graduate advisors, Dr. Douglas Noll and Dr. Luis Hernandez-Garcia, who supported me throughout my graduate career. I was very fortunate to have the opportunity to work with both of them. I am also deeply grateful for the understanding and support they displayed during very trying times. Doug has been a role model and a wonderful mentor for me who has always been available to offer guidance and suggestions, but just as importantly, afforded me freedoms that helped me grow as an individual, beyond a researcher and a doctoral student. Luis introduced me to arterial spin labeling techniques and helped me in different aspects of my project from the beginning. His guidance, constant ideas and continual enthusiasm for this work had huge impacts on the progress of my work. In addition to mentoring me, he has been a great friend and has helped me in difficult times.

I would also like to give special thanks to Dr. Scott Peltier for involving me in his remarkable real-time fMRI project. In addition I would like to thank the members of my committee, Dr. Fowlkes and Dr. Zubieta, for their time and effort.

My thanks to other students, researchers and support staff in the fMRI lab such as Dr. Greg Lee, Dr. William Grissom, Dr. Valur Olafsson, Dr. Yoon Chung Kim, Dr. Kumar Pandey, Dr. Chunyu Yip, Dr. Jon Nielsen, Daehyun Yoon, the late Eve Gochis, Yash Shah, Alan Chu, Feng Zhao and Keith Newnham among others for all their help during my stay here. Particularly, I would like to thank Ruth Halsey for her kindness and for all the positive changes that she has made since she joined the fMRI lab.

Special thanks also go to Chuck Nicholas, Katherine Guarino and particularly Maria Steel, for their administrative help during my graduate school.

I would like to thank my parents, Aliasghar Jahanian and Maryam Mizamohammadi.

Without their tremendous sacrifices, I would have not been able to be here. This thesis is the result of their constant encouragement, unwavering support, guidance and strong faith in me. I want to thank my brother and sister Pedram and Ronak for all their love and support they have given me.

Last, but not least, I would like to thank my wife Azadeh for all the love and support she has given me during our time together. She has always wanted the best for me and stood by me during difficult times. She has picked me up when I was down and cheered me on when needed. For that I will be forever in debt to her. Thank you, Azadeh, from the bottom of my heart.

Hesamoddin Jahanian

July 2012

Table of contents

List of Figures

List of Tables

Chapter 1

Introduction

1.1. Functional Magnetic Resonance Imaging (fMRI)

Functional Magnetic Resonance Imaging (fMRI) refers to MRI technique that goes beyond the anatomy to measure aspects of local physiology of the brain in order to explore neuropsychological and cognitive principles underlying brain function [1-3]. Since it does not require contrast agents, fMRI has emerged as a non-invasive tool and has created a revolution in research on the basic functions of the healthy human brain. In addition, due to its increasing use and accessibility, fMRI holds the promise of being used to diagnose central nervous system pathology and used as a tool for neurosurgical mapping and planning [4]. Over the years, several fMRI techniques have been developed, but the most popular one employed at present is Blood Oxygen Level Dependent (BOLD) [1, 2, 5].

1.2. Blood Oxygen Level Dependent (BOLD) fMRI

BOLD fMRI technique does not image neuronal activity directly, but rather the changes in vascular physiology associated with neuronal activity. BOLD utilizes oxygenation dependent magnetic susceptibility difference between oxygenated and deoxygenated hemoglobin for image contrast. Deoxyhemoglobin produces magnetic field gradients around and through the blood vessels that decrease the MR signal. Brain activation is characterized by a drop in the local oxygen extraction fraction (OEF) and a corresponding drop in the local concentration of deoxyhemoglobin. Increase in metabolic and vascular demand in brain regions surrounding active neurons will result in increased

cerebral blood flow (CBF), cerebral blood volume (CBV), and to a lesser extent, oxygen metabolism and extraction which will eventually, cause a decrease in the local oxygen extraction fraction (OEF). The reduction in deoxyhemoglobin during activation then produces a small increase in the MR signal [1, 2, 5-7]. These changes take place on a much slower timescale (seconds) and over a wider region than the neuronal activity itself. BOLD fMRI is currently the dominant technique for functional imaging due to its higher signal to noise ratio (SNR), better sensitivity, ability to detect activation from single events and higher temporal resolution compared to other fMRI techniques [5, 6, 8].

1.3. Shortcomings of BOLD fMRI

Blood Oxygenation Level Dependent (BOLD) contrast fMRI is currently the dominant technique for functional imaging and has yielded a wealth of information about brain function. The observed BOLD contrast arises from a combination of several indirect phenomena that correlate with neuronal brain activation, such as increases in cerebral blood volume (CBF) and cerebral blood flow (CBF) and a decrease in the concentration of deoxy-hemoglobin, that causes the observed BOLD signal intensity to increase in the active area. However, this signal increase is a non-linear function of many physiological parameters as well as the scanner's own characteristics [9-12]. As a consequence, BOLD imaging results are typically reported as unitless statistical significance maps without a clear, quantitative, physiological interpretation.

One issue plaguing the BOLD effect technique is that, since the BOLD effect is based on sensitivity to local changes in magnetic susceptibility, artifacts due to susceptibility gradients are also greatly exacerbated. These artifacts are especially problematic in areas of the brain that lie near air spaces, such as the roof of the mouth, nose and ear canals, as well as the sinuses [3, 6].

The structure of the drift noise in the BOLD signal within a session has been shown to be autoregressive [13] and difficult to remove or model. Furthermore, the height and shape of the BOLD response depend on the baseline perfusion and metabolic levels, and thus

effects of interest can be confounded by the conditions of the experimental resting state [14, 15]. Thus, noise properties and drift of the BOLD signal make studies with long activation periods nearly impossible, as the effects of interest are confounded with the slow scanner drifts [16]. The same reasons prevent BOLD fMRI studies from answering questions about baseline conditions. For example, what is the effect of a given drug, therapy, or training regimen on the baseline activity of a brain structure of interest? How do the neural substrates of a specific cognitive function change with age?

Hence, there is a clear need for development of alternative and/or complementary quantitative methods to BOLD imaging for fMRI. As technology develops a paradigm shift toward quantitative methods that offer meaningful physiological interpretation and comparison across laboratories is expected.

1.4. Physiological Parameters for Quantitative fMRI

Recently several MRI techniques have been proposed for dynamic measurement of quantifiable physiological parameters such as oxygen consumption, cerebral blood volume (CBV) and cerebral blood flow (CBF). These methods can be used for quantitative functional imaging.

Cerebral blood volume (CBV) is a readily quantifiable physiological parameter. Recent blood volume imaging techniques, such as VASO [17] and AVIS [18], hold promise for quantitative fMRI, but they are severely hampered in terms of signal to noise ration (SNR), temporal resolution, and multi-slice imaging capability in their present state. Moreover, the corresponding models for quantification of CBV using these methods require many assumptions and/or multiple measurements per time point. [19-21].

Other methods that indirectly measure the rate of oxygen consumption by the brain are also available, but they require CBF data and calibration studies involving hypercapnia experiments [22, 23]. Thus, at this stage, they are not practical for dynamic quantitative functional imaging and will not be the focus of this chapter.

Cerebral blood flow (CBF) is also a readily quantifiable physiological parameter, and is easier to relate to neuronal metabolism than the BOLD response. Furthermore, animal studies conducted at high field, and high spatial resolution have indicated that neuronal activity produces CBF changes that are more localized to the parenchyma than the BOLD effect, consistent with the notion that the BOLD effect is more weighted toward draining veins and away from the active tissue [24, 25]. Thus, a fast, repeatable technique to measure CBF directly would be very desirable and complementary to BOLD imaging. Therefore we will focus on techniques for the measurement of CBF in the rest of this chapter.

1.5. Methods for measurement of cerebral blood flow (CBF)

Blood flow through any organ has been used as an important measure of its health and functionality for a long time [26]. As such, many techniques have been developed to measure blood flow based on tracer injections. The central idea behind these is always the same: some substance that can be detected easily (ie - radioactivity or fluorescence) gets injected somewhere upstream of the organ of interest, either an artery feeding of the tissue, a vein, or directly into the left ventricle of the heart. Then the concentration of the tracer is measured with the appropriate detector as it travels through the tissue of interest. Perfusion can then be calculated from the uptake curve of the tracer in the tissue.

With the advent of new imaging techniques, the detection process was incorporated into the imaging process, as in autoradiography, positron emission tomography (PET), or Single-photon emission computed tomography (SPECT) scanners. These imaging modalities use radioactive tracers to generate the raw signals from which the images are reconstructed. Hence, it was a straightforward leap to use the timing information in order to quantify perfusion through the existing tracer kinetic models.

In the case of MRI, perfusion can also be obtained by imaging the passage of a tracer through the tissue. Instead of being radioactive, though, MRI tracers are molecules that change the relaxation rates of blood and tissue (typically gadolinium compounds, such as

Gd-DOTA or Gd-DTPA). MRI has the added benefit that it allows for fairly rapid imaging (1-2 seconds for a whole brain volume) so one can sample the wash-in and wash-out of the tracer through the tissue. One can also simultaneously measure the amount of dispersion of the bolus that occurs during the transit from the injection site to the region of interest. Knowledge of this dispersion provides a more accurate estimate of the tissue's blood flow rate. Unfortunately, one can only do one contrast injection at a time, as the tracer takes many hours to clear the body, so it is not a very useful technique for fMRI.

In the pursuit of a practical and noninvasive method for cerebral blood flow another category of techniques, collectively known as arterial spin labeling (ASL), has been developed which employ magnetically labeled arterial water as an endogenous tracer [27-29]. The principle behind ASL imaging is conceptually simple. As with other techniques, the measurement consists of measuring the concentration of a tracer as it passes through a tissue of interest.

ASL deviates from the usual tracer strategy in two ways. First and foremost, no tracer is injected. Instead, the tracer is "created" inside the arteries feeding the organ by radio frequency (RF) electromagnetic pulses. These pulses are generated by standard MRI coils and invert the magnetization state of the water protons in the blood. After allowing a short period of time for inflow of the tracer into the tissue of interest, an image is collected. Just like in previous techniques, blood flow can be quantified by measuring the signal change due to the tracer – typically by subtracting the image with the tracer from a control image without the tracer. The second important difference is that the tracer used in ASL decays very quickly, since the longitudinal relaxation rate of arterial blood is in the order of 1600 ms. As a result, there is a significant penalty in the signal-to-noise ratio (SNR) but, on the bright side, the experiment can be repeated immediately and as many times as desired. One can think of ASL as a tracer (also referred to as "label" or "tag") that is completely non-toxic, rapidly decaying and it can be selectively injected into any artery tracer [27-29].

1.6. Examples of functional ASL studies

Due to above mentioned properties of functional arterial spin labeling (fASL), it is particularly useful for the study of gradual changes in neural activity, longitudinal and multi-site studies. We use the term fASL to indicate ASL time series used for fMRI purposes, but there is no technical difference between fASL and ASL. fASL has been used in several basic and cognitive neuroscience applications. It has been used in many studies to investigate visual, motor and language functions at 1.5T and 3T [30-37] and has been compared to BOLD fMRI [30, 32, 33, 36-38] indicating that the intra-individual reproducibility of fASL in terms of the area of activation and activation quantification is comparable to that of BOLD fMRI. fASL however, detects smaller activation volumes than BOLD fMRI but the areas had a high degree of co-localization between subjects. fASL also shows higher specificity compared to BOLD fMRI while maintaining high sensitivity in activation detection in the activated area [37].

Due to the drift in the BOLD signal, study of slow changes in neural activity using BOLD is quit challenging. fASL is a suitable tool for these studies as well. Motor learning is an example of the gradual changes in the neural activity over time, which cannot be easily assessed using BOLD fMRI. In [39] Olson et al. used fASL to study continuous, gradual changes in neural activity during motor learning. Subjects were required to use four fingers to press keys as quickly and as accurately as possible in response to the presentation of visual cues. Olson et al. reported that subjects performing this task demonstrated a reduction of neural activity in response to motor execution after training as compared to the start of training. Because the change in performance is slow and continuous, it is assumed for this study that the neural correlate of performance improvement during training is a gradual reduction in regional activity. The authors used fASL to detect these neural changes and reported reliable correlations between performance improvements and decreases in blood flow in premotor cortex and the inferior parietal lobe. This study suggests that fASL is a suitable tool for the study of the slow changes in the neural activity resulting from different cognitive tasks.

fASL has also been used in higher-level cognitive activation studies. There is an increasing body of evidence pointing to a neurobiological basis of personality. Characterizing the biological bases of personality dimensions is important to explaining individual differences in brain activity associated with more dynamic changes in experience (e.g., a psychotic episode) and cognition (e.g.,activation paradigms in functional MRI) [40]. In [40] O' Gorman et al. explored the biological bases of the major dimensions of models of personality using fASL. In this study, the correlation between personality factors with regional brain function was successfully investigated using fASL. The authors reported associations between perfusion in brain regions (including basal ganglia, thalamus, inferior frontal gyrus, cerebellum and cuneus) and different personality dimensions. These results suggest that variations in perfusion in certain brain regions correlated with variations in personality dimensions may reflect variations in brain function [40].

fASL provides quantification of absolute cerebral blood flow (CBF) along with excellent reproducibility over long time periods, making ASL a sensitive technique for visualization of brain function during the resting state as well as during task performance. This property allowed Rao et al. [41] to employ ASL to investigate the effect of genetic variation of the human serotonin transporter gene on resting brain function of healthy individuals. They studied the alteration of resting brain function in emotion-related regions (including the amygdala and ventromedial prefrontal cortex) in healthy individuals caused by the 5-HTTLPR genotype. Valid and reliable inferences of resting activity for applications such as this study could not be derived from BOLD fMRI because it only measures relative changes in neural activity, and the changes in signal intensity from scanner drift are much larger then the effects of interest.

Also, using ASL, authors [41] demonstrated an association of 5-HTTLPR genotype with resting amygdala and ventromedial prefrontal cortex function in the healthy human brain. Such alterations suggest a broad role of the 5-HTT gene in brain function that may be associated with the genetic susceptibility for mood disorders such as depression.

Neuronal modulations found using functional ASL (fASL), such as those reported in [40, 41], may also be important in interpretation of the different manifestations of BOLD response (which typically rely on the modulation of cerebral hemodynamics for detection of task-induced activation) to a particular stimuli in different groups.

The presence of low frequency signal drift in the BOLD signal impedes using a long task block. This problem makes it difficult to investigate slow processes such as learning, emotion, sustained attention and behavioral states in healthy and clinical populations. Because of its efficacy in longitudinal designs and low frequency paradigms, fASL is a good candidate for these studies. Kim et al. [42] successfully utilized fASL to study an uninterrupted 6-min continuous performance of the two high-level cognitive tasks (visual sustained attention and verbal working memory) which prior to fASL was only feasible for suboptimal short data acquisition blocks (40-90s). Understanding the neural correlates of these cognition function is very important because sustained attention is also implicated in various clinical disorders including attention deficit hyperactivity disorder, traumatic brain injury, and Alzheimer's disease [42].

In another study, Rao et al. [43] used fASL and BOLD to measure brain activation patterns associated with natural vision while subjects were freely viewing a cartoon movie. Rao et al. reported that cerebral blood flow increases in multiple visual pathway areas and frontal areas, and decreases in ventromedial frontal cortex and superior temporal cortex during movie viewing compared to resting states. Concurrent BOLD contrast revealed similar but weaker activation and deactivation patterns. This study demonstrates the feasibility of using fASL for imaging both sustained and dynamic effects in neural activation during natural and ecologically valid situations [43].

With excellent reproducibility over long-term time periods, fASL is ideal for imaging a sustained behavioral state, such as stress. Wang et al [44] used fASL to measure perfusion changes associated with mild to moderate stress. The authors demonstrated that a positive correlation exists between the change in perfusion induced by the stress task and subjective stress rating in the ventral right prefrontal cortex and left insula/putamen area. This study provides neuroimaging evidence that psychological stress induces

negative emotion and vigilance and that the ventral right prefrontal cortex plays a key role in the central stress response.

Pharmacological functional (phMRI) studies are making a significant contribution to our understanding of drug effects on brain systems. Since noise spectrum of arterial spin labeling signal contains relatively less power at low frequencies, it is particularly useful for phMRI studies in which a change in brain activity is expected over the course of minutes, hours, or days to asses low frequency between- and within-session drug-induced changes [45]. As an example, Gollub et al. [46] used fASL to measure neuronal activation during visual stimulation before and after cocaine and saline infusions. The authors used fASL to determine whether acute intravenous cocaine use would change global cerebral blood flow and demonstrated that cortical gray matter cerebral blood flow was unchanged after saline infusion but decreased after cocaine infusion.

These studies demonstrate that fASL can be successfully utilized for the investigation of the cerebral blood flow changes associated with development of human brain, personality, high level cognitive operations, the behavioral states such as attention, natural vision, psychological stress and assessing low frequency drug effects. Increased applications of fASL to the investigation of cognitively impaired populations are expected to follow.

1.7. Methods for Arterial Spin Labeling (ASL)

Any ASL sequence is basically made up of: 1) labeling period, during which the labeled (tagged) spin is created, 2) some delay time to allow the label to reach the tissue of interest, and 3) an imaging pulse sequence where the image is acquired. There may be additional pulses to shape the input function before the acquisition part, and there may be multiple coils involved in some variants, but in general, the structure remains the same. Thus, it is convenient to discuss labeling and imaging schemes independently, as they can be combined in multiple ways.

1.7.1. Labeling (tagging) schemes

There are a number of MRI pulse sequence strategies that can be used to label the blood spins. The first class of arterial spin labeling pulse sequences is "Continuous arterial spin labeling" (CASL) that attempts to continuously label (tag) blood as it passes a particular plane known as labeling (tagging) plane [27, 28]. Another class of arterial spin labeling pulse sequences is "Pulsed arterial spin labeling" (PASL) that employs a single pulse to define a volume and label the containing arterial blood [47, 48]. Whereas the pulsed approach only requires 1-2 seconds for the label to reach its maximum concentration in the tissue the continuous approach requires approximately 3 seconds before a steady state concentration of tag is reached. However, because of the longer inversion times of the continuous labeling scheme, the amount of tag to be detected is much larger and thus, the SNR of the method is also larger [11, 49], however, the benefits can be hampered by imperfect practical implementation of CASL. The tradeoff between PASL and CASL is primarily one of speed versus SNR.

Recently, beside conventional pulsed (PASL) and continuous (CASL) RF pulses, an intermediate method, called Pseudo-continuous ASL (pCASL) is proposed [50, 51]. pCASL utilizes a train of discrete RF pulses to mimic continuous tagging that is often unavailable on imagers due to the requirement of continuous RF transmit capabilities. pCASL has the potential of combining the merits of PASL, including less hardware demand, and CASL, which includes a longer tagging bolus and thus higher SNR. These improvements provide a better balance between tagging efficiency and SNR [50, 51].

1.7.1.1. Continuous Arterial Spin Labeling (CASL)

In the original continuous ASL formulation [27, 28], low-power, long pulses (in the order of a second or two) are applied at a plane inferior to the brain. Typically this is below the circle of Willis where the arterial supply to the brain is perpendicular to the labeling plane (see Figure 1.1.a). As usual, in order to achieve slice selection, the long RF pulses are applied at some frequency offset and in the presence of a slice-selective gradient.

These pulses have very different effects on the stationary and the moving spins. While the stationary spins at the labeling plane become saturated and lose phase coherence (essentially destroying their magnetization), the spins that are moving through the labeling plane experience a gradual change of their resonant frequency (recall that the resonant frequency is directly proportional to the magnetic field). The difference between the resonance frequency of the protons and the transmission frequency changes from positive through negative as the spins move through the inversion plane and is zero at the center of it.

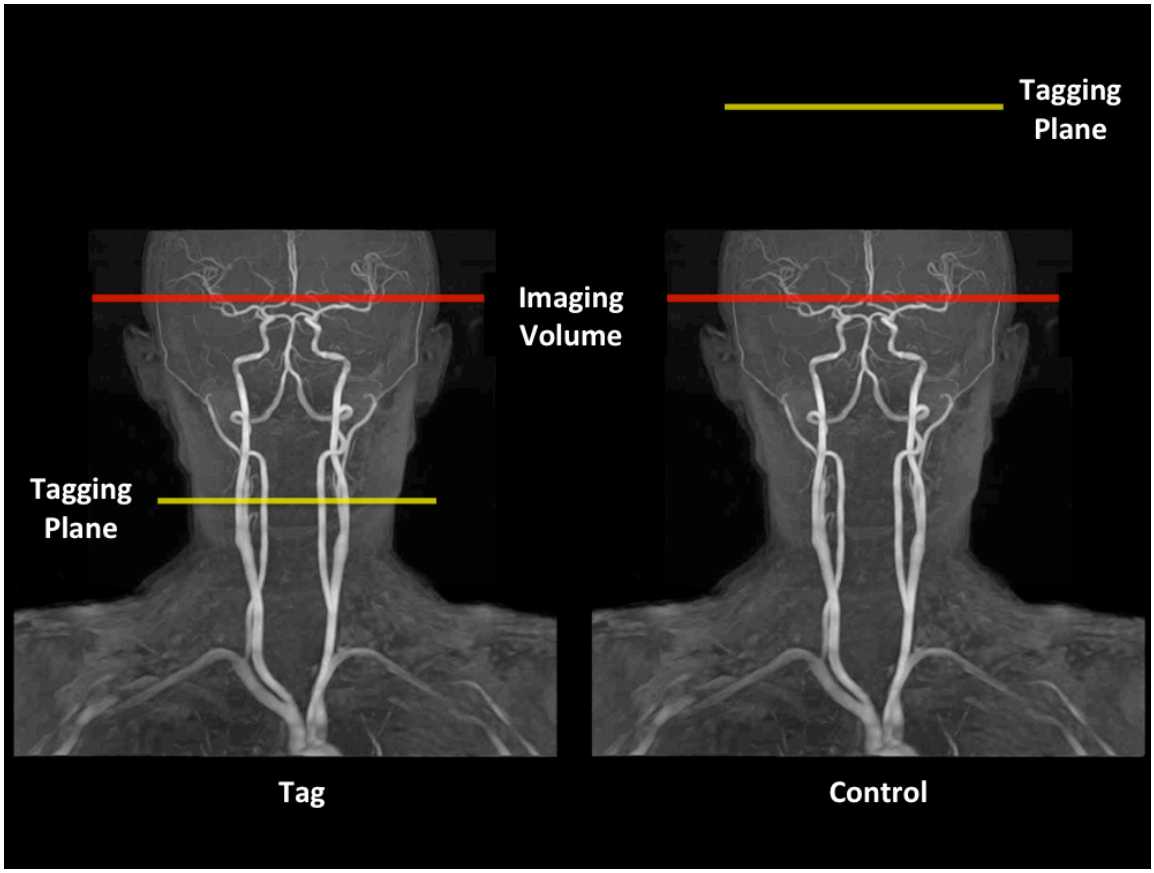

(a) **(b)**

Figure 1.1. Illustration of the relative locations of the inversion plane and imaging volume in the original continuous arterial spin labeling (CASL): **a)** during tagging period **b)** during control period. Note that using this technique only one slice can be imaged.

Because of this effective "frequency sweep", the net magnetic field generated by the combination of the main magnetic field (B_0), the applied RF field (B_{1eff}) and the magnetic field resulting from the spin's precession itself (ω/γ) experiences a rotation from pointing along the direction of the main magnetic field to pointing against it (see Figure 1.2). If this rotation is slow relative to the precession frequency, the effect of the constant RF pulse on these moving spins is to create a "spin-locked" state. This means that the flowing proton's magnetization precesses around the effective magnetic field and follows it as it rotated from pointing up to pointing down.

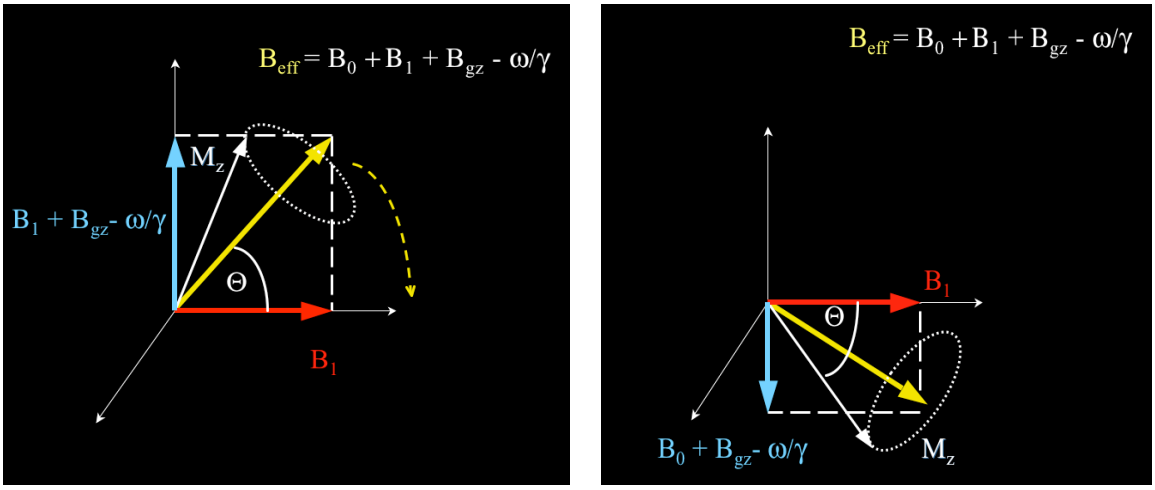

(a) **(b)**

Figure 1.2. The adiabatic inversion process: **(a)** In the rotating frame of reference the magnetic fields due to the scanner's main magnetic field (B_0), the RF coil's field (B_1), the slice select gradient (B_{gz}) and the opposing magnetization field add up to an "effective magnetic field" (B_{eff}). The arterial water's magnetization vector precesses around B_{eff}. **(b)** As the spins move, the contribution from the slice select changes from positive to negative. As this happens, the magnetization vector continues to precess around the effective field, resulting in the inversion of the magnetization vector.

As the protons move through the inversion plane, the "effective" field (B_{eff}) to which they are locked rotates from pointing along the direction of the main magnetic field to pointing against it. The end result is that when the flowing spins leave the plane, their magnetization is inverted. This phenomenon is referred to as "flow driven adiabatic

inversion" and is the basis for continuous arterial spin labeling techniques. It is important to note that immediately after inversion, the spins experience T_1 relaxation and the label effectively decays in a matter of a couple of seconds.

The main caveat of continuous ASL is that the long inversion pulses applied at the neck for labeling purposes also produce a significant amount of magnetization transfer (MT) [27, 28] in the spins at the tissue of interest. Briefly, magnetization transfer consists of signal loss during acquisition when it is preceded by RF pulses, even if those are not applied on resonance. As a result of MT, subtracting a tagged image from a control image would indicate not only the perfusion effects but also the degree of magnetization transfer, which is of no interest to the investigator.

This would constitute a major obstacle, but a number of solutions have been devised. The original solution to this problem was to apply an MT preparation pulse with identical properties to those of the labeling pulse before collecting the control image. This preparation pulse was identical to labeling pulse but with a reversed slice select gradient such that the pulse would be centered above the head (see Figure 1.1.b). In that case, there is only magnetization transfer but no arterial spin labeling. While this works in principle, it is difficult to collect more than one slice at a time while appropriately compensated magnetization transfer symmetrically for all the slices. Another solution was to simply use a separate RF coil for labeling whose field pattern will not reach the brain [52-54]. While this approach works quite well and is relatively simple to implement in principle, it requires additional hardware that can be synchronized with the main MRI scanner's pulse sequence. It is also generally uncomfortable for the subjects to wear the additional neck coil.

Several other strategies to overcome the magnetization transfer problem have been tried to overcome this problem, such as amplitude modulated CASL [55] (see Figure 1.3) in which by having two labeling planes for collecting control images, the effect of MT will be almost the same for control and tag images. The second labeling plane, undoes the labeling effect of the fist labeling plane and therefore spins passing through the two labeling planes will not be inverted for collecting the control images.

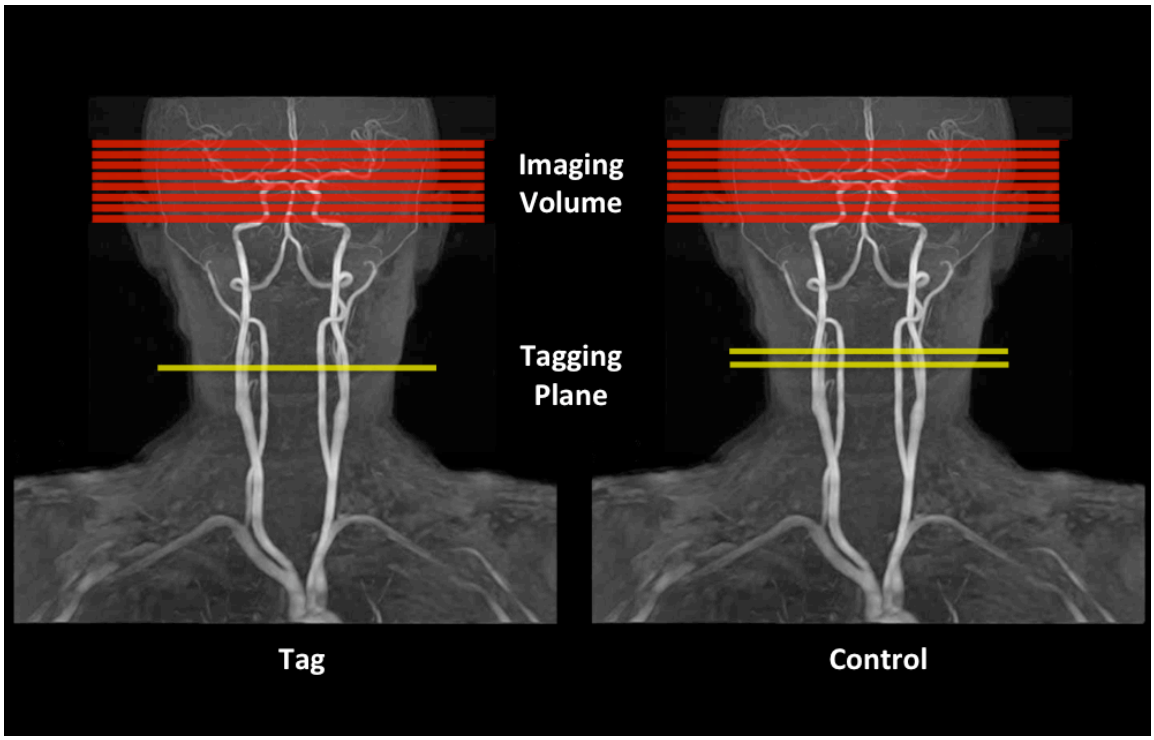

(a) **(b)**

Figure 1.3. Illustration of the relative locations of the inversion plane and imaging volume in the amplitude modulated continuous arterial spin labeling: (**a**) during tagging period **(b)** during control period.

1.7.1.2. Pseudo-continuous Arterial Spin Labeling (pCASL)

The most promising technique to solve the magnetization transfer problem in CASL is to break up the continuous labeling pulse into a train of pulses applied in rapid succession to achieve the same adiabatic inversion effect. In the control case, however, the same pulse train is applied but the phase of every other pulse is shifted by 180 degrees, such that every other pulse "un-does" the flip of the previous pulse. The end result is that both the control and the labeled image receive the same amount of magnetization transfer, the flowing blood's magnetization gets inverted prior to collecting the labeled image but it remains un-inverted during the collection of the control image. This technique, known as

pseudo-continuous arterial spin labeling (pCASL) has greatly facilitated the use of continuous ASL because it addresses the magnetization transfer issue and is relatively easy to implement [50, 51]. The caveat is that pCASL is sensitive to magnetic field inhomogeneity (off-resonance) at the inversion plane. This effect can severely affect the efficiency of the labeling process, crippling the technique, and is exacerbated at higher magnetic fields.

1.7.1.3. Pulsed Arterial Spin Labeling (PASL)

In pulsed arterial spin labeling technique a slab containing the arterial supply to the organ of interest is labeled with a short RF inversion pulse and then allow the inverted spins to flow from that slab into the tissue of interest. The difference in signal intensity between the label and control images is provided by the spins that flowed into the imaging slices during the inversion delay. This signal intensity difference can then be readily quantified and translated into perfusion images. This process mimics the injection of a bolus of tracer, rather than a constant infusion, as in the case of continuous ASL.

The simplest form of pulsed ASL is the EPISTAR technique [48], in which the inversion pulse (typically a hyperbolic secant) applied just below the region of interest (see Figure 1.4) followed by a delay to allow the inverted blood to flow into the tissue before collecting the image. Hyperbolic secant pulses are relatively short adiabatic pulses and exhibit no significant magnetization transfer effects, so there is no need for pre-compensation pulses before collecting the reference image. In the FAIR technique (the original pulsed ASL technique) the control image is preceded by an inversion pulse applied over the entire brain, followed by a short delay [47, 56].

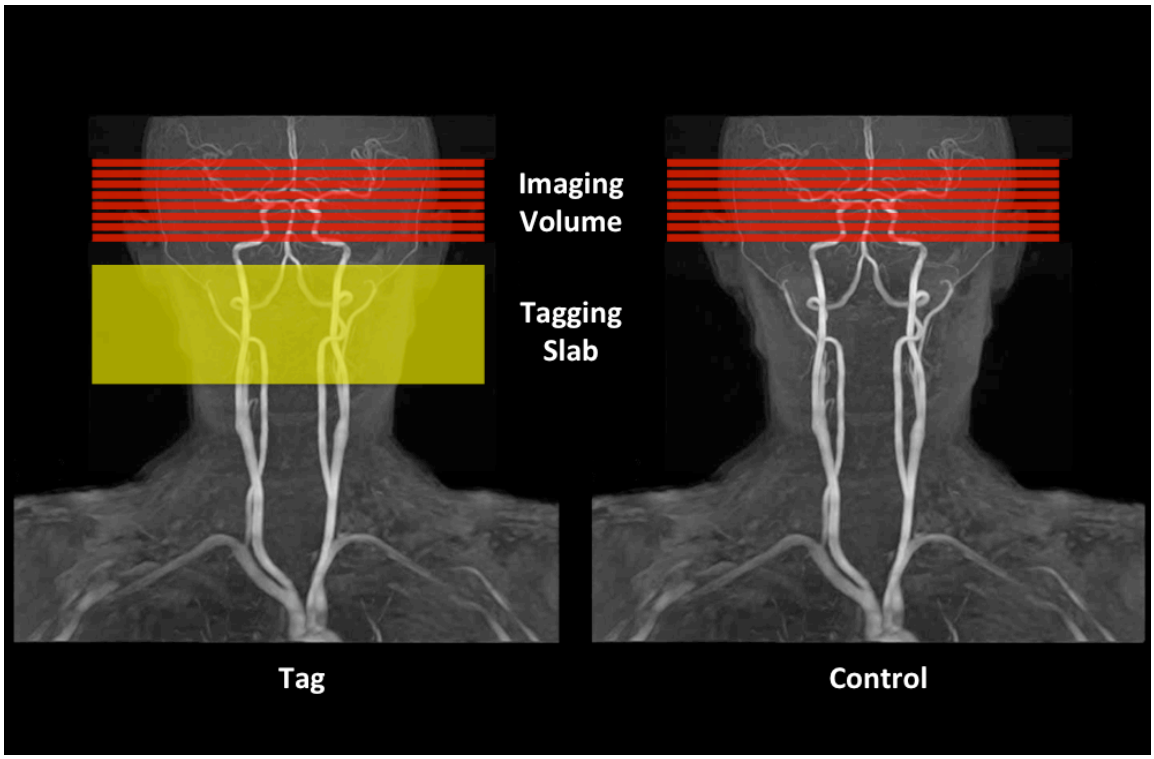

(a) **(b)**

Figure 1.4. Illustration of the relative locations of the tagging slab and imaging volume in the in EPISTAR. For the tag image the technique uses selective inversion slab below the imaging volume **(a)** and no pulse during the control period **(b).**

The tagged image is collected following a similar hyperbolic secant inversion pulse, except that it is applied only over the slices of interest, followed again by the same short delay to allow for inflow of blood into the imaging region (see Figure 1.5). There are many variants on this theme, but perhaps the most popular pulsed ASL technique is QUIPSS which uses additional pulses to saturate the trailing edges of the label, thus producing a clearly defined bolus [57, 58].

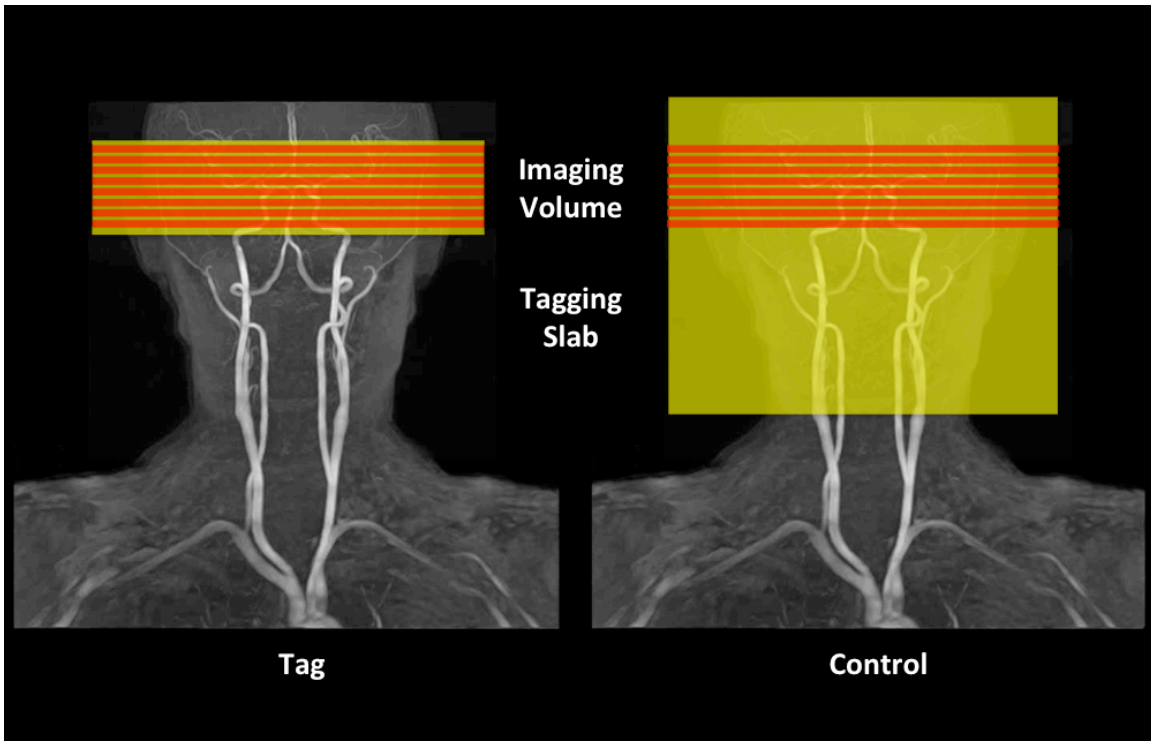

(a) **(b)**

Figure 1.5. Illustration of the flow alternating inversion recovery (FAIR) technique. For the tag image a selective inversion slab around the imaging volume is used **(a)** and for the control image a nonselective global inversion pulse is employed in this technique **(b)**.

1.7.2. ASL Image Acquisition

Image collection following the spin labeling process can be done in a number of ways, but it is important to take into account the goals of the specific application. As usual in MRI, there is a trade-off between acquisition speed, SNR and resolution.

In clinical and resting state applications, typical ASL scans use more standard image acquisition pulse sequences since the speed consideration is relaxed. Fast spin-echo acquisitions are a popular method because of their insensitivity to off-resonance artifacts and relatively high SNR and speed. For example [59, 60] used a 3D GRASE acquisition

sequence in conjunction with continuous ASL in order to boost the SNR of the acquired images in a functional imaging study of the medial temporal lobe.

Functional MRI requires fast image acquisition in order to capture the hemodynamic changes that take place during mental activity adequately. Fast imaging techniques that take advantage of echo-planar and echo-volumar acquisition and parallel imaging allow us to image the whole brain in a matter of a second or two with high spatial resolution. The flows in and out of the tissue while decaying is such that we are constrained to roughly a half a second to acquire the whole volume. This acquisition time window means that there is a significant constraint in the number of slices that one can get after a single labeling period. For instance, using a fast spiral acquisition typically allows for acquisition of a single slice in at least 25 ms. At this rate one can acquire 20 slices in half a second, which is adequate but requires thick slices of about 6 mm thickness, assuming a 12 cm brain.

In this regard, there is recent interest in the development of 3D echo-planar and echo-volumar acquisition schemes. 3D imaging schemes can ensure the same acquisition delay for the entire imaging volume relative to the labeling period. The SNR of 3D imaging can be greater than 2D multislice because a larger volume contributes to each echo. For example, Gunther et al [61] proposed a multi-echo 3D acquisition that allows collection of a k-space plane at each echo. Unfortunately, this acquisition scheme imposes a T2 weighting on each plane of k-space depending on the acquisition order. The result is typically a severe blur of the volume along the z-direction. One can think of this as a blurring filter applied along the slice direction, and the shape of that filter's point spread function (PSF) is that of the T2 decay.

Another 3D alternative is to use multi-shot readouts as in [53] but these typically require the use of low flip angles to preserve the magnetization throughout all the kz encoding steps. Low flip angles however result in reduction of the available signal. Gai et al [62] have experimented with an increasing flip-angle schedule starting at 10 degrees that produces a constant signal along kz according to the Ernst formula. This approach produces a flat point spread function, but at the cost of SNR. Recently, Nielsen et al [63]

have proposed a segmented low-flip-angle spiral readout with RF-soiling that can improve temporal SNR 2-fold relative to 2D multislice. They employed a cubic flip angle schedule to minimize the blurring in the ASL difference images.

1.8. Challenges facing ASL

So far, in this chapter we have illustrated the utility of ASL in functional MRI, but ASL is not a panacea. Arterial spin labeling techniques pose a number of challenges. These challenges must be overcome so that ASL techniques can take a more central role in the study of brain function. ASL is challenged by low SNR, since less than 10% of the water in a given voxel is contributed by blood [64, 65] and the label decays quickly. This problem can be partially alleviated by continuous arterial spin labeling, which increases the amount of label that is introduced into the tissue. Gains in the SNR have also been made with the development of pulse sequences that employ background suppression pulses, as these dramatically reduce the noise contribution from stationary tissue [66]. These background suppression pulses however, interfere with the ability to quantify perfusion and therefore they limit the measurement to relative CBF measures.[67]

Another major challenge to ASL techniques is low temporal resolution because ASL measurements take from 3 to 6 seconds depending on the amount of time spent labeling the arterial blood. Collecting multi-slice data can be challenging because the imaging RF pulses can interfere with the inversion label of the arterial water [68].

Lastly, all slices must be acquired within a short period of time in order to sample the label before it clears from the tissue of interest. As we have discussed earlier, functional MRI experiments often require the ability to scan the whole brain at a rapid rate in order to localize and characterize brief, subtle changes in cerebral activity (i.e., event related experiments). Collecting multi-slice ASL images in a rapid manner is challenging, given the SNR and clearance rate of the label. While one can collect images at a rate roughly equivalent to the transit time of the blood between the labeling plane and the imaging

volume (roughly 1.5 seconds) the number of slices at this rate is limited to less than twelve at the present time [63].

1.9. Conclusions

In this chapter we have examined arterial spin labeling as a technique for functional MRI. As we have seen, there are some clear advantages to collecting ASL data for functional studies in some circumstances, but other times it may not be beneficial. ASL is really well suited for longitudinal studies and studies with long blocks of activation (block design), but it may not be so well suited for event related experiments. ASL offers quantitative measures of perfusion at rest and activation. On a per subject basis, the technique's limitations are low SNR and temporal resolution, but there are significant gains in terms of population variance and contrast between resting and active states.

The goal of this dissertation is to improve ASL technique in terms of signal to noise ratio and temporal resolution so that it can take a more significant role in functional neuroimaging studies.

1.10. Dissertation outline

This dissertation includes three studies which are either published or ready for submission to peer-review journals. The first chapter is intended to introduce the reader to the relevant concepts, motivations and background not explicitly covered in each of the three studies. The last chapter of the dissertation summarizes the findings of all three studies as a whole and discusses future work and preliminary results stemming directly from these initial studies. All studies in this dissertation are focused on the pseudo-continuous arterial spin labeling (pCASL) technique.

In chapter 2, we discuss the effects of magnetic field inhomogeneity on tagging efficiency and signal to noise ratio of pCASL pulse sequence. We investigate these effects using computer simulation, phantom study and In-vivo experiments. We also

propose a method to correct for the degrading effects of magnetic field inhomogeneity on pCASL pulse sequence and to optimize the signal to noise ratio of the technique. Chapter 2 has been published in the *NMR in Biomedicine* journal [69]

In chapter 3, we present two applications of the optimized pCASL pulse sequence proposed in chapter 2. First we present the implementation of real-time acquisition and analysis of pCASL-based fMRI time series. In this implementation, all calculations, including image reconstruction and activation detection is executed within a single TR (4 s). Second, employing the optimized pCASL pulse sequence, we propose a reduced specific absorption rate (SAR) version of pCASL pulse sequence that allows the reduction of the flip angle of RF pulses without compromising the signal to noise ratio of the measurements. The main application of this method would be in ultra-high-field MRI (≥ 7T) ASL studies. Parts of chapter 3 have been published in *Magnetic Resonance in Medicine* journal [70].

In chapter 4, we propose a new framework for dynamic imaging of arterial blood volume using pCASL pulse sequence. We discuss the kinetics of arterial spin labeling signal and find the parameters that provides an ASL signal primarily determined by arterial blood volume rather than arterial blood flow. We evaluate the proposed method by comparing it to the conventional perfusion ASL and BOLD techniques using functional MRI experiments.

Chapter 5 summarizes the conclusions from the previous chapters, and places these results in the context of fMRI applications as a whole. In addition, potential future work stemming from these earlier studies is described.

1.11. References

[1] S. Ogawa, and T. M. Lee, "Magnetic resonance imaging of blood vessels at high fields: in vivo and in vitro measurements and image simulation," *Magn Reson Med,* vol. 16, no. 1, pp. 9-18, Oct, 1990.

[2] S. Ogawa, T. Lee, A. Kay, and D. Tank, "Brain magnetic resonance imaging with contrast dependent on blood oxygenation.," *Proc Natl Acad Sci U S A,* vol. 87, no. 24, pp. 9868-72, Dec, 1990.

[3] K. Kwong, J. Belliveau, D. Chesler, I. Goldberg, R. Weisskoff, B. Poncelet, D. Kennedy, B. Hoppel, M. Cohen, R. Turner, and a. et, "Dynamic magnetic resonance imaging of human brain activity during primary sensory stimulation.," *Proc Natl Acad Sci U S A,* vol. 89, no. 12, pp. 5675-9, Jun 15, 1992.

[4] T. Rohlfing, J. B. West, J. Beier, T. Liebig, C. A. Taschner, and U. W. Thomale, "Registration of functional and anatomical MRI: accuracy assessment and application in navigated neurosurgery," *Comput Aided Surg,* vol. 5, no. 6, pp. 414-25, 2000.

[5] S. Ogawa, R. S. Menon, D. W. Tank, S. G. Kim, H. Merkle, J. M. Ellermann, and K. Ugurbil, "Functional brain mapping by blood oxygenation level-dependent contrast magnetic resonance imaging. A comparison of signal characteristics with a biophysical model," *Biophys J,* vol. 64, no. 3, pp. 803-12, Mar, 1993.

[6] P. A. Bandettini, E. C. Wong, R. S. Hinks, R. S. Tikofsky, and J. S. Hyde, "Time course EPI of human brain function during task activation," *Magn Reson Med,* vol. 25, no. 2, pp. 390-7, Jun, 1992.

[7] K. Kwong, "Functional magnetic resonance imaging with echo planar imaging.," *Magn Reson Q,* vol. 11, no. 1, pp. 1-20, Mar, 1995.

[8] J. A. Detre, and J. Wang, "Technical aspects and utility of fMRI using BOLD and ASL," *Clin Neurophysiol,* vol. 113, no. 5, pp. 621-34, May, 2002.

[9] G. Boynton, S. Engel, G. Glover, and D. Heeger, "Linear systems analysis of functional magnetic resonance imaging in human V1.," *J Neurosci,* vol. 16, no. 13, pp. 4207-21, Jul 1, 1996.

[10] R. Buxton, and L. Frank, "A model for the coupling between cerebral blood flow and oxygen metabolism during neural stimulation.," *J Cereb Blood Flow Metab,* vol. 17, no. 1, pp. 64-72, Jan, 1997.

[11] R. Buxton, L. Frank, E. Wong, B. Siewert, S. Warach, and R. Edelman, "A general kinetic model for quantitative perfusion imaging with arterial spin labeling.," *Magn Reson Med,* vol. 40, no. 3, pp. 383-96, Sep, 1998.

[12] A. Vazquez, and D. Noll, "Nonlinear aspects of the BOLD response in functional MRI.," *Neuroimage,* vol. 7, no. 2, pp. 108-18, Feb, 1998.

[13] T. E. Lund, K. H. Madsen, K. Sidaros, W. L. Luo, and T. E. Nichols, "Non-white noise in fMRI: does modelling have an impact?," *Neuroimage,* vol. 29, no. 1, pp. 54-66, Jan 1, 2006.

[14] E. R. Cohen, K. Ugurbil, and S. G. Kim, "Effect of basal conditions on the magnitude and dynamics of the blood oxygenation level-dependent fMRI response," *J Cereb Blood Flow Metab,* vol. 22, no. 9, pp. 1042-53, Sep, 2002.

[15] T. A. Mulderink, D. R. Gitelman, M. M. Mesulam, and T. B. Parrish, "On the use of caffeine as a contrast booster for BOLD fMRI studies," *Neuroimage,* vol. 15, no. 1, pp. 37-44, Jan, 2002.

[16] A. M. Smith, B. K. Lewis, U. E. Ruttimann, F. Q. Ye, T. M. Sinnwell, Y. Yang, J. H. Duyn, and J. A. Frank, "Investigation of low frequency drift in fMRI signal," *Neuroimage,* vol. 9, no. 5, pp. 526-33, May, 1999.

[17] H. Lu, X. Golay, J. J. Pekar, and P. C. M. van Zijl, "Functional magnetic resonance imaging based on changes in vascular space occupancy," *Magnetic Resonance in Medicine,* vol. 50, no. 2, pp. 263-274, 2003.

[18] A. L. Vazquez, G. R. Lee, L. Hernandez-Garcia, and D. C. Noll, "Application of selective saturation to image the dynamics of arterial blood flow during brain activation using magnetic resonance imaging," *Magnetic Resonance in Medicine,* vol. 55, no. 4, pp. 816-825, 2006.

[19] T. Jin, and S.-G. Kim, "Improved cortical-layer specificity of vascular space occupancy fMRI with slab inversion relative to spin-echo BOLD at 9.4 T," *Neuroimage,* vol. 40, no. 1, pp. 59-67, 2008.

[20] C. B. Glielmi, R. A. Schuchard, and X. P. Hu, "Estimating cerebral blood volume with expanded vascular space occupancy slice coverage," *Magnetic Resonance in Medicine,* vol. 61, no. 5, pp. 1193-1200, 2009.

[21] M. J. Donahue, E. Sideso, B. J. MacIntosh, J. Kennedy, A. Handa, and P. Jezzard, "Absolute arterial cerebral blood volume quantification using inflow vascular-

space-occupancy with dynamic subtraction magnetic resonance imaging," *Journal of Cerebral Blood Flow & Metabolism,* vol. 30, no. 7, pp. 1329-1342, 2010.

[22] R. Hoge, J. Atkinson, B. Gill, G. Crelier, S. Marrett, and G. Pike, "Investigation of BOLD signal dependence on cerebral blood flow and oxygen consumption: the deoxyhemoglobin dilution model.," *Magn Reson Med,* vol. 42, no. 5, pp. 849-63, Nov, 1999.

[23] T. L. Davis, K. K. Kwong, R. M. Weisskoff, and B. R. Rosen, "Calibrated functional MRI: mapping the dynamics of oxidative metabolism," *Proc Natl Acad Sci U S A,* vol. 95, no. 4, pp. 1834-9, Feb 17, 1998.

[24] T. Duong, E. Yacoub, G. Adriany, X. Hu, K. Ugurbil, J. Vaughan, H. Merkle, and S. Kim, "High-resolution, spin-echo BOLD, and CBF fMRI at 4 and 7 T.," *Magn Reson Med,* vol. 48, no. 4, pp. 589-93, Oct, 2002.

[25] J. Pfeuffer, G. Adriany, A. Shmuel, E. Yacoub, P. Van De Moortele, X. Hu, and K. Ugurbil, "Perfusion-based high-resolution functional imaging in the human brain at 7 Tesla.," *Magn Reson Med,* vol. 47, no. 5, pp. 903-11, May, 2002.

[26] N. A. Lassen, and W. Perl, *Tracer kinetic methods in medical physiology*, New York: Raven Press, 1979.

[27] J. Detre, J. Leigh, D. Williams, and A. Koretsky, "Perfusion imaging.," *Magn Reson Med,* vol. 23, no. 1, pp. 37-45, Jan, 1992.

[28] D. Williams, J. Detre, J. Leigh, and A. Koretsky, "Magnetic resonance imaging of perfusion using spin inversion of arterial water.," *Proc Natl Acad Sci U S A,* vol. 89, no. 1, pp. 212-6, Jan 1, 1992.

[29] D. C. Alsop, and J. A. Detre, "Reduced transit-time sensitivity in noninvasive magnetic resonance imaging of human cerebral blood flow," *J Cereb Blood Flow Metab,* vol. 16, no. 6, pp. 1236-49, Nov, 1996.

[30] G. Aguirre, J. Detre, E. Zarahn, and D. Alsop, "Experimental design and the relative sensitivity of BOLD and perfusion fMRI.," *Neuroimage,* vol. 15, no. 3, pp. 488-500, Mar, 2002.

[31] J. Wang, G. Aguirre, D. Kimberg, A. Roc, L. Li, and J. Detre, "Arterial spin labeling perfusion fMRI with very low task frequency.," *Magn Reson Med,* vol. 49, no. 5, pp. 796-802, May, 2003.

[32] S. Kemeny, F. Q. Ye, R. Birn, and A. R. Braun, "Comparison of continuous overt speech fMRI using BOLD and arterial spin labeling," *Hum Brain Mapp,* vol. 24, no. 3, pp. 173-83, Mar, 2005.

[33] T. Tjandra, J. C. Brooks, P. Figueiredo, R. Wise, P. M. Matthews, and I. Tracey, "Quantitative assessment of the reproducibility of functional activation measured with BOLD and MR perfusion imaging: implications for clinical trial design," *Neuroimage,* vol. 27, no. 2, pp. 393-401, Aug 15, 2005.

[34] O. Leontiev, and R. B. Buxton, "Reproducibility of BOLD, perfusion, and CMRO2 measurements with calibrated-BOLD fMRI," *Neuroimage,* vol. 35, no. 1, pp. 175-84, Mar, 2007.

[35] B. M. Ances, O. Leontiev, J. E. Perthen, C. Liang, A. E. Lansing, and R. B. Buxton, "Regional differences in the coupling of cerebral blood flow and oxygen metabolism changes in response to activation: implications for BOLD-fMRI," *Neuroimage,* vol. 39, no. 4, pp. 1510-21, Feb 15, 2008.

[36] J. J. Chen, M. Wieckowska, E. Meyer, and G. B. Pike, "Cerebral blood flow measurement using fMRI and PET: a cross-validation study," *Int J Biomed Imaging,* vol. 2008, pp. 516359, 2008.

[37] H. Raoult, J. Petr, E. Bannier, A. Stamm, J. Y. Gauvrit, C. Barillot, and J. C. Ferre, "Arterial spin labeling for motor activation mapping at 3T with a 32-channel coil: reproducibility and spatial accuracy in comparison with BOLD fMRI," *Neuroimage,* vol. 58, no. 1, pp. 157-67, Sep 1, 2011.

[38] M. Hermes, D. Hagemann, P. Britz, S. Lieser, J. Rock, E. Naumann, and C. Walter, "Reproducibility of continuous arterial spin labeling perfusion MRI after 7 weeks," *MAGMA,* vol. 20, no. 2, pp. 103-15, Apr, 2007.

[39] I. R. Olson, H. Rao, K. S. Moore, J. Wang, J. A. Detre, and G. K. Aguirre, "Using perfusion fMRI to measure continuous changes in neural activity with learning," *Brain Cogn,* vol. 60, no. 3, pp. 262-71, Apr, 2006.

[40] R. L. O'Gorman, V. Kumari, S. C. Williams, F. O. Zelaya, S. E. Connor, D. C. Alsop, and J. A. Gray, "Personality factors correlate with regional cerebral perfusion," *Neuroimage,* vol. 31, no. 2, pp. 489-95, Jun, 2006.

[41] H. Rao, S. J. Gillihan, J. Wang, M. Korczykowski, G. M. Sankoorikal, K. A. Kaercher, E. S. Brodkin, J. A. Detre, and M. J. Farah, "Genetic variation in serotonin transporter alters resting brain function in healthy individuals," *Biol Psychiatry,* vol. 62, no. 6, pp. 600-6, Sep 15, 2007.

[42] J. Kim, J. Whyte, J. Wang, H. Rao, K. Z. Tang, and J. A. Detre, "Continuous ASL perfusion fMRI investigation of higher cognition: quantification of tonic CBF changes during sustained attention and working memory tasks," *Neuroimage,* vol. 31, no. 1, pp. 376-85, May 15, 2006.

[43] H. Rao, J. Wang, K. Tang, W. Pan, and J. A. Detre, "Imaging brain activity during natural vision using CASL perfusion fMRI," *Hum Brain Mapp,* vol. 28, no. 7, pp. 593-601, Jul, 2007.

[44] J. Wang, H. Rao, G. S. Wetmore, P. M. Furlan, M. Korczykowski, D. F. Dinges, and J. A. Detre, "Perfusion functional MRI reveals cerebral blood flow pattern under psychological stress," *Proc Natl Acad Sci U S A,* vol. 102, no. 49, pp. 17804-9, Dec 6, 2005.

[45] R. G. Wise, and I. Tracey, "The role of fMRI in drug discovery," *J Magn Reson Imaging,* vol. 23, no. 6, pp. 862-76, Jun, 2006.

[46] R. L. Gollub, H. C. Breiter, H. Kantor, D. Kennedy, D. Gastfriend, R. T. Mathew, N. Makris, A. Guimaraes, J. Riorden, T. Campbell, M. Foley, S. E. Hyman, B. Rosen, and R. Weisskoff, "Cocaine decreases cortical cerebral blood flow but does not obscure regional activation in functional magnetic resonance imaging in human subjects," *J Cereb Blood Flow Metab,* vol. 18, no. 7, pp. 724-34, Jul, 1998.

[47] S. Kim, and N. Tsekos, "Perfusion imaging by a flow-sensitive alternating inversion recovery (FAIR) technique: application to functional brain imaging.," *Magn Reson Med,* vol. 37, no. 3, pp. 425-35, Mar, 1997.

[48] R. Edelman, and Q. Chen, "EPISTAR MRI: multislice mapping of cerebral blood flow.," *Magn Reson Med,* vol. 40, no. 6, pp. 800-5, Dec, 1998.

[49] E. Wong, R. Buxton, and L. Frank, "A theoretical and experimental comparison of continuous and pulsed arterial spin labeling techniques for quantitative perfusion imaging.," *Magn Reson Med,* vol. 40, no. 3, pp. 348-55, Sep, 1998.

[50] W. Dai, D. Garcia, C. de Bazelaire, and D. C. Alsop, "Continuous flow-driven inversion for arterial spin labeling using pulsed radio frequency and gradient fields," *Magn Reson Med,* vol. 60, no. 6, pp. 1488-97, Dec, 2008.

[51] W. C. Wu, M. Fernandez-Seara, J. A. Detre, F. W. Wehrli, and J. Wang, "A theoretical and experimental investigation of the tagging efficiency of pseudocontinuous arterial spin labeling," *Magn Reson Med,* vol. 58, no. 5, pp. 1020-7, Nov, 2007.

[52] W. Zhang, A. Silva, D. Williams, and A. Koretsky, "NMR measurement of perfusion using arterial spin labeling without saturation of macromolecular spins.," *Magn Reson Med,* vol. 33, no. 3, pp. 370-6, Mar, 1995.

[53] S. Talagala, F. Ye, P. Ledden, and S. Chesnick, "Whole-brain 3D perfusion MRI at 3.0 T using CASL with a separate labeling coil.," *Magn Reson Med,* vol. 52, no. 1, pp. 131-40, Jul, 2004.

[54] L. Hernandez-Garcia, G. R. Lee, A. L. Vazquez, and D. C. Noll, "Fast, pseudo-continuous arterial spin labeling for functional imaging using a two-coil system," *Magnetic Resonance in Medicine,* vol. 51, no. 3, pp. 577-585, 2004.

[55] J. Wang, Y. Zhang, R. Wolf, A. Roc, D. Alsop, and J. Detre, "Amplitude-modulated Continuous Arterial Spin-labeling 3.0-T Perfusion MR Imaging with a Single Coil: Feasibility Study.," *Radiology,* vol. 235, no. 1, pp. 218-28, Apr, 2005.

[56] S. Kim, "Quantification of relative cerebral blood flow change by flow-sensitive alternating inversion recovery (FAIR) technique: application to functional mapping.," *Magn Reson Med,* vol. 34, no. 3, pp. 293-301, Sep, 1995.

[57] E. Wong, R. Buxton, and L. Frank, "Implementation of quantitative perfusion imaging techniques for functional brain mapping using pulsed arterial spin labeling.," *NMR Biomed,* vol. 10, no. 4-5, pp. 237-49, Jun-Aug, 1997.

[58] E. Wong, R. Buxton, and L. Frank, "Quantitative imaging of perfusion using a single subtraction (QUIPSS and QUIPSS II)." *Magn Reson Med,* vol. 39, no. 5, pp. 702-8, May, 1998.

[59] M. A. Fernandez-Seara, J. Wang, Z. Wang, M. Korczykowski, M. Guenther, D. A. Feinberg, and J. A. Detre, "Imaging mesial temporal lobe activation during scene encoding: comparison of fMRI using BOLD and arterial spin labeling," *Hum Brain Mapp,* vol. 28, no. 12, pp. 1391-400, Dec, 2007.

[60] M. A. Fernandez-Seara, Z. Wang, J. Wang, H. Y. Rao, M. Guenther, D. A. Feinberg, and J. A. Detre, "Continuous arterial spin labeling perfusion measurements using single shot 3D GRASE at 3 T," *Magn Reson Med,* vol. 54, no. 5, pp. 1241-7, Nov, 2005.

[61] M. Gunther, K. Oshio, and D. A. Feinberg, "Single-shot 3D imaging techniques improve arterial spin labeling perfusion measurements," *Magn Reson Med,* vol. 54, no. 2, pp. 491-8, Aug, 2005.

[62] N. D. Gai, S. L. Talagala, and J. A. Butman, "Whole-brain cerebral blood flow mapping using 3D echo planar imaging and pulsed arterial tagging," *J Magn Reson Imaging,* vol. 33, no. 2, pp. 287-95, Feb, 2011.

[63] J.-F. Nielsen, and L. Hernandez-Garcia, "Functional perfusion imaging using pseudocontinuous arterial spin labeling with low-flip-angle segmented 3D spiral readouts," *Magnetic Resonance in Medicine*, pp. n/a-n/a, 2012.

[64] G. Pawlik, A. Rackl, and R. Bing, "Quantitative capillary topography and blood flow in the cerebral cortex of cats: an in vivo microscopic study.," *Brain Res,* vol. 208, no. 1, pp. 35-58, Mar 9, 1981.

[65] H. Weiss, E. Buchweitz, T. Murtha, and M. Auletta, "Quantitative regional determination of morphometric indices of the total and perfused capillary network in the rat brain.," *Circ Res,* vol. 51, no. 4, pp. 494-503, Oct, 1982.

[66] D. Garcia, G. Duhammel, and D. Alsop, "Slow Magnetization Transfer Dominates Inefficiency of Suppressed Arterial Spin Labeling ". p. 1151.

[67] D. D. Shin, H.-L. Liu, E. C. Wong, and T. T. Liu, "Effect of background suppression on CBF quantitation in pseudo continuous arterial spin labeling," *Proceedings of International Society for Magnetic Resonance in Medicine* pp. 2101, 2011.

[68] A. Silva, W. Zhang, D. Williams, and A. Koretsky, "Multi-slice MRI of rat brain perfusion during amphetamine stimulation using arterial spin labeling.," *Magn Reson Med,* vol. 33, no. 2, pp. 209-14, Feb, 1995.

[69] H. Jahanian, D. C. Noll, and L. Hernandez-Garcia, "B0 field inhomogeneity considerations in pseudo-continuous arterial spin labeling (pCASL): effects on tagging efficiency and correction strategy," *NMR in Biomedicine,* vol. 24, no. 10, pp. 1202-1209, 2011.

[70] L. Hernandez-Garcia, H. Jahanian, M. K. Greenwald, J.-K. Zubieta, and S. J. Peltier, "Real-time functional MRI using pseudo-continuous arterial spin labeling," *Magnetic Resonance in Medicine,* vol. 65, no. 6, pp. 1570-1577, 2011.

Chapter 2

Optimizing the tagging efficiency and signal to noise ratio of pseudo-continuous ASL pulse sequence

2.1. Abstract

Pseudo-continuous arterial spin labeling (pCASL) is a very powerful technique to measure cerebral perfusion which circumvents problems affecting other continuous arterial spin labeling schemes such as magnetization transfer and duty cycle. However, some variability in the tagging efficiency of pCASL technique has been reported. In this chapter we investigate the effect of B0 field inhomogeneity on the tagging efficiency of pCASL pulse sequence as a possible cause of this variability. Both theory and simulated data predict that the efficiency of pseudo-continuous labeling pulses can be degraded in the presence of off-resonance effects. These findings are corroborated with human in-vivo measurements of tagging efficiency.

Based on this theoretical framework, a method utilizing the B0 field map information is proposed to correct for the possible loss in tagging efficiency of pCASL pulse sequence. The efficiency of the proposed correction method is evaluated using numerical simulations and in-vivo implementation. The data show that the proposed method can effectively recover the lost tagging efficiency and signal-to-noise ratio of pCASL due to off-resonance effects.

2.2. Introduction

Perfusion is a well-known indicator of brain function. It is used to study normal physiology and pathology of brain [1-3]. Arterial Spin Labeling (ASL) techniques permit quantitative measurement of perfusion with MRI without injection of exogenous tracers [4].

Beside the steady state perfusion measurements, ASL is capable of estimating transient perfusion changes, which can be used for studying brain function [5-7]. Perfusion-based functional MRI through ASL has remarkable potential as a tool to study brain function because of its quantifiable nature and close relation to neuronal activity. Although it is possible to saturate the tissue of interest with tagged blood by using longer RF tagging pulses (continuous ASL or CASL) [8, 9] and improve the SNR of perfusion measurement, ASL techniques still suffer from low signal to noise ratio (SNR) and magnetization transfer effects, which make multi-slice measurements problematic.

The recent introduction of pseudo-continuous inversion pulses (pCASL) [10, 11] facilitates the use of CASL by providing multi-slice cerebral perfusion measurements while compensating for magnetization transfer effects in an effective manner without using additional hardware or losing tagging efficiency, yet limiting the specific absorption rate (SAR). pCASL employs a rapidly repeated gradient and radio frequency (RF) pulses to mimic the effect of continuous labeling without the need for continuous RF transmit capabilities.

However, it has been reported that the tagging efficiency of pCASL can vary greatly for different subjects and also for different tagging locations in the same subject. These findings have been observed at 3T [12, 13], 7T [14, 15] and 11.75T [16] ASL studies.

Any loss in the tagging efficiency of pCASL, causes loss in SNR which can not be neglected, given the inherently low SNR of ASL. Furthermore, any unaccounted loss of tagging efficiency also results in significant quantification errors. In this paper, we investigate the effects of B0 field inhomogeneity on the efficiency of the pseudo-continuous inversion pulses as a possible cause for these variations in the tagging

efficiency and propose a method to fix this. We propose to restore the loss in tagging efficiency by correcting the phase of the RF pulses in combination with an average gradient compensation scheme. We demonstrate the effects of field-inhomogeneity and efficacy of the method using numerical simulations and in vivo experimental data.

2.3. Theory

As discussed in chapter 1, adiabatic inversion occurs when spins experience a radiofrequency magnetic field, B1, of sweeping frequency relative to their resonance frequency [17]. In the case of flow-driven inversions (e.g. continuous arterial spin labeling) the frequency sweep is achieved by the spins moving in the direction of a magnetic field gradient. In other words, the frequency of the B1 field is constant, but the resonant frequency of the spins changes as they move in the direction of the gradient [17].

Pseudo-continuous inversion pulses produce the flow driven adiabatic inversion effect in a piecewise manner by exciting the magnetization vector and allowing a small amount of position-dependent phase accumulation in the transverse plane, between RF pulses. Assuming that slice selective gradient is applied along the Z direction, the phase accumulation is caused by the imbalance in the slice selective gradient (G_{ss}) providing a net average gradient (G_{av}) between pulses. The net movement of the magnetization vector closely resembles the motion of continuous adiabatic inversions [10, 11].

Consider a single cycle in a pseudo-continuous inversion pulse as depicted in Figure 2.1 [10, 11]. Ideally, for a flowing spin moving at the velocity V, along the Z direction, which is at distance Z(t) from iso-center, the amount of phase accumulation between nth and (n+1)th RF pulses is :

$$
\begin{aligned}
\Delta\phi(n) &= \int_{t=n\delta}^{(n+1)\delta} \gamma G_{ss}(t) Z(t)\ dt \\
&= \int_{t=n\delta}^{(n+1)\delta} \gamma G_{ss}(t)(Z(t=n\delta) + Vt\ )dt \\
&= \int_{t=n\delta}^{(n+1)\delta} \gamma G_{ss}(t)(Z(t=0)\ + (n-1)V\delta + Vt\ )dt \\
&= \gamma Z(t=0)\ G_{av}\delta + \gamma(n-1)VG_{av}\delta^2 + \int_{t=n\delta}^{(n+1)\delta} \gamma G_{ss}(t) Vt\ dt
\end{aligned}
\tag{2.1}
$$

in which G_{ss}, δ and G_{av} represent slice selective gradient (assumed to be applied along the Z direction), time interval between two RF pulses, average gradient over the time between RF pulses ($G_{av} = A_{extra}/\delta$), respectively. In this formulation, t=0 represents the start of RF pulse. The first term in Eq. 2.1 depends on the position of tagging plane with respect to the system iso-center. This term needs to be compensated if the tagging plane is not located at the system iso-center. Adding a linear phase to the tagging/control RF pulses can compensate for the position dependent term in Eq. 2.1 and makes the phase accumulation of flowing spins independent of the distance from the system iso-center.

However, the field homogeneity in the tagging plane is often perturbed by the presence of the head and/or by imperfect shimming. In particular, the air-tissue interfaces in the mouth and throat and any dental work have profound effect. We can model the local field inhomogeneities at the tagging plane of pCASL pulse as a constant shift plus a linear Z-gradient and we refer to them as off-resonance (ΔB_0) and off-resonance gradient (ΔG), respectively, throughout the paper. In that case, the amount of error introduced to the phase accumulation ($\Delta\varphi_{error}$) between two RF pulses for the pCASL pulse sequence (Figure. 2.1) can be calculated using Eq. 2.2.

$$
\Delta\phi_{error} = \gamma\ \Delta B_0\ \delta + \frac{1}{2}\gamma\ V\ \Delta G\ \delta^2 \tag{2.2}
$$

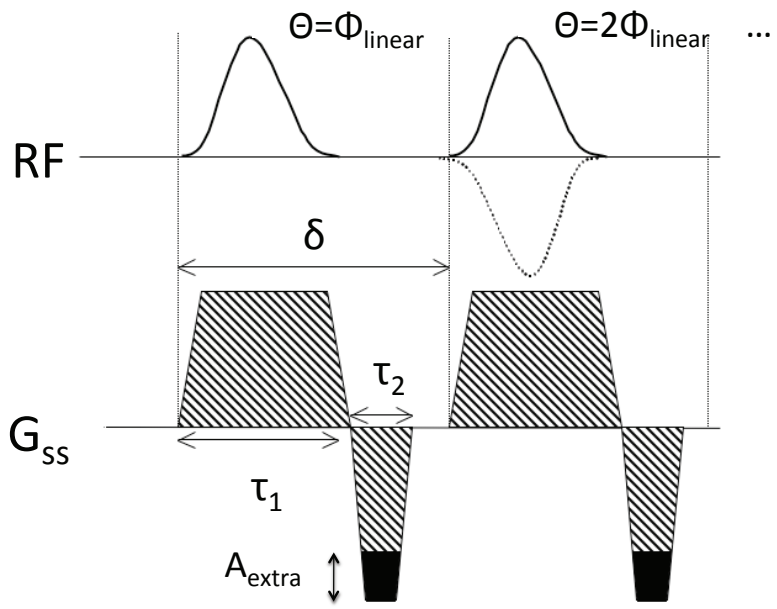

Figure 2.1. One cycle of the repeated pattern of radio frequency (RF) and slice-select gradient (G_{ss}) pulses used for pseudo-continuous inversion where the control sequence is shown with dashed line. θ denotes the phase of each RF pulse.

ΔB0 and ΔG can be estimated from a field map collected within the tagging plane, using a first order linear fit. As can be seen in Eq. 2.2, ΔG induces an unwanted velocity-dependent phase in the magnetization vector during the interval between RF pulses that can degrade the adiabatic inversion. Off-resonance (ΔB_0) produces a position-dependent phase error in the magnetization vector that can further degrade the inversion.

We propose to compensate for ΔG by updating the area of the refocusing lobe of the slice select gradient (see Figure 2.1) by ΔA_{extra}, such that

$$\Delta A_{extra} = -\Delta G\, \delta \tag{2.3}$$

This change will restore the change in average gradient (G_{av}) and consequently the frequency sweep. It also rewinds the velocity dependent portion of the $\Delta\varphi_{error}$ (Eq. 2.2)

without the need for making any assumption about the flow velocity. Note that the linear phase initially added to compensate for the position dependent phase accumulation term (Eq. 2.1), needs to be updated accordingly as well. The remainder of $\Delta\varphi_{error}$, caused by off-resonance effects (ΔB_0), will then be compensated by adding a linear phase, φ_{linear} , to the RF pulses (Figure 2.1). φ_{linear} can be calculated by

$$\phi_{linear} = \gamma \, \Delta B_0 \, \delta \tag{2.4}$$

Applying these changes to the pulse sequence provides us with the proper frequency sweep and phase accumulation between two RF pulses, needed for achieving high inversion efficiency.

2.4. Methods

2.4.1. Simulation

We simulated the behavior of the net magnetization vector of an ensemble of moving spins in the presence of a pseudo-continuous inversion pulse sequence using a numerical implementation of the Bloch equation. The step size in the simulations was one microsecond and the behavior of spins was simulated over a 500ms window (250ms before and 250ms after passing the tagging plane) using 500000 data points. The spins were moving along the Z direction, perpendicular to the tagging. At the static magnetic field strength of 3T, T1 and T2 were 1664 ms and 250 ms, respectively [18, 19]. It consisted of a 500 ms train of Hanning-window shaped radio frequency (RF) pulses (500 us width), with 1500 us between pulses, during a slice-select gradient (0.6 G/cm) and followed by a re-focusing gradient. We unbalanced the area of the refocusing gradient by

a variable amount to achieve a net average gradient (G_{av}). In the control pulse sequence, we reversed the sign of every other RF pulse (dotted plot in Figure 2.1).

The ensemble of spins moved with laminar flow in a cylinder with the radius of 0.4 cm [20]. To have a more realistic simulation, we considered a distribution of peak velocities for laminar flow. We derived this peak velocity distribution from a model for carotid blood flow velocity waveform suggested in [21] with minimum and maximum velocities of 20 and 108 cm/s. We used the derived distribution shown in Figure 2.2 for weighted averaging the tagging efficiency calculated for each velocity to obtain the overall tagging efficiency.

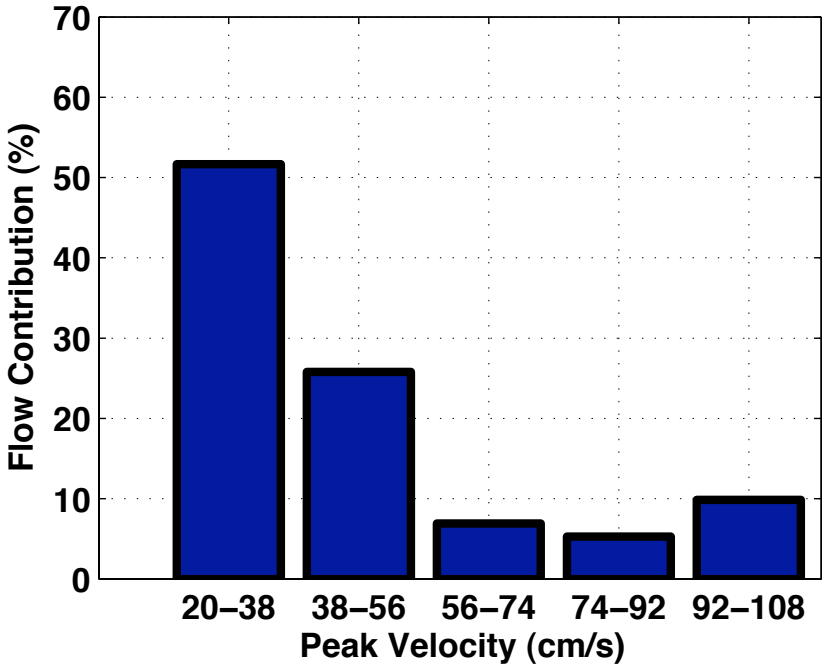

Figure 2.2. Contribution of different peak blood velocities in the blood flow transporting to the brain.

The tagging efficiency (α) for each velocity was measured at the end of the pulse train, (i.e., 250 ms after the spins crossed the tagging plane) using Eq. 2.5.

$$\alpha = \frac{\left| \vec{M}_{z\ control} - \vec{M}_{z\ tag} \right|}{2\left| \vec{M}_{z\ control} \right|} \tag{2.5}$$

We introduced an artifactual shift in resonance frequency and off-resonance gradient (ΔB_0 and ΔG) to the pulse sequence in order to simulate the field inhomogeneity effects described earlier. We corrected the effect of these errors using the proposed method by directly measuring the field inhomogeneity within the tagging plane and adjusting the RF phase and mean gradients in the pCASL pulse accordingly to compensate for the off-resonance fields. Using the simulated pCASL sequence we performed the following studies:

Study 1: Finding optimum values of G_{av} and flip angle under ideal conditions (i.e. no off-resonance or gradient distortion).

Study 2: Investigating the effect of field inhomogeneity on the inversion efficiency by adding artifactual off-resonance and off-resonance gradient to the simulation.

Study 3: Evaluating the efficiency of the proposed method in recovering the degraded inversion efficiency.

2.4.2. Phantom Study

The pCASL pulse sequence shown in Figure 2.1 was implemented on a 3.0 T Signa Excite scanner (General Electric, Waukesha, WI). The experiment was carried out using the simulation study parameters, variable G_{av} and Flip angle = 35°. The tagging/control

duration was 900 ms. Image acquisition was performed right after the tagging/control pulses using a gradient-echo spiral imaging sequence (TR= 1000 ms, TE = 3 ms, flip angle = 90°, number of slices = 1, sl. thickness = 7 mm, FOV = 24 cm, 48 frames). We did not use any flow compensated sequence. We also estimated a magnetic field inhomogeneity map from two sagittal images acquired with a TE difference of 1 ms [22].

We imaged a flow phantom consisted of a polyurethane tube carrying tap water, which was recirculated with a Master-Flex LS peristaltic pump (Cole Parmer, Vernon Hills, IL) with flow velocity = 30 cm/s, using the described pCASL sequence. We located the tagging plane 3 cm below the imaging plane in the phantom. We measured the tagging efficiency within the tube of flow phantom using Eq. 2.5. We measured the tagging efficiency for different values of average gradient and linear phase. We measured the tagging efficiency as a function of linear phase correction to the RF pulses (φlinear) at several levels of average gradient (G_{av}). The optimum parameters were compared to those predicted by the proposed technique using the off-resonance and off-resonance gradients estimated from the magnetic field inhomogeneity map. We derived the off-resonance values within the tube located inside the tagging plane (~2cm thick). We estimated the shift in the resonance frequency and off-resonance gradient by fitting a line to the derived off-resonance values using least square error fitting technique.

2.4.3. In-vivo Experiments

5 subjects were scanned using a 3.0 T Signa Excite scanner (General Electric, Waukesha, WI) in accordance to the University of Michigan's IRB regulations. The experiment was carried out using the optimum set of pCASL pulse sequence parameters found in our simulation study (G_{av} = 0.039 (G/cm), flip angle = 35°). G_{av} and φ_{linear} were then modified according to the proposed method (Eq 2.3 and 2.4).

Tagging/Control was applied for 1800 ms followed by a post-inversion delay of 1700 ms before image acquisition. Tagged and control images were collected alternately during 16 image acquisitions. The tagging plane was located at the carotid arteries (approximately 6

cm below the circle of Willis. Images were collected using a gradient echo spiral imaging sequence (TR= 4000 ms, TE = 3 ms, number of slices = 9, sl. thickness = 7 mm, FOV = 24 cm). We did not use any flow compensated sequence.

We calculated a coronal magnetic field map of the tagging region for each subject prior to the ASL study, from two images acquired with a TE difference of 1 ms [22]. Using the obtained coronal field inhomogeneity maps, we estimated off-resonance and off-resonance gradient for each subject by fitting a line to the off-resonance values within each artery. We manually defined the location of arteries on the field inhomogeneity map using the associated anatomical images. For each artery, we derived the off-resonance values within the artery located inside the tagging plane (~2cm thick). We estimated the shift in the resonance frequency and off-resonance gradient by fitting a line to the derived off-resonance values using least square error fitting technique. Finally we averaged the estimated values together. We performed standard shimming on the whole brain including the tagging and the imaging plane in the beginning of each study and kept the shimming values the same for all scans including field map estimation.

For each subject we performed two ASL studies: 1) Using the initial parameters obtained from the simulation study 2) Using the modified parameters suggested by the proposed method.

To evaluate the efficiency of the proposed method, for each subject, we estimated the signal to noise ratio (SNR) and tagging efficiency (Eq. 2.5) before and after correction. We acquired a high-resolution (256x256) T1-weighted anatomical image using the same prescription used for ASL studies. We created a grey matter mask by segmentation of the T1-weighted image after co-registration to the perfusion images. Using the grey matter mask, we calculated SNR as the mean gray matter signal change over the time course divided by its temporal standard deviation.

To check if the proposed method was successful in providing the optimum tagging efficiency for each subject, we measured the tagging efficiency in the carotid arteries, by tagging at ~ 6 cm below the circle of willis and imaging one axial slice at ~3 cm below the circle of willis (TR = 500ms, tagging/control time = 400ms, no post inversion delay,

16-shot spiral image acquisition with 128 x 128 matrix, FOV = 20). We measured the tagging efficiency for different φ_{linear} values between 0 and -π (tagging efficiency curve) for the average gradient suggested by the proposed method and the one proposed by simulation study (Eq. 2.3).

2.5. Results

2.5.1. Simulation Study Results

Figure 2.3 shows the simulated tagging efficiency for a range of flip angles and average slice select gradients under ideal conditions (homogeneous magnetic field). There is a broad region of G_{av} and flip angle that can provide high (i.e. > 80%) tagging efficiency. We chose the parameters highlighted with a green dot (G_{av} = 0.039 (G/cm), flip angle = 35°) as the starting working point for subsequent studies. The tagging efficiency achieved at this point was 87%. The phase accumulation between RF pulses is a function of G_{av} and blood velocity (Eq. 2.1). Therefore, employing higher G_{av} does not necessarily lead to higher inversion efficiency.

Figure 2.4.a shows the tagging efficiency achieved using the optimal parameters obtained above, but in the presence of different amounts of off-resonance and off-resonance gradient. The negative tagging efficiencies in Figure 2.4.a. represent the situations in which the order of tagging and control effectively changed due to shifts greater than π in the phase of RF pulses. We then applied the proposed correction method to recover the compromised tagging efficiencies at each point. Figure 2.4.b shows the obtained tagging efficiencies after correction. As an example, the M_z profile of a spin passing the pCASL tagging plane at three different situations is shown in Figure 2.5: a) ideal case without any field inhomogeneity b) with field inhomogeneity (ΔG = -0.01 G/cm and off-resonance = -125 Hz) before correction and c) with field inhomogeneity after correction.

Note the shift in the tagging plane from its original place due to off-resonance (blue curve compared to the black one). As can be seen, the proposed correction method successfully restored the compromised inversion efficiencies for all amounts of off-resonance and off-resonance gradients.

2.5.2. Phantom Study Results

We measured the tagging efficiency curve for different amounts of G_{av} in a flow phantom consisting of a tube with known velocity (30 cm/s). These curves are shown in Figure 2.6. The black arrow in Figure 2.6 points to the starting working point suggested by simulation study in the ideal situation (i.e. no field inhomogeneity) and the green arrow points to the modified working point suggested by the proposed method using the field inhomogeneity map information (off-resonance = 55 Hz and ΔG = -0.01 G/cm at the tagging plane). As can be seen modifying G_{av} and adding the linear phase (φ_{linear}) according to the proposed method improved the tagging efficiency by ~40%.

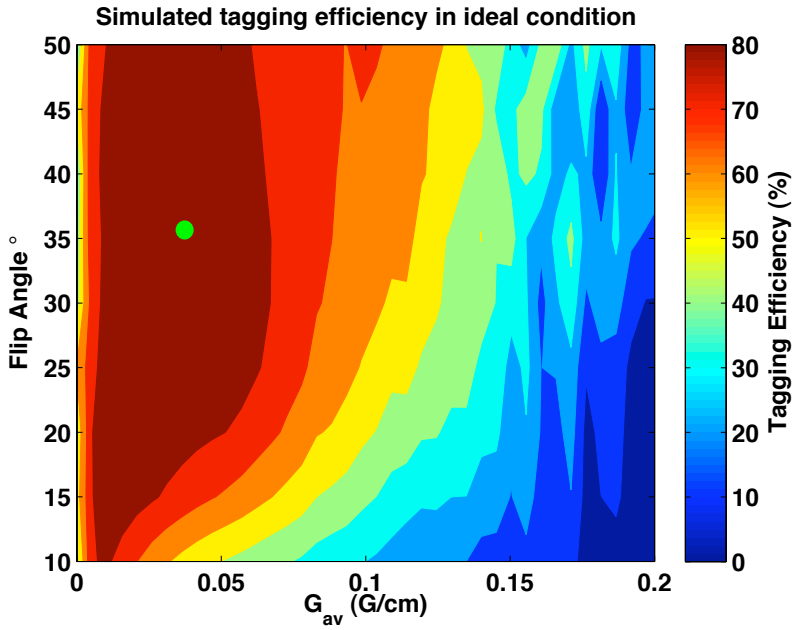

Figure 2.3. Simulated tagging efficiency in the ideal case for different values of Flip angle and Average gradient. The working point chosen for the use in later studies is highlighted with a green dot.

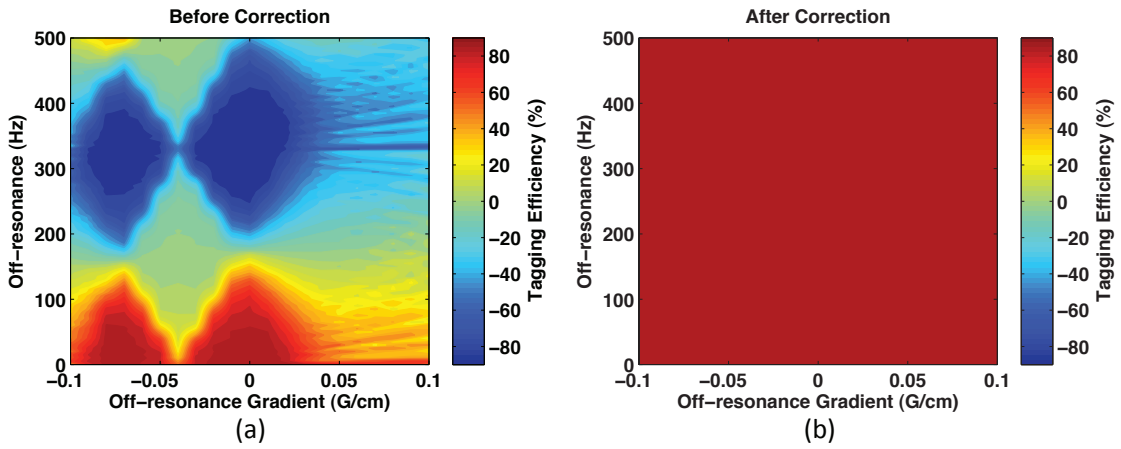

Figure 2.4. Simulation study results: tagging efficiencies measured for different amounts of off-resonance and off-resonance gradient; **(a)** before correction **(b)** after correction using the proposed method. The negative tagging efficiencies represent the situations in which the order of tagging and control changed due to RF pulse phase shifts greater than π.

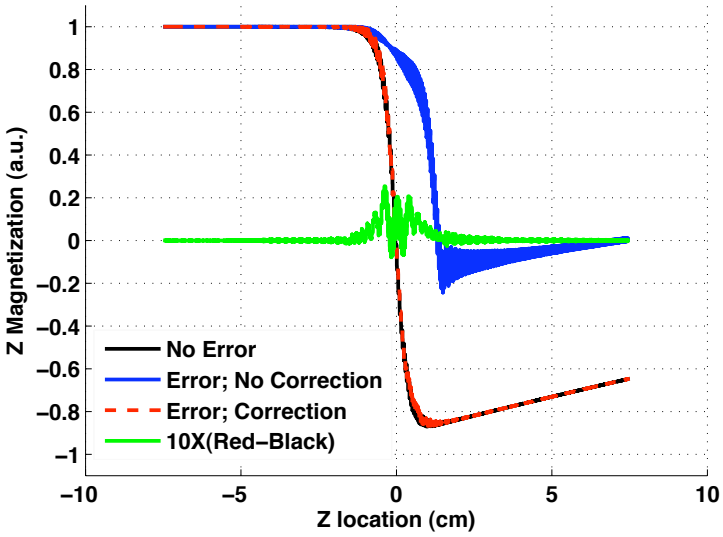

Figure 2.5. Simulated profile of the magnetization vector of a spin in Z direction (Mz) passing the pCASL tagging plane located at Z=0 cm: No field inhomogeneity (Black), with field inhomogeneity (ΔG = -0.01 G/cm and off-resonance = -125 Hz) before correction (Blue) and with field inhomogeneity after correction (Red) (Note overlap between Red/Black). The magnified difference (X10) between red and black lines is also shown (Green).

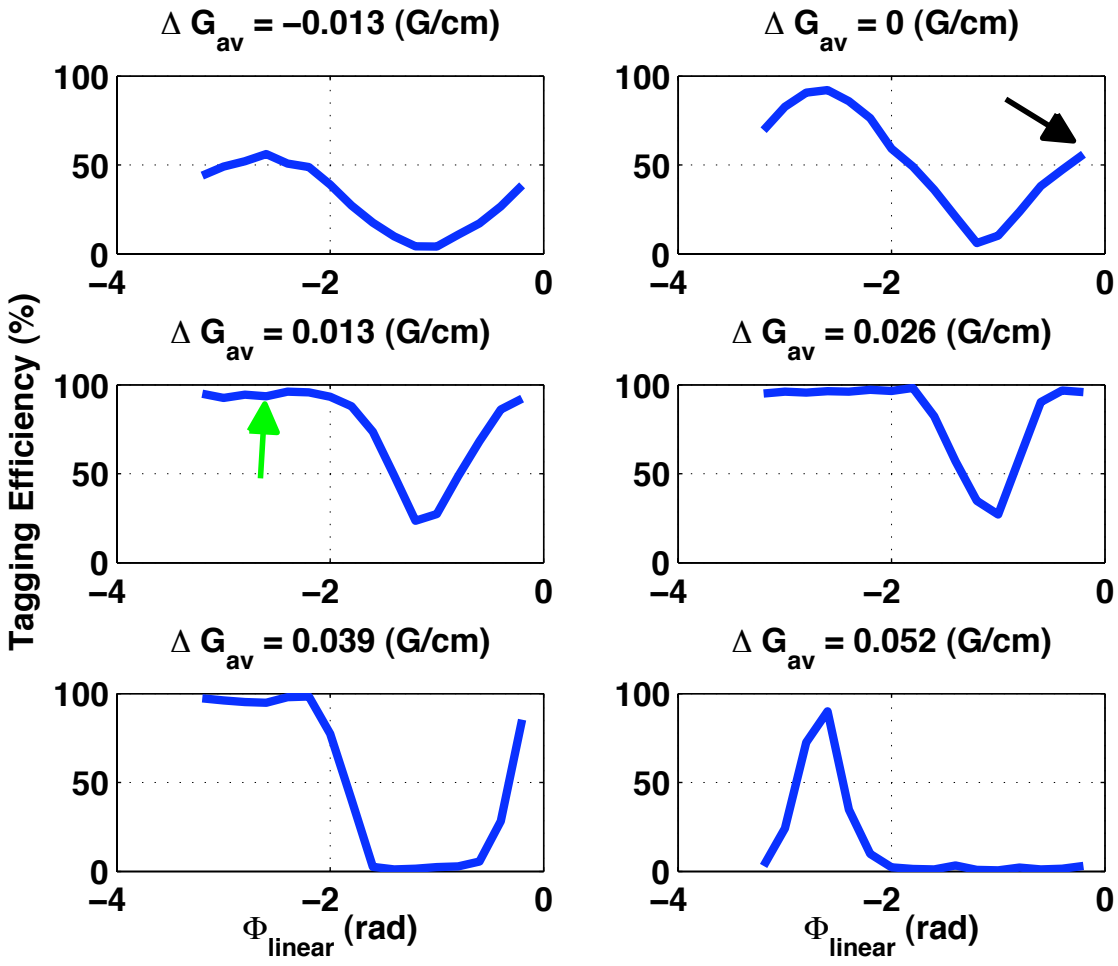

Figure 2.6. The tagging efficiency curve measured in a flow phantom for different average gradients. The working points suggested by simulation under ideal conditions (homogeneous magnetic field) and by the proposed method (using field inhomogeneity map information) are shown with black and green arrows respectively.

2.5.3. In-vivo Results

For each subject, the signal-to-noise-ratio and tagging efficiency were measured before and after the correction using the proposed method. The measured SNRs and tagging efficiencies along with the corresponding estimated off-resonance and off-resonance gradient are presented in Table 2.1 and Table 2.2. As can be seen, the proposed method considerably improved the SNR and tagging efficiency in subjects (1,2 and 3). The field

inhomogeneity map estimated for subject #1 which had shown the biggest improvement, is shown in Figure 2.7. Perfusion difference images for this subject before and after correction using the proposed method are presented in Figures 2.8.a and b. The tagging efficiency curves of this subject measured are also shown in Figures 2.8.c and d. The black arrow points to the working point suggested by our simulation study in the ideal situation (no field inhomogeneity) and used for acquisition of perfusion images in Figure 2.8.a. The green arrow points to the working point suggested by the proposed method and used for acquisition of perfusion image in Figure 2.8.b. As can be seen the proposed method successfully recovered the degraded tagging efficiency.

The variations observed in the tagging efficiency of different arteries/subjects before correction using the proposed method, are due to different off-resonance and off-resonance gradients at the tagging plane. Graphical representations of the measured tagging efficiencies and SNRs, before and after correction are also shown in Figure 2.9.

Table 2.1. In vivo measurements of the tagging efficiency and the SNR of the subtraction images before and after the proposed correction.

Subject #	**1**	**2**	**3**	**4**	**5**
Tagging Efficiency before Correction	17%	62%	38%	79%	78%
Tagging Efficiency after Correction	73%	80%	77.5%	75%	77%
SNR before Correction	0.18	4.26	2.88	5.98	4.80
SNR after Correction	11.45	7.84	7.12	5.54	4.90

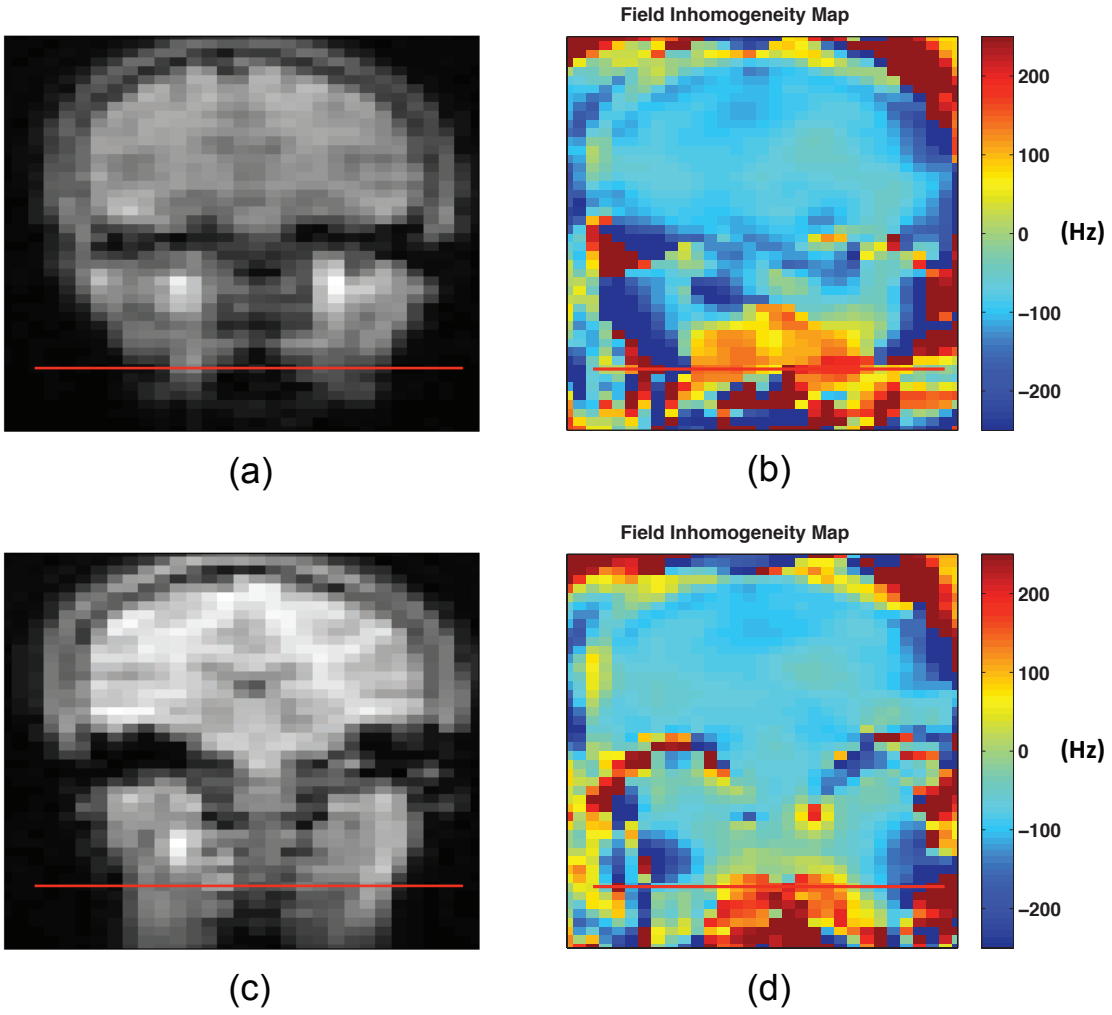

Figure 2.7. Estimated field inhomogeneity map for subject #1. The location of tagging plane is shown with the red line in the pictures. **(a,b)** The anatomical image and corresponding field inhomogeneity map at the level of carotid arteries **(c,d)** The anatomical image and corresponding field inhomogeneity map at the level of vertebral arteries.

2.6. Discussion

The method proposed in this chapter is intended to compensate for inhomogeneity of magnetic field in the tagging region by using phase corrected RF pulses. In a sense, it can be considered as an RF shimming method for pCASL. In a situation where there is a

Table 2.2. In vivo measurements of magnetic field off-resonance and off-resonance gradient at the tagging plane for different arteries. In this table, LC, RC, LV and RV represent left carotid artery, right carotid artery, left vertebral artery and right vertebral artery respectively.

Subject #		**1**	**2**	**3**	**4**	**5**
Off-resonance (Hz)	**LC**	79	-120	-167	53	-88
	RC	89	-117	-166	50	-78
	LV	115	-173	-189	60	-113
	RV	160	-168	-190	55	-120
	mean	111	-144	-178	54	-100
Off-resonance Gradient (G/cm)	**LC**	-0.021	-0.005	0.003	0.001	0.013
	RC	-0.020	0.006	0.003	0.001	0.009
	LV	-0.004	-0.003	0.004	-0.001	0.006
	RV	-0.010	0.005	0.003	-0.001	0.017
	mean	-0.014	0.001	0.003	0.000	0.011

procedure that can provide ideal shimming in both the imaging and the tagging locations, the proposed correction method will not be necessary. Our experience, however, is quite the opposite. We used standard and high order shimming procedures on the whole brain including the tagging and the imaging planes, but our efforts were not successful and in some cases higher order shimming even led to further distortion of the field at the tagging or the imaging planes. Thus, in cases where shimming is insufficient, as is the case at

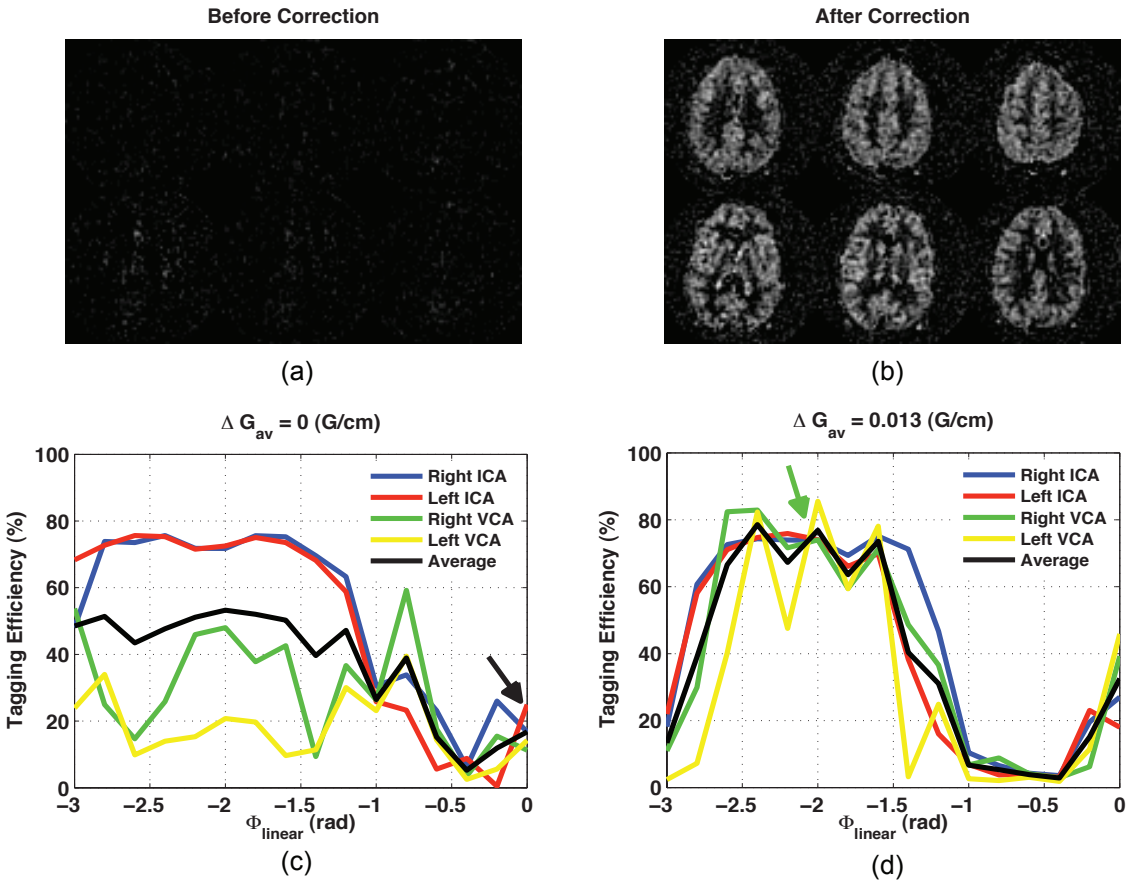

Figure 2.8. Perfusion difference images for subject #1 acquired **(a)** before and **(b)** after correction with the proposed method. Tagging efficiency curve measured in the left and right carotid arteries (CA) and vertebral arteries (VA) **(c)** before and **(d)** after correction for the same subject. The black and green arrows point to the working point suggested by the simulation study and the proposed method respectively.

higher field (≥ 7T), this straightforward phase correction technique can provide the necessary tagging efficiency.

Besides modulating the average gradient and phase accumulation between RF pulses, there is another mechanism involved in degradation of tagging efficiency as a result of a shift in the resonance frequency. Off-resonance shifts the spatial location of tagging plane. It also shifts the frequency sweep profile. However, since G_{av} is much smaller than G_{max}, (0.039 G/cm vs 0.6 G/cm in this study) a shift in resonance frequency shifts the tagging slab slightly, but it shifts the frequency sweep by a lot more (See Figure 2.5 and

note the shift in the blue curve compared to the black one). The mismatch between RF pulse profile and the frequency sweep profile can lead to further degradation of tagging efficiency. By applying the proposed corrections, besides correcting the frequency sweep and phase accumulation, we also shift the frequency sweep back to the intended location.

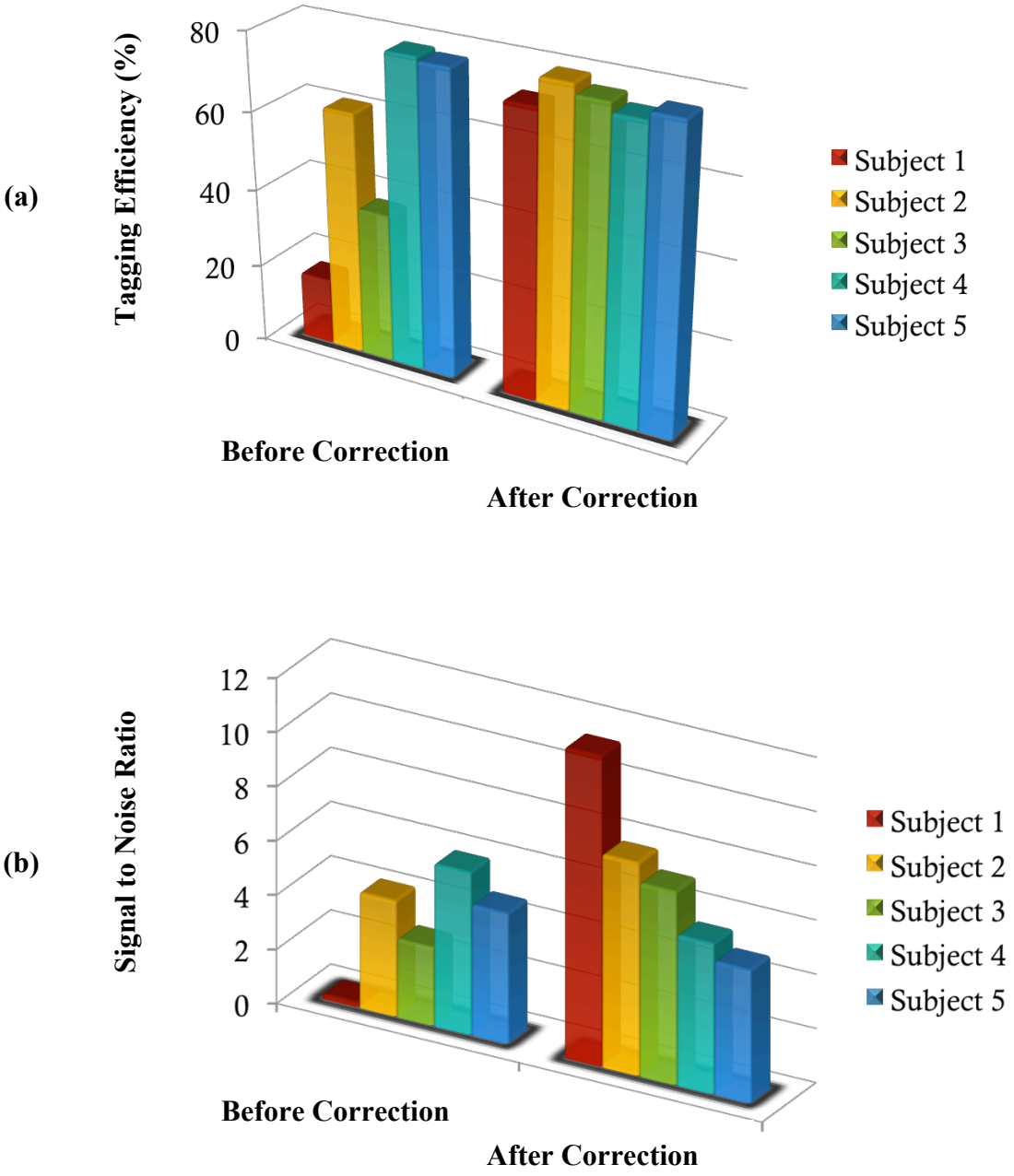

Figure 2.9. Measured tagging efficiencies **(a)** and signal to noise ratios **(b)** before and after correction using the proposed method.

An orientation offset between an artery and the applied gradient direction will change the effective velocity of the blood spins along the gradient direction, which can change the phase accumulation of spins between RF pulses depending on the angle between artery and gradient direction. In addition the presence of a through plane gradients in this situation will further modulate the phase accumulation and can degrade the tagging efficiency. Therefore in practice it is better to place the tagging plane in an area in which the arteries are align with the applied gradient direction as much as possible.

Since it is not possible to find the optimum parameters in the ideal situation (i.e. no field inhomogeneity) using experimental data, we used numerical simulation of the Bloch equation to find the starting working point. In order to make our simulations as realistic as possible, we considered a laminar blood flow with a distribution of velocities derived from the measured mean blood flow waveform suggested in [21] instead of assuming plug flow, as in previous studies [10]. In pulsatile blood flow of arteries, there is also an acceleration pattern, which can further change the amount of phase accumulation between RF pulses. But given the fact that blood velocity is fairly high in the arteries and the tagging plane is relatively narrow (~2cm), we only considered the distribution of blood velocity in the pulsatile flow of arteries and neglected the effect of acceleration of blood within the tagging plane. The simulated ranges of off-resonance and off-resonance gradient are wider that what we observed in our results (Table 2.2) because we did not intentionally put our tagging plane on areas with high off-resonance and gradient errors. But on a given field inhomogeneity map it is possible to find areas with off-resonance and off-resonance gradient as high as those in our simulated study.

Upon inspection of the tagging efficiency curves of our phantom study (Figure 2.6), it is apparent that it is possible to achieve a high tagging efficiency only by adding a proper linear phase alone for a wide range of average gradients. In that case, Eq. 2.2 should be used for estimating the proper linear phase instead of Eq. 2.4, which requires knowledge (or an assumption) about the blood velocity. In addition, the blood flow velocity at the carotids is higher than the flow velocity of our flow phantom (30 cm/s) and, as a result, we expect the correction to be more sensitive to the choice of G_{av} in human studies. In addition, as can be seen in Figure 2.4.a, having a proper average gradient makes the

pCASL pulse sequence less sensitive to the selection of linear phase (i.e. more robustness to the errors in estimation of the proper linear phase).

In our subjects, the mean off-resonance and off-resonance gradient values worked fine for all of the arteries. However, this might not be the case in all subjects. If the off-resonance values at arteries are so different then, it might not be possible to find a correction values that works for all of them. It that case, the difference of off-resonance between arteries can be eliminated by adding a small in-plane gradients similar to what is proposed in [23].

We note that, without this correction applied to the data set presented in this chapter, two of the subjects (out of five) would have still yielded accurate perfusion maps with reasonable SNR. However, in 2 of them, we would have faced with considerably lower tagging efficiencies and SNR maps. In these cases, the quantification of perfusion maps, without the measurements of tagging efficiencies would have resulted in significant errors. For one of the subjects, the perfusion measurement was simply not possible without the proposed correction method.

2.7. Conclusion

This study shows that, even if the pCASL sequence has been theoretically optimized, the tagging efficiency of pCASL can be compromised by local shifts in the magnetic field, and thus, the resonance frequency, at the tagging plane. Loss in tagging efficiency leads to lower signal to noise perfusion maps and also can cause considerable quantification errors if unaccounted.

Our preliminary results showed that estimating these field inhomogeneities using B0 field map information and compensating for them using the proposed method can effectively recover the compromised tagging efficiency. This may allow the use of pCASL in a wider range of conditions (clinical or research) including high field scanning, where it may have otherwise been impractical.

2.8. References

[1] C. Huang, L. O. Wahlund, O. Almkvist, D. Elehu, L. Svensson, T. Jonsson, B. Winblad, and P. Julin, "Voxel- and VOI-based analysis of SPECT CBF in relation to clinical and psychological heterogeneity of mild cognitive impairment," *Neuroimage,* vol. 19, no. 3, pp. 1137-44, Jul, 2003.

[2] T. D. Farr, and S. Wegener, "Use of magnetic resonance imaging to predict outcome after stroke: a review of experimental and clinical evidence," *J Cereb Blood Flow Metab,* vol. 30, no. 4, pp. 703-17, Apr, 2010.

[3] D. C. Alsop, J. A. Detre, and M. Grossman, "Assessment of cerebral blood flow in Alzheimer's disease by spin-labeled magnetic resonance imaging," *Ann Neurol,* vol. 47, no. 1, pp. 93-100, Jan, 2000.

[4] D. Williams, J. Detre, J. Leigh, and A. Koretsky, "Magnetic resonance imaging of perfusion using spin inversion of arterial water.," *Proc Natl Acad Sci U S A,* vol. 89, no. 1, pp. 212-6, Jan 1, 1992.

[5] S. Kim, "Quantification of relative cerebral blood flow change by flow-sensitive alternating inversion recovery (FAIR) technique: application to functional mapping.," *Magn Reson Med,* vol. 34, no. 3, pp. 293-301, Sep, 1995.

[6] L. Hernandez-Garcia, G. R. Lee, A. L. Vazquez, and D. C. Noll, "Fast, pseudo-continuous arterial spin labeling for functional imaging using a two-coil system," *Magnetic Resonance in Medicine,* vol. 51, no. 3, pp. 577-585, 2004.

[7] T. Liu, E. Wong, L. Frank, and R. Buxton, "Analysis and design of perfusion-based event-related fMRI experiments.," *Neuroimage,* vol. 16, no. 1, pp. 269-82, May, 2002.

[8] D. C. Alsop, and J. A. Detre, "Multisection cerebral blood flow MR imaging with continuous arterial spin labeling," *Radiology,* vol. 208, no. 2, pp. 410-6, Aug, 1998.

[9] E. Wong, R. Buxton, and L. Frank, "A theoretical and experimental comparison of continuous and pulsed arterial spin labeling techniques for quantitative perfusion imaging.," *Magn Reson Med,* vol. 40, no. 3, pp. 348-55, Sep, 1998.

[10] W. C. Wu, M. Fernandez-Seara, J. A. Detre, F. W. Wehrli, and J. Wang, "A theoretical and experimental investigation of the tagging efficiency of pseudocontinuous arterial spin labeling," *Magn Reson Med,* vol. 58, no. 5, pp. 1020-7, Nov, 2007.

[11] W. Dai, D. Garcia, C. de Bazelaire, and D. C. Alsop, "Continuous flow-driven inversion for arterial spin labeling using pulsed radio frequency and gradient fields," *Magn Reson Med,* vol. 60, no. 6, pp. 1488-97, Dec, 2008.

[12] D. D. Shin, T. T. Liu, E. C. Wong, A. Shankaranarayanan, and Y. Jung, "Pseudocontinuous arterial spin labeling with optimized tagging efficiency," *Magn Reson Med*, Jan 3, 2012.

[13] Y. Jung, E. C. Wong, and T. T. Liu, "Multiphase pseudocontinuous arterial spin labeling (MP-PCASL) for robust quantification of cerebral blood flow," *Magn Reson Med,* vol. 64, no. 3, pp. 799-810, Sep, 2010.

[14] E. Ghariq, W. M. Teeuwisse, A. G. Webb, and M. J. van Osch, "Feasibility of pseudocontinuous arterial spin labeling at 7 T with whole-brain coverage," *MAGMA,* vol. 25, no. 2, pp. 83-93, Apr, 2012.

[15] W. M. Luh, S. L. Talagala, T. Q. Li, and P. A. Bandettini, "Pseudo-continuous arterial spin labeling at 7 T for human brain: Estimation and correction for off-resonance effects using a Prescan," *Magn Reson Med*, Apr 9, 2012.

[16] G. Duhamel, V. Callot, M. Tachrount, D. C. Alsop, and P. J. Cozzone, "Pseudo-continuous arterial spin labeling at very high magnetic field (11.75 T) for high-resolution mouse brain perfusion imaging," *Magn Reson Med,* vol. 67, no. 5, pp. 1225-36, May, 2012.

[17] W. T. Dixon, L. N. Du, D. D. Faul, M. Gado, and S. Rossnick, "Projection angiograms of blood labeled by adiabatic fast passage," *Magn Reson Med,* vol. 3, no. 3, pp. 454-62, Jun, 1986.

[18] H. Lu, C. Clingman, X. Golay, and P. van Zijl, "Determining the longitudinal relaxation time (T1) of blood at 3.0 Tesla.," *Magn Reson Med,* vol. 52, no. 3, pp. 679-82, Sep, 2004.

[19] G. A. Wright, B. S. Hu, and A. Macovski, "1991 I.I. Rabi Award. Estimating oxygen saturation of blood in vivo with MR imaging at 1.5 T," *J Magn Reson Imaging,* vol. 1, no. 3, pp. 275-83, May-Jun, 1991.

[20] J. O. Arndt, J. Klauske, and F. Mersch, "The diameter of the intact carotid artery in man and its change with pulse pressure," *Pflugers Arch Gesamte Physiol Menschen Tiere,* vol. 301, no. 3, pp. 230-40, 1968.

[21] D. W. Holdsworth, C. J. Norley, R. Frayne, D. A. Steinman, and B. K. Rutt, "Characterization of common carotid artery blood-flow waveforms in normal human subjects," *Physiol Meas,* vol. 20, no. 3, pp. 219-40, Aug, 1999.

[22] C. Y. Yip, J. A. Fessler, and D. C. Noll, "Advanced three-dimensional tailored RF pulse for signal recovery in T2*-weighted functional magnetic resonance imaging," *Magn Reson Med,* vol. 56, no. 5, pp. 1050-9, Nov, 2006.

[23] E. C. Wong, "Vessel-encoded arterial spin-labeling using pseudocontinuous tagging," *Magn Reson Med,* vol. 58, no. 6, pp. 1086-91, Dec, 2007.

Chapter 3

Two applications of the optimized pseudo-continuous ASL pulse sequence: "*real-time functional ASL*" and "*Reduced specific absorption rate pseudo-continuous ASL*"

3.1. Abstract

Optimized tagging efficiency of the pseudo-continuous ASL (pCASL), after correction using the method presented in the previous chapter, provides an optimized signal to noise ratio that makes it possible to extend the applications of pCASL. In this chapter two of the applications of the optimized pCASL are presented: "*real-time functional ASL"* and "*reduced specific absorption rate (SAR) pCASL"*.

The first implementation of real-time acquisition and analysis of Arterial Spin Labeling (ASL) based functional MRI time series is presented in this chapter. The implementation uses the optimized pseudo-continuous labeling scheme followed by a spiral k-space acquisition trajectory. Real-time reconstruction of the images, preprocessing and regression analysis of the fMRI data were implemented on a laptop computer interfaced with the MRI scanner. The method allowed the user to track the current raw data, subtraction images, and the cumulative t-statistic map overlaid on a cumulative subtraction image. The user was also able to track the time course of individual time courses, and interactively select an ROI as a nuisance covariate. The pulse sequence allows the user to adjust acquisition and labeling parameters while observing their effect on the image within a single pair of TRs. This method is illustrated on a stimulation paradigm consisting of simultaneous finger-tapping and visual stimulation and on a bimanual finger tapping task alternating hands.

One of the challenges facing the application of pCASL at higher field (7T and higher) scanners is

the high specific absorption rate of pCASL sequence. Reducing the flip angle of pCASL radio frequency (RF) pulses reduces the SAR level but at the same time compromises the tagging efficiency and SNR of the technique. A reduced specific absorption rate (SAR) version of pCASL pulse sequence is designed using the improved tagging efficiency of the optimized pCASL technique discussed in chapter 2. Using simulation and in-vivo studies, a set of pCASL pulse sequence parameters is found that allows reducing the flip angle of pCASL RF pulses without losing the tagging efficiency.

3.2. Real-time functional ASL

Conventional functional magnetic resonance imaging (fMRI) collects BOLD-sensitive MR images of a subject's brain while performing a cognitive task, whereas subsequent image reconstruction and analysis are performed offline. Real-time functional magnetic resonance imaging (rtfMRI) is an exciting extension to conventional fMRI techniques that enables the user to analyze fMRI data as it is being collected. Thus, in rtfMRI the results are immediately available as the subject is being scanned, and can be used to reveal and guide the subject's cognitive processes. It can also facilitate the experimenter's parameter selections or a clinician's interventions [1].

Several real-time analysis methods have been implemented for online processing of BOLD data, including cumulative correlation [2], sliding-window correlations with reference vector optimization [3], online general linear model (GLM) analysis [4], and combined methods to collect behavioral, physiological and MRI data while performing near real-time statistical analysis [5]. All the above methods can facilitate real-time analysis, e.g. the incremental algorithms are useful in monitoring ongoing activation, and the sliding window approaches can improve localization of dynamic activity in time [4]. Given current computer processing speed, any of these approaches can be used to display real-time activation maps. This allows for several real-time applications: online data quality control, real-time functional activation monitoring, interactive paradigms based on the subject's dynamic functional activity (fMRI biofeedback or brain-computer interface [6], and autonomous control of neural activation using real-time fMRI. These techniques have been used to study subjects' modulation of motor-area cortical activation

[7-11].

However, despite the efficiency of BOLD-sensitive MR images to detect and localize active site in fMRI, the BOLD signal is difficult to quantify in a physically meaningful way because it results from intricate relationships between cerebral oxygenation, blood flow and volume, as well as the scanner's unique characteristics. Due to very limited processing time available in rtfMRI applications, quantifying the BOLD signal in real-time poses substantial challenges. Furthermore, the baseline of the BOLD signal drifts over time within a session and this could be quite problematic in experiments where the periodicity of the paradigm is quite long. Lack of meaningful physical units in BOLD data, in addition to these drifts, challenges the use of BOLD imaging for studies of baseline activity and confounds long-term activation studies considerably [12].

Given the quantitative nature of its signal and its insensitivity to scanner signal drifts, perfusion based functional MRI using arterial spin labeling (ASL) techniques have emerged as an alternative to BOLD fMRI. ASL techniques [13-15] employ magnetically labeled arterial water as an endogenous tracer to quantify the perfusion rate. This type of measurement is particularly desirable for longitudinal studies and studies with low stimulation frequency, where the BOLD signal drifts are confounded with the signal of interest [16-18].

In this chapter, the first implementation of real-time, ASL-based, functional MRI is introduced. We will report on the technical feasibility of acquiring perfusion based functional images using ASL in real-time, and the necessary software interfaces and analysis methods for image acquisition and process. Our implementation uses an optimized pseudo-continuous labeling scheme [19] followed by a spiral k-space acquisition trajectory. It allows interactive adjustment of parameters, data smoothing, differencing, statistical analysis and display during acquisition of individual ASL images. It also enables the user to track the time course of individual voxels, and select an ROI as a nuisance covariate interactively. The interface is implemented on a laptop computer interfaced with the MRI scanner.

We demonstrate our implementation of real-time ASL, on a simple visual-motor activation experiment, and a bimanual finger opposition task, although the long-term application motivating this work is fMRI-guided biofeedback to train nicotine-dependent subjects to control

their cigarette craving.

3.2.1. Implementation of Real-time functional ASL

This work was performed on a 3.0T GE Signa scanner (Waukesha, WI) interfaced with an Apple MacBook (Cupertino, CA) with a 2.4 GHz dual core processor and 4GB of RAM. The acquisition pulse sequence was a pCASL sequence [20] with (a) phase corrections (discussed in the previous chapter) [19] for optimization of labeling efficiency and (b) real-time communication support (c) spiral image acquisition (FOV = 24 cm, slice thickness = 6 mm, data matrix = 64 x 64 x 8 slices). Each slice generated 4712 complex data points of raw k-space data. The pCASL pulse train had the following parameters: TR=4000 ms, tagging time=2100 ms, post inversion delay=1500 ms, pCASL flip angle=35, fractional moment=0.9, pCASL TR=1.5 ms, pCASL phase correction=2.2 radians).

A diagram of the data flow is shown in Figure 3.1. Data transfer between the scanner and the MacBook was done through Ethernet using custom C functions modified from the RDS Client software (General Electric Medical Systems, Waukesha, WI). Data were transferred directly from the scanner's data acquisition board to the laptop's memory via TCP/IP connection, without disk storage. Reconstruction, processing and display were performed off-line by the MacBook using custom Matlab Software (South Nattick, MA). Transfer and reconstruction were performed after each slice acquisition. To reduce memory requirements, the reconstructed images were analyzed as single precision floating point numbers instead of Matlab's default double precision. Data were spatially smoothed with a Gaussian kernel, and running subtraction was performed on the images to yield perfusion-weighted images. A reference function reflecting the effects of interest (i.e., the perfusion response to the stimulation paradigm) was constructed prior to the experiment. This function was used to create a design matrix for GLM analysis that also included a nuisance regressor, which was updated during the data acquisition, and a baseline regressor. As the nth image was acquired, a temporary design matrix was updated from the first n rows of the whole design matrix. The parameters of this temporary GLM were estimated by ordinary least squares and a t-statistic map was computed for the contrast of interest. T-maps were overlaid on the mean perfusion-weighted image and thresholded at a liberal $|t| > 3.0$.

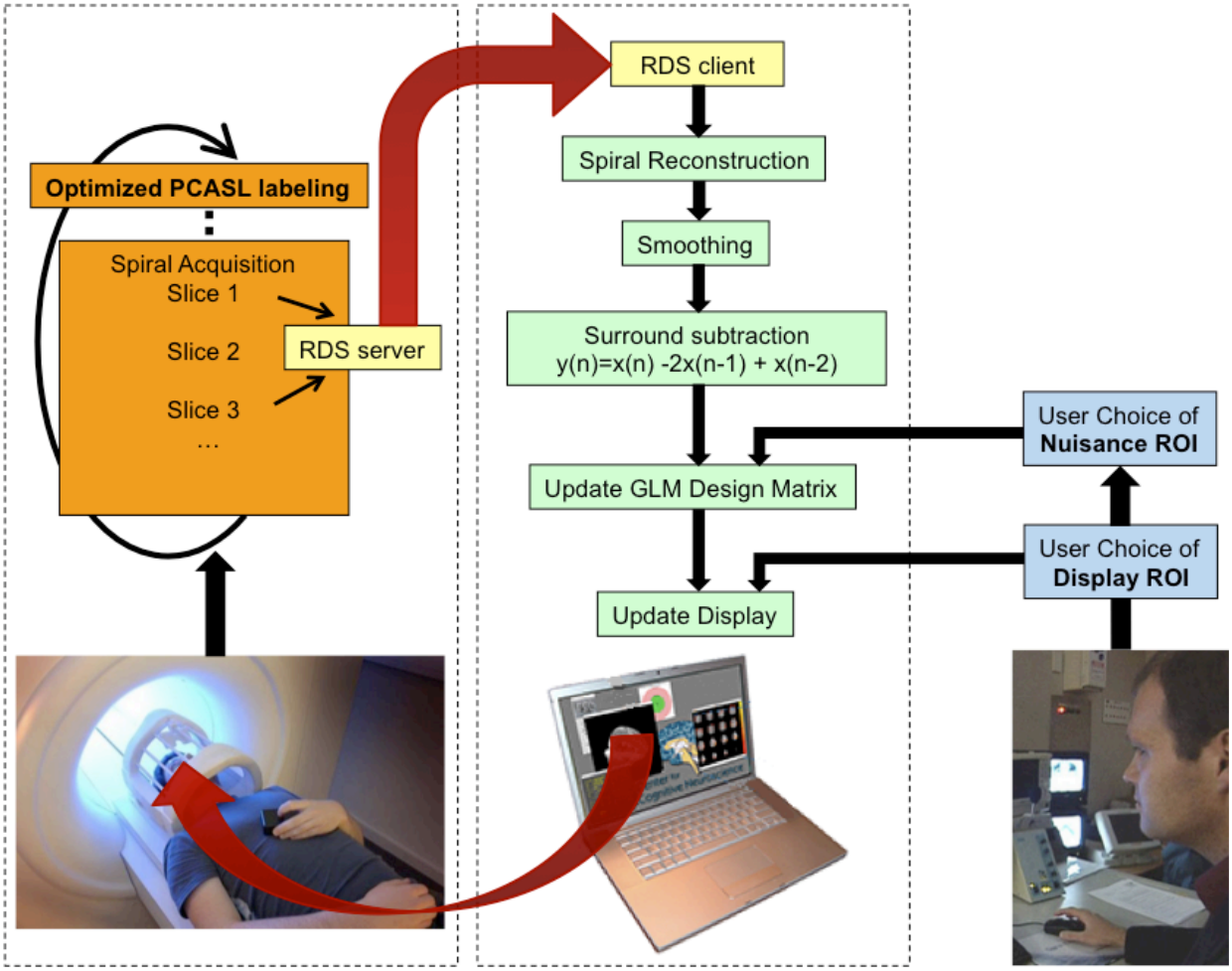

Figure 3.1. Real-time processing stream for ASL fMRI experiment. Data were transferred directly from the scanner's data acquisition board to laptop memory without disk storage. Reconstruction, processing and display were performed off-line by the MacBook using custom Matlab software. Transfer and reconstruction were performed after each slice acquisition. The user interacts with the system by selecting the ROI for the nuisance regressor and a second ROI for time series display.

The aforementioned nuisance regressor consisted of the time course at an region of interest (ROI) selected by the user in real-time. This ROI was chosen from a while matter region to remove physiological fluctuations or other spatial correlations in ASL data.

The global mean time course, the reference function, and the time courses of the user-defined

"nuisance region" and a second ROI were displayed in real-time. This allowed the user to monitor activation in any specific brain area and to visually inspect the nuisance regressor for correlations with the reference function. The user was thus able to choose both ROIs in real-time.

For testing and demonstration purposes, two subjects were scanned in accordance with the University of Michigan's Internal Review Board's policies, as follows. A real-time pCASL time series was collected while the first subject performed a finger-tapping task consisting of 20 sec tapping with the left hand while a checkerboard pattern flashed in front of her eyes at 8 Hz. The activation period was followed by 30 sec of rest. This 50-sec cycle was repeated over a 320 sec period. The second subject was instructed to perform a finger-tapping task with the right hand for 20 sec, followed by 20 sec finger tapping with the left hand. This procedure was repeated for 320 sec. In both cases, the data were transferred, reconstructed and processed, as described above, while the user updated the nuisance ROI, and monitored the image acquisition quality and statistical map in real-time.

3.2.2. Real-time functional ASL: Results

After every acquisition, the following displays were updated: (1) current reconstructed image, (2) with the most recent perfusion weighted image, (3) the thresholded t-statistic map overlaid on the mean perfusion weighted image, (4) a time course of the spatial mean ASL signal over the field of view, a user-selected ROI, and a second ROI that serves as a nuisance regressor. The model waveform was also displayed for reference. The Matlab reconstruction, processing, and display program was able to keep in real-time (processing lag < 2TR) with the acquisition. Each slice reconstruction from the spiral k-space data took 0.02 sec, on average. The computation time of the OLS over the whole volume increased linearly with the number of time points available, from 0.38 sec at the third acquisition up to 0.57 sec at the 80th acquisition.

For each subject, a sample screen shot of the user interface taken after 80 acquisitions is displayed in Figures 3.2 and 3.3, respectively. Positive t-scores are displayed in a red color scale, while negative ones are displayed on a blue scale. As expected, the visual-motor task (subject 1) produced increases in perfusion that correlated with the reference function in the right

motor cortex and the visual cortex. The bimanual motor task (subject 2) resulted in perfusion increases that were correlated with the reference function on the left motor cortex and anti-correlated on the right motor cortex. Figure 3.4 shows the evolution of the t-statistic map throughout the acquisition for the first subject.

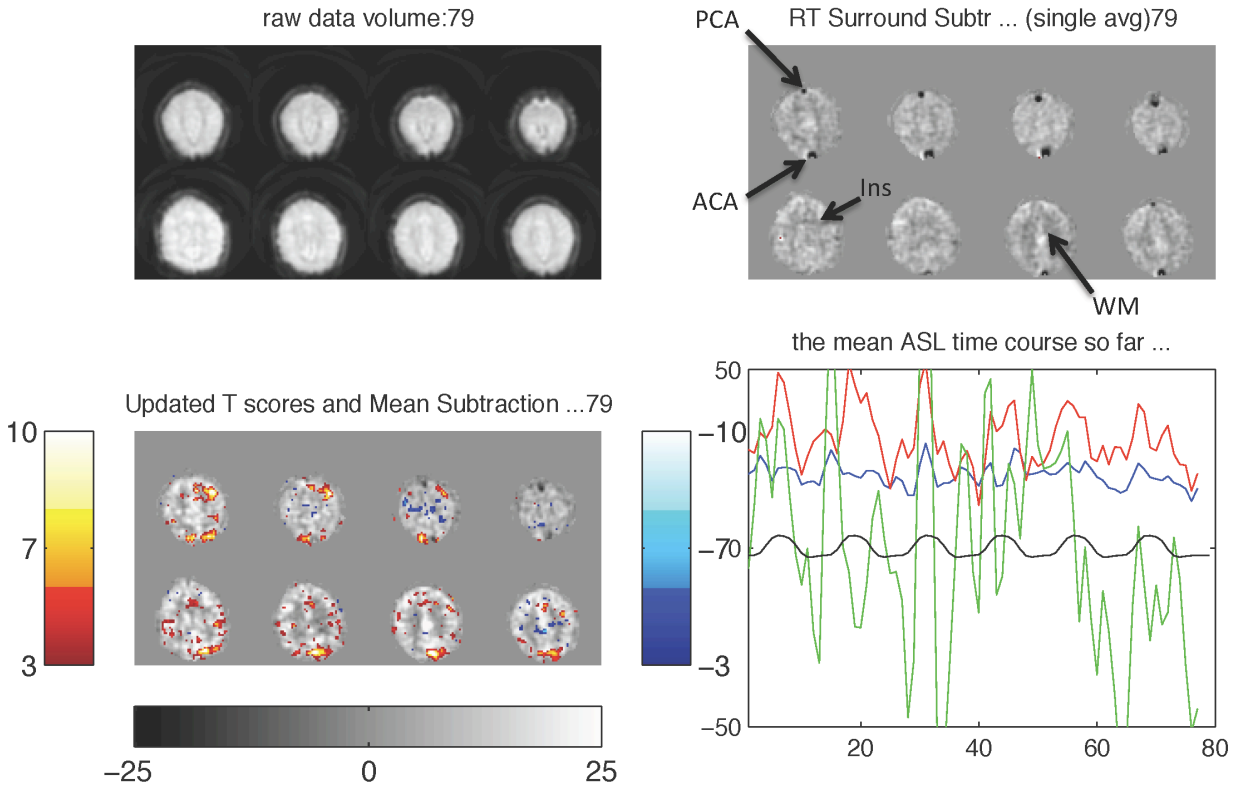

Figure 3.2. User interface of real-time system: visual-motor task. Clockwise from the top-left, the windows display (1) the current raw unsubtracted image, (2) the most recent surround subtracted image, (3) a plot of the several time courses of interest and (4) the most current update of the thresholded t-map overlaid on top of the cumulative mean subtracted image. The time courses were: the proposed model or reference function (black); the global mean signal (blue); a user-defined ROI (red); and a second user-defined ROI from which the nuisance covariate was extracted (green). The user was allowed to update the ROI locations at will and the display was updated after every acquisition. Four ROIs used as nuisance covariates are indicated in the top-right panel. These ROIs consisted of a 3 x 3 voxel region sampled at a single slice. The regions were placed on the Posterior Cerebral Artery (PCA), the Anterior Cerebral Artery (ACA), a white mater region (WM) and a heavily vascularized left insula region (Ins).

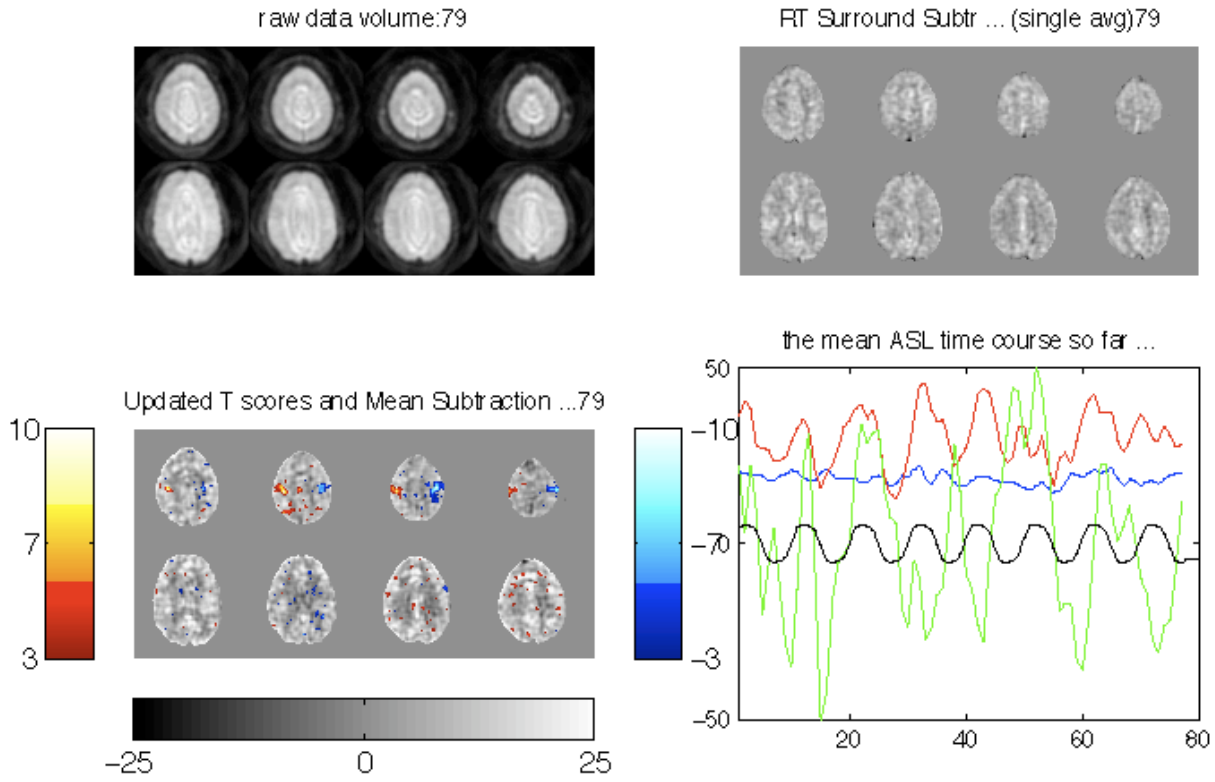

Figure 3.3. User interface of real-time system: alternating finger-tapping task. As in Figure 3.2, the raw image, subtracted images, statistical maps and time courses are displayed in real-time. In this case, the activation maps indicated correlation with the reference function in the left motor cortex and anti-correlation on the right motor cortex, corresponding to the alternating finger tapping task.

3.2.3. Real-time functional ASL: Discussion

Real-time imaging with arterial spin labeling is facilitated by the fact that there is a long period of labeling between image acquisitions. This labeling period affords the user ample time for reconstruction, image corrections, and analysis "on the fly". We are presently developing more sophisticated methods to analyze the data, including pattern recognition methods based on support vector machine classification [21]. In our current implementation, the 4 second TR offered ample time to process the data using linear regression, even as the size of the data and design matrices increased. For longer time series or reduced TR times, such as those using Turbo-CASL techniques [22, 23], sliding-window or incremental regression techniques [4, 24] may be necessary.

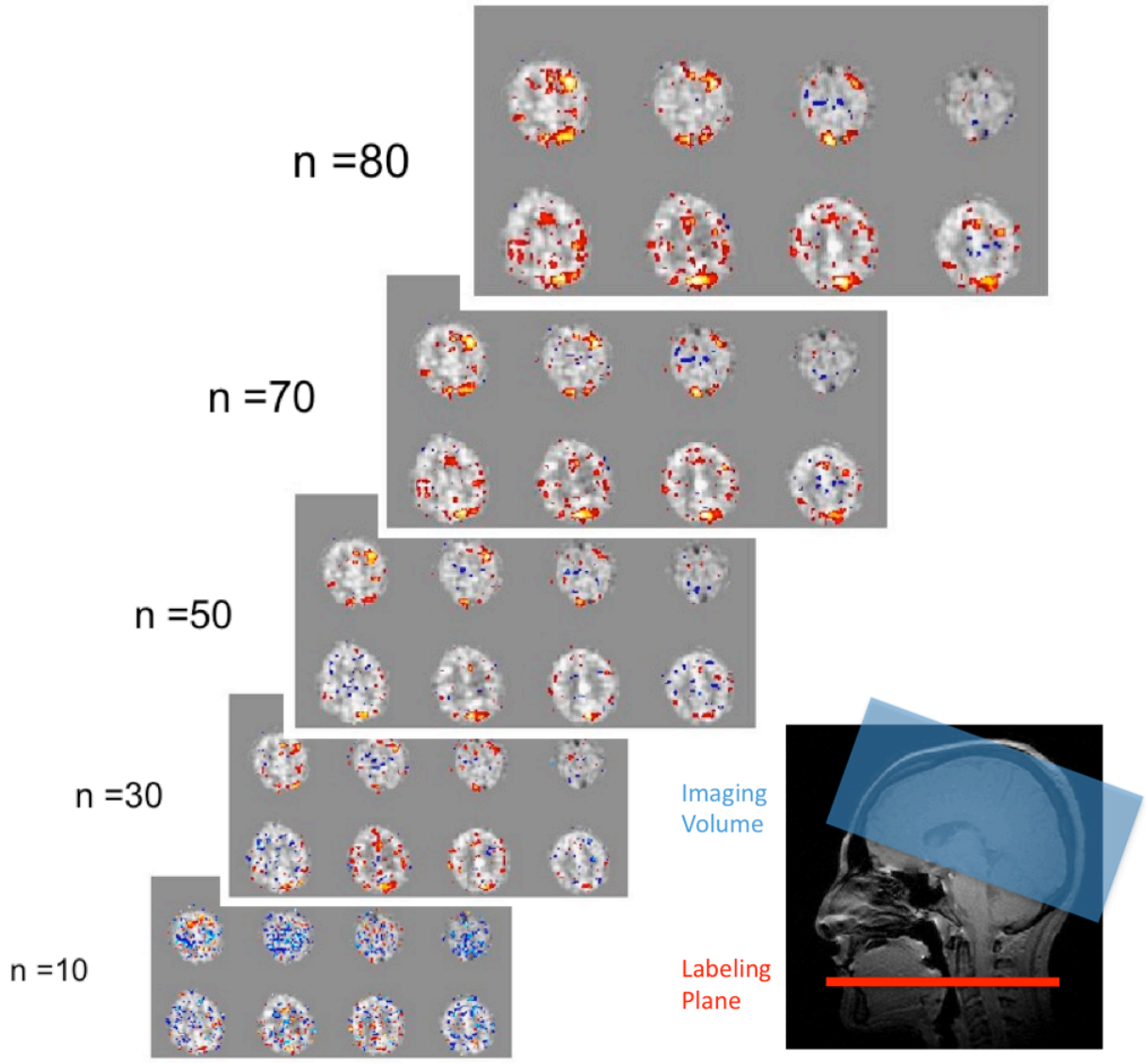

Figure 3.4. Evolution of the statistical map during visual-motor stimulation task. As more data were available, the statistical maps became more detailed with a lower number of false positives and more significant scores in the active regions. The placement of the inversion plane and the imaging slices relative to each other is shown on a sagittal view.

As with other ASL fMRI acquisitions, the number of slices that can be acquired is restricted by system acquisition speed. The kinetics of the inversion label are such that the entire volume should be collected within an approximately 500-ms window to ensure that the label has

sufficient time to arrive at the tissue but not enough to have washed out completely. While our acquisition scheme used a sequential slice acquisition, 3D imaging schemes for data acquisition may also prove to be beneficial, as demonstrated by [25]. Parallel imaging will also increase acquisition speed, although at a penalty of computation time [26] so it may require a faster computing framework.

We note that, in the realm of clinical perfusion imaging with ASL, Xie et al. [27] have developed an adaptive sampling scheme that can determine an optimal set of inversion times (TI) for baseline perfusion quantification with pulsed ASL images. This method examines the images collected and determines the choice of TI for the next image within the acquisition period, i.e., in real-time, but it must be noted that this technique is not related to time series functional MRI.

Using the ROI's time course as a nuisance covariate improved the analyses. An in-depth study of noise removal by nuisance ROI covariates is outside the scope of this study; however, we note that Wang et al. demonstrated that using the global mean signal as a covariate modestly improved sensitivity by removing spatially coherent noise from the time series, provided the global signal was not correlated with the reference function [28]. Behzadi et al. [29] also noted that using time courses from pixels with high variance to construct nuisance covariates had a significant effect for noise removal, and that these high variance ROIs corresponded largely with the arterial vasculature. Arterial fluctuations are visible to the naked eye in ASL time series data, especially when displayed as a movie. As ASL data are collected and displayed in real-time, the signal intensity in arteries fluctuates with the cardiac cycle, and the subtraction process enhances this fluctuation making the arteries evident to the user. These fluctuations are also pervasive on the rest of the image, although to a less dramatic extent, so it is not surprising that including their time course as a nuisance regressor was beneficial for the analysis. Thus, real-time acquisition and processing greatly facilitated the choice of a nuisance regressor. The user can thus pick one such region as a nuisance covariate and immediately observe its effect on the time course of the region of interest as well as on the t-map obtained from the GLM estimation. This approach must be used with care, however, and with some prior knowledge of the expected activation pattern and brain vasculature. In general, standard angiographic techniques are not necessary to identify major arteries, as the oscillations in the ASL signal make them apparent to the user. It is important, however, that the user not select a nuisance region whose activity is task related, as

that can result in a loss of sensitivity and detection power. Hence, it is useful to display the reference time course along with the nuisance regressor to identify potential correlations. We also note that including additional nuisance regressors always results in loss of degrees of freedom and, while reducing the residual variance and boosting the t-statistics, they can potentially reduce the statistical significance of the result.

3.3. Reduced specific absorption rate (SAR) pseudo-continuous arterial spin labeling

The high SAR of the original pseudo-continuous arterial spin labeling pulse sequence [20, 30] is an important challenge at ultra-high-field MRI (≥ 7T) that limits the tagging duration and/or increases the repetition time of the pulse sequence resulting in lower signal to noise time per unit time. In this section, we discuss a novel method employing the optimized pCASL pulse sequence presented in chapter 2, to mitigate this problem. In the original implementation of pCASL, due to its sensitivity to field inhomogeneity, a reduction in the flip angle of radio frequency (RF) pulses will lead to loss in inversion efficiency and signal to noise ratio. To solve this problem, the reduced SAR pCASL technique proposed here, utilizes the optimized pCASL pulse sequence which compensates for field inhomogeneity using filed map information [19]. Using simulation and experimental studies, a set of pCASL pulse sequence parameters is found that allows reducing the flip angle of pCASL RF pulses (and consequently SAR) without losing the inversion efficiency. The proposed set of parameters employs smaller slice selective gradients which leads to less acoustic noise as well. This makes the pulse sequence more desirable, especially for functional MRI studies.

3.3.1. Reduced SAR pCASL: Simulation Study

The behavior of the magnetization vector of an ensemble of moving spins (laminar flow with peak velocity = 100 cm/s, T1/T2=1600/250 ms) in the presence of a pCASL pulse sequence (Hanning-shaped RF of 500μs duration) was simulated using a numerical implementation of the Bloch equations. The area of the refocusing gradient was unbalanced by a variable amount to achieve a net average gradient (G_{av}). We measured the inversion efficiency for different amounts

of average gradients and flip angles and repeated the simulation for different gradient amplitudes during RF pulse (G_{max}). A set of parameters providing high inversion efficiency (IE>90%) yet having the lowest SAR were found from the simulation results.

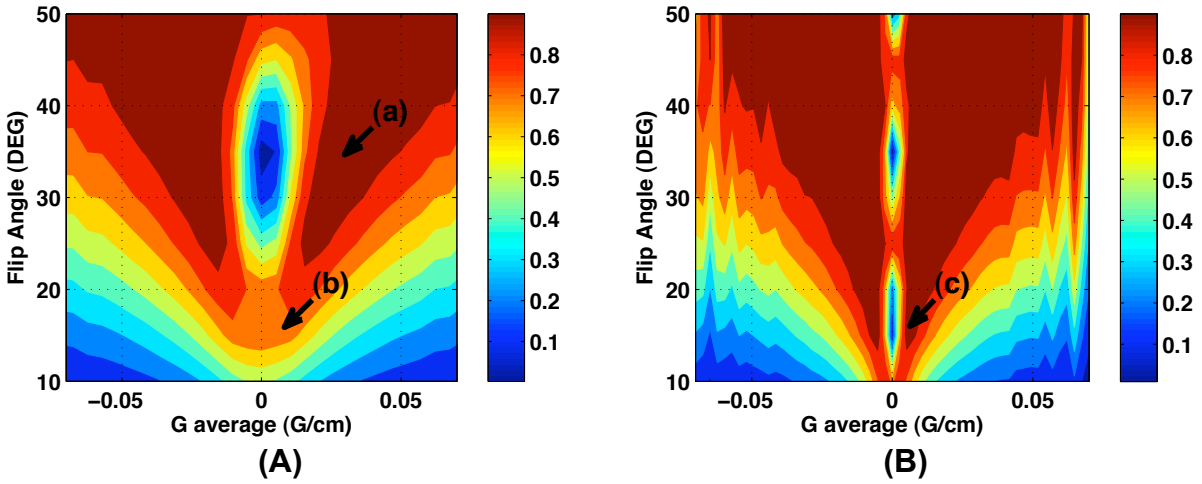

Figure 3.5. Contour maps of simulated inversion efficiencies achieved using different amounts of average gradient (G_{av}) and Flip angles for **(A)** gradient amplitude (G_{max})= 0.6 G/cm and **(B)** G_{max}= 0.3 G/cm. Parameters used for the In-vivo study (Figure 3.2) are shown with arrows. Simulated inversion efficiencies for points a, b and c were 97%, 72% and 95% respectively.

3.3.2. Reduced SAR pCASL: In-vivo Study

We performed an In-vivo study to verify the results of our simulation study. The pCASL pulse sequence was implemented on a 3.0 T Signa Excite scanner (General Electric, Waukesha, WI). Three In-vivo perfusion studies (8 pairs of control-tag for each study) were performed using the parameters marked with arrows in Figure 3.5: a) Standard pCASL b) Standard pCASL with low flip angle 3) Modified pCASL with low flip angle. Each experiment was also corrected for field inhomogeneity effects (3) to make sure that the highest possible efficiency is achieved.

A high-resolution (256x256) T1-weighted anatomical image was also acquired using the same prescription used for perfusion images. A grey matter mask was created by segmentation of the T1-weighted image after co-registration to the perfusion images. Signal to noise ratio (SNR) of each perfusion experiment was calculated as the mean gray matter perfusion over the time course, divided by its temporal standard deviation.

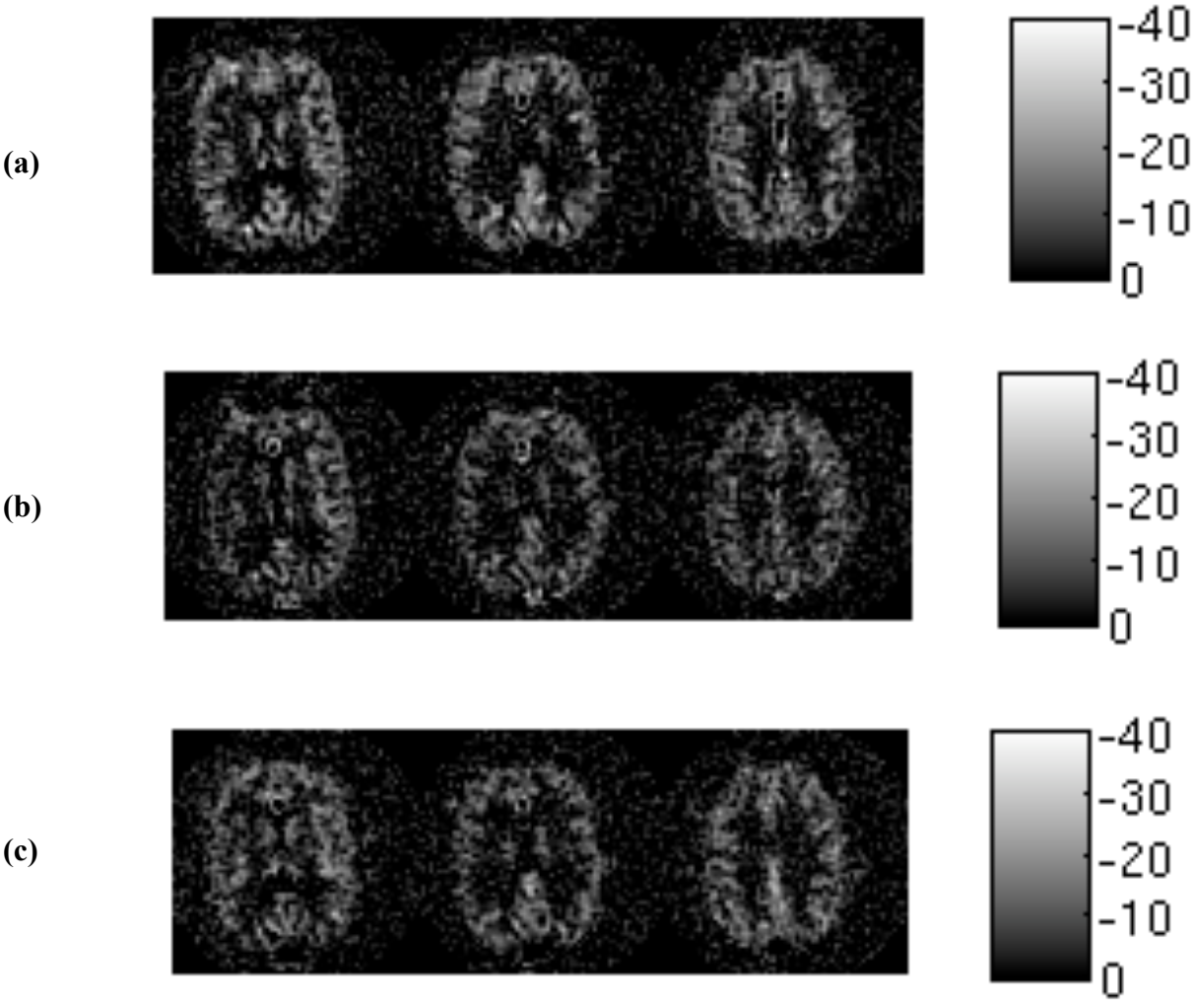

Figure 3.6. Perfusion difference images acquired using: **(a)** Flip angle = 35°, G_{max} =0.6 (G/cm) **(b)** Flip angle = 15°, G_{max} =0.6 (G/cm) and **(c)** Flip angle = 15°, G_{max} =0.3 (G/cm).

3.3.3. Reduced SAR pCASL: Results

Simulation results obtained using different G_{max} values showed that using smaller G_{max} it is possible to use lower flip angles and still achieve high inversion efficiency (IE>90%). Figure 3.5. Shows simulated inversion efficiencies for G_{max} = 0.6 and 0.3 G/cm. Point (a) on the contour map corresponds to the parameters used in the standard pCASL experiments. The flip angle in this regime is 35 degrees. Using lower flip angles (e.g. 15 degree corresponding to point (b) on

the contour map), will lead to significant loss in labeling efficiency and signal to noise ratio. As can be seen in Figure 3.5, changing the maximum gradient changes the amount of phase accommodation between RF pulses and consequently modifies the pattern of the obtained inversion efficiency in the contour plot. By lowering G_{max}, according to our simulation results, it will be possible to achieve high inversion efficiencies even at flip angles as low as 15 degrees (point (c) on the contour map). However, since there is a narrow area with high inversion efficiency at low flip angles, the pulse sequence will be so sensitive to field inhomogeneity and therefore in practice, off resonance effects, will severely degrade the inversion efficiency and signal to noise ratio of the perfusion images. To solve this problem we use the off resonance correction method presented in chapter 2 to make the method robust to field inhomogeneity and prevent the loss in inversion efficiency.

Figure 3.6 shows three slices of perfusion difference images acquired using the parameters (a),(b) and (c) marked in Figure 3.5. For each dataset, SNR values were measured inside the grey matter mask obtained from the high-resolution T1 images. The measured SNR values for these studies were: (a) 8.22, (b) 3.77 and (c) 9.98 indicating the success of the proposed reduced SAR pCASL method in providing the image quality and SNR comparable to the standard pCASL technique.

3.3.4. Reduced SAR pCASL: Discussion

Using G_{max} values proposed in the original implementation of pCASL [20, 30] the area with high inversion efficiency at low flip angles is quite narrow. Thus, the original pulse sequence is so sensitive to field inhomogeneity, variations in velocity across the vessel, and across the cardiac cycle at low flip angles. Consequently, in accordance with our experimental results, reducing the flip angle of RF pulse train severely degrades the inversion efficiency of the original pulse sequence. Our results, however, indicate that employing a low G_{max} (0.03 G/cm) along with an off-resonance correction scheme can mitigate this problem.

Decreasing G_{max} also reduces the acoustic noise of the pCASL pulse sequence, which is particularly desirable for functional MRI studies. This reduction, however, increases the spatial

width of the inversion plane, which may limit the choice of tagging plane location particularly above the circle of Willis. The reduced SAR pulse will also be more sensitive to the gradient of the inhomogeneity at the tagging plane and employing the optimized pCASL sequence and correcting for field inhomogeneity will be critical for achieving high inversion efficiency.

3.4. Conclusion

In this chapter, we demonstrated that real-time arterial spin labeling fMRI reconstruction, display, and analysis could be performed on a personal computer. Our target application is to provide neuroimaging feedback to experimental subjects undergoing stimulation paradigms with very long periodicity (> 45 sec). Having said that, real-time ASL scanning can be quite useful in the fMRI setting for many applications, in addition to our own application. Primarily, it allows the operator to evaluate data quality immediately. This point is important because ASL data have an inherently low signal to noise ratio, exacerbated by low inversion efficiency, which can be a problem in certain ASL implementations [19, 31]. Hence, we find it extremely useful to be able to evaluate data quality and make decisions about tuning the labeling parameters immediately. The technique also affords the user the opportunity to quickly evaluate the subject's performance during the scanning session itself. Furthermore, it allows the investigator to determine the subject's compliance with the task and/or to make decisions about subsequent stimuli or interactions with the subject.

In this chapter, we also presented a reduced SAR version of pCASL pulse sequence. Decreasing the flip angle (and consequently SAR) of pCASL pulse sequence without changing other parameters compromises the inversion efficiency and SNR of the pCASL experiment. However by properly decreasing the gradient amplitude during the RF pulses (G_{max}) and using the optimized pCASL sequence, it is possible to use smaller flip angles without losing the inversion efficiency.

3.5. References

[1] R. C. deCharms, "Applications of real-time fMRI," *Nat Rev Neurosci,* vol. 9, no. 9, pp. 720-9, Sep, 2008.

[2] R. W. Cox, A. Jesmanowicz, and J. S. Hyde, "Real-time functional magnetic resonance imaging," *Magn Reson Med,* vol. 33, no. 2, pp. 230-6, Feb, 1995.

[3] D. Gembris, J. G. Taylor, S. Schor, W. Frings, D. Suter, and S. Posse, "Functional magnetic resonance imaging in real time (FIRE): sliding-window correlation analysis and reference-vector optimization," *Magn Reson Med,* vol. 43, no. 2, pp. 259-68, Feb, 2000.

[4] T. Nakai, E. Bagarinao, K. Matsuo, Y. Ohgami, and C. Kato, "Dynamic monitoring of brain activation under visual stimulation using fMRI--the advantage of real-time fMRI with sliding window GLM analysis," *J Neurosci Methods,* vol. 157, no. 1, pp. 158-67, Oct 15, 2006.

[5] J. T. Voyvodic, "Real-time fMRI paradigm control, physiology, and behavior combined with near real-time statistical analysis," *Neuroimage,* vol. 10, no. 2, pp. 91-106, Aug, 1999.

[6] S. S. Yoo, T. Fairneny, N. K. Chen, S. E. Choo, L. P. Panych, H. Park, S. Y. Lee, and F. A. Jolesz, "Brain-computer interface using fMRI: spatial navigation by thoughts," *Neuroreport,* vol. 15, no. 10, pp. 1591-5, Jul 19, 2004.

[7] S. S. Yoo, and F. A. Jolesz, "Functional MRI for neurofeedback: feasibility study on a hand motor task," *Neuroreport,* vol. 13, no. 11, pp. 1377-81, Aug 7, 2002.

[8] S. Posse, D. Fitzgerald, K. Gao, U. Habel, D. Rosenberg, G. J. Moore, and F. Schneider, "Real-time fMRI of temporolimbic regions detects amygdala activation during single-trial self-induced sadness," *Neuroimage,* vol. 18, no. 3, pp. 760-8, Mar, 2003.

[9] R. C. deCharms, K. Christoff, G. H. Glover, J. M. Pauly, S. Whitfield, and J. D. Gabrieli, "Learned regulation of spatially localized brain activation using real-time fMRI," *Neuroimage,* vol. 21, no. 1, pp. 436-43, Jan, 2004.

[10] K. L. Phan, D. A. Fitzgerald, K. Gao, G. J. Moore, M. E. Tancer, and S. Posse, "Real-time fMRI of cortico-limbic brain activity during emotional processing," *Neuroreport,* vol. 15, no. 3, pp. 527-32, Mar 1, 2004.

[11] A. Caria, R. Veit, R. Sitaram, M. Lotze, N. Weiskopf, W. Grodd, and N. Birbaumer, "Regulation of anterior insular cortex activity using real-time fMRI," *Neuroimage,* vol. 35, no. 3, pp. 1238-46, Apr 15, 2007.

[12] G. Boynton, S. Engel, G. Glover, and D. Heeger, "Linear systems analysis of functional magnetic resonance imaging in human V1.," *J Neurosci,* vol. 16, no. 13, pp. 4207-21, Jul 1, 1996.

[13] D. Alsop, and J. Detre, "Reduced transit-time sensitivity in noninvasive magnetic resonance imaging of human cerebral blood flow.," *J Cereb Blood Flow Metab,* vol. 16, no. 6, pp. 1236-49, Nov, 1996.

[14] J. Detre, J. Leigh, D. Williams, and A. Koretsky, "Perfusion imaging.," *Magn Reson Med,* vol. 23, no. 1, pp. 37-45, Jan, 1992.

[15] D. Williams, J. Detre, J. Leigh, and A. Koretsky, "Magnetic resonance imaging of perfusion using spin inversion of arterial water.," *Proc Natl Acad Sci U S A,* vol. 89, no. 1, pp. 212-6, Jan 1, 1992.

[16] G. Aguirre, J. Detre, E. Zarahn, and D. Alsop, "Experimental design and the relative sensitivity of BOLD and perfusion fMRI.," *Neuroimage,* vol. 15, no. 3, pp. 488-500, Mar, 2002.

[17] T. Liu, and E. Wong, "A signal processing model for arterial spin labeling functional MRI.," *Neuroimage,* vol. 24, no. 1, pp. 207-15, Jan 1, 2005.

[18] T. Liu, E. Wong, L. Frank, and R. Buxton, "Analysis and design of perfusion-based event-related fMRI experiments.," *Neuroimage,* vol. 16, no. 1, pp. 269-82, May, 2002.

[19] H. Jahanian, D. C. Noll, and L. Hernandez-Garcia, "B0 field inhomogeneity considerations in pseudo-continuous arterial spin labeling (pCASL): effects on tagging efficiency and correction strategy," *NMR in Biomedicine,* vol. 24, no. 10, pp. 1202-1209, 2011.

[20] W. Dai, D. Garcia, C. de Bazelaire, and D. C. Alsop, "Continuous flow-driven inversion for arterial spin labeling using pulsed radio frequency and gradient fields," *Magn Reson Med,* vol. 60, no. 6, pp. 1488-97, Dec, 2008.

[21] S. LaConte, S. Strother, V. Cherkassky, J. Anderson, and X. Hu, "Support vector machines for temporal classification of block design fMRI data," *Neuroimage,* vol. 26, no. 2, pp. 317-29, Jun, 2005.

[22] L. Hernandez-Garcia, G. R. Lee, A. L. Vazquez, and D. C. Noll, "Fast, pseudo-continuous arterial spin labeling for functional imaging using a two-coil system," *Magnetic Resonance in Medicine,* vol. 51, no. 3, pp. 577-585, 2004.

[23] L. Hernandez-Garcia, G. R. Lee, A. L. Vazquez, C.-Y. Yip, and D. C. Noll, "Quantification of perfusion fMRI using a numerical model of arterial spin labeling that accounts for dynamic transit time effects," *Magnetic Resonance in Medicine,* vol. 54, no. 4, pp. 955-964, 2005.

[24] E. Bagarinao, K. Matsuo, T. Nakai, and S. Sato, "Estimation of general linear model coefficients for real-time application," *Neuroimage,* vol. 19, no. 2 Pt 1, pp. 422-9, Jun, 2003.

[25] M. Gunther, K. Oshio, and D. A. Feinberg, "Single-shot 3D imaging techniques improve arterial spin labeling perfusion measurements," *Magn Reson Med,* vol. 54, no. 2, pp. 491-8, Aug, 2005.

[26] J. E. Perthen, M. Bydder, K. Restom, and T. T. Liu, "SNR and functional sensitivity of BOLD and perfusion-based fMRI using arterial spin labeling with spiral SENSE at 3 T," *Magn Reson Imaging,* vol. 26, no. 4, pp. 513-22, May, 2008.

[27] J. Xie, S. Clare, D. Gallichan, R. N. Gunn, and P. Jezzard, "Real-time adaptive sequential design for optimal acquisition of arterial spin labeling MRI data," *Magn Reson Med,* vol. 64, no. 1, pp. 203-10, Jul, 2010.

[28] Z. Wang, G. K. Aguirre, H. Rao, J. Wang, M. A. Fernandez-Seara, A. R. Childress, and J. A. Detre, "Empirical optimization of ASL data analysis using an ASL data processing toolbox: ASLtbx," *Magn Reson Imaging,* vol. 26, no. 2, pp. 261-9, Feb, 2008.

[29] Y. Behzadi, K. Restom, J. Liau, and T. T. Liu, "A component based noise correction method (CompCor) for BOLD and perfusion based fMRI," *Neuroimage,* vol. 37, no. 1, pp. 90-101, Aug 1, 2007.

[30] W. C. Wu, M. Fernandez-Seara, J. A. Detre, F. W. Wehrli, and J. Wang, "A theoretical and experimental investigation of the tagging efficiency of pseudocontinuous arterial spin labeling," *Magn Reson Med,* vol. 58, no. 5, pp. 1020-7, Nov, 2007.

[31] Y. Jung, E. C. Wong, and T. T. Liu, "Multiphase pseudocontinuous arterial spin labeling (MP-PCASL) for robust quantification of cerebral blood flow," *Magn Reson Med,* vol. 64, no. 3, pp. 799-810, Sep, 2010.

Chapter 4

Arterial cerebral blood volume (aCBV) weighted functional MRI using pseudo-continuous arterial spin labeling

4.1. Abstract

A variant of arterial spin labeling (ASL) technique was developed in order to image arterial cerebral blood volume (aCBV) with little or no contributions from the parenchyma. The proposed technique takes advantage of the kinetics of the label through the vasculature and is suitable for dynamic, functional imaging experiments. Dynamic imaging of arterial blood volume (aCBV) can be a very powerful tool for the study of brain function in both diseased and healthy human brains since neurovascular regulation, including responses to neural activation that give rise to the BOLD effect, occurs mainly at the arterial and arteriolar level. While current CBF-based and CBV-based fMRI techniques suffer from poor sensitivity and low temporal resolution, the method proposed here offers sensitivity to brain activation that is on par with BOLD imaging and superior to other CBF-based methods.

4.2. Introduction

Cerebral blood volume is a very important measurement for the study of a number of neurodegenerative disorders that involve vascular dysregulation such as hypertension, stroke [1, 2], small brain infarcts [3], Alzheimers disease [4], astrocytoma and other brain tumors [5, 6] and cerebral stenoses [7]. The ability to separate the arterial compartment from the venous compartment of CBV may provide additional information not obtainable

from total CBV (e.g. in steno-occlusive disease of the internal carotid artery [8]) and also provide insights into vascular control mechanisms in healthy and diseased [6, 8, 9].

Imaging of arterial cerebral blood volume (aCBV) can also be important for the study of human brain function and cognition. aCBV regulates the tissue perfusion and can be an essential indicator of vascular reactivity [9]. aCBV can also provide critical information for understanding the blood oxygen level-dependent (BOLD) contrast [10]. Moreover, functional magnetic resonance imaging using physiological parameters such as cerebral blood flow or cerebral blood volume, unlike BOLD fMRI, provides a quantifiable contrast and is also more closely related to neural activity [11-13]. These methods can also be much less sensitive to the local susceptibility artifacts which is an issue plaguing the BOLD effect especially in areas of the brain that lie near air spaces [14].

Therefore, CBF and CBV based functional MRI methods have recently received attention as alternative and complementary techniques to BOLD fMRI. These methods, however, generally have been hampered in terms of signal to noise ratio (SNR), temporal resolution and multi-slice imaging capability.

Different methods have been proposed for non-invasive measurement of aCBV in animals [15] and humans [16-19]. iVASO [19] uses the difference in T1 relaxation time of blood and tissue to assess the arterial blood volume. This method [20] is based on a set of assumptions about the arterial transit time and T1 values, which requires further verification. aCBV can also be estimated from the arterial blood information present in the signal obtained from arterial spin labeling (ASL) techniques. Some techniques obtain ASL images at different post labeling delays and quantifying the aCBV by modeling the collected signal [16-18]. The difference between ASL measurements with and without flow-crusher gradients is related to aCBV and several techniques have estimated aCBV by this approach [16, 20-22]. The MOTIVE technique [15], uses magnetization transfer along with arterial spin labeling technique to modulate the tissue and blood signals and estimate the aCBV in animals. While all these methods have been shown to be useful in various applications, many are not suitable for real world human fMRI experiments due

to the long acquisition time, need for multiple measurements, poor temporal resolution and very limited slice coverage.

The purpose of this study is to develop a method that provides aCBV-weighted signal suitable for functional imaging experiments using ASL technique. We propose a novel dynamic aCBV measurement technique based on pseudo-continuous arterial spin labeling (pCASL) technique [23, 24]. In the proposed method we tailor the tagging time and TR for each subject to achieve a contrast that depends on arterial cerebral blood volume (aCBV) with little or no contamination from perfusion signal, similar to our previous approach [25]. The approach presented here, however, allows for a much faster acquisition rate, making it more suitable for dynamic fMRI experiments.

We employ a 3D imaging pulse sequence with multi-shot (segmented) readouts for imaging the aCBV signal. Besides improving the SNR efficiency relative to 2D multislice, the 3D acquisition ensures the same acquisition delay for the entire imaging volume relative to the tagging period and therefore provides us with the capability to measure the aCBV in a volume rather than a single slice [26].

The method proposed here offers sensitivity to brain activation that is on par with BOLD imaging and superior to CBF ASL, while maintaining many advantages of CBF ASL imaging in terms of less sensitivity to susceptibility artifact, quantifiable signal and less signal drift. We demonstrate the proposed method using numerical simulations and in vivo experimental data. We compare the proposed method with standard CBF ASL and BOLD techniques in terms of sensitivity, reproducibility, locus of activation and temporal response for fMRI experiments.

4.3. Materials and Methods

4.3.1. Theory

We consider a voxel of tissue as three separate compartments through which arterial water flows: arterial compartment, capillary and tissue compartment, and a venous compartment. In an ASL experiment, the labeled water enters the voxel via the arterial compartment and exchanges through the capillaries/tissue on its way to the venous compartment, from which it leaves the voxel. At 3 Tesla and below, T1 decay prevents the labeled spins from retaining their label by the time they reach the venous compartment, so it can be safely neglected.

Therefore, for our purposes, the observed ASL signal can be split into an arterial and a tissue compartment ($S_{total} = S_a + S_t$) and modeled separately. The signal contribution by the labeled arterial spins, S_a, in a continuous ASL experiment can be expressed by adapting the general kinetic model [27] for magnetization difference between tagged and control images as follows:

$$\begin{aligned} S_a(t) &= \Delta M_a(t) = 2\alpha . M_{a0} . aCBV . c(t) \\ c(t) &= rect(t,w) * [k(t-\tau_1) . m(t)] \\ k(t) &= \left[\frac{s^{(1+SP)}}{\Gamma(1+SP)} t^{SP} e^{-st} \right] \\ m(t) &= e^{-t/T_{1a}} \end{aligned} \qquad (4.\ 1)$$

where M_{a0} is the equilibrium magnetization of arterial blood, *aCBV* is the arterial blood volume fraction in a given voxel, α is the inversion efficiency, *rect(t,w)* describes a rectangular labeling function of duration w. The mean time it takes to reach the voxel is τ_1, or "arterial arrival time". This input experiences longitudinal relaxation, as well as dispersion of velocities as it moves up the arterial network. The dispersion of the tag during travel to the imaging plane can be approximated by convolving the input function with a Gamma kernel *k(t)* [28, 29].

The arterial label in turn serves as an input to the tissue compartment, whose signal can be expressed as a second convolution

$$S_t(t) = S_a(t).f * \left\{ e^{-\frac{f}{\lambda}(t-\tau_2)} . e^{-(t-\tau_2)T_{1t}} \right\} \quad (4.2)$$

Here, the second term in the convolution captures the clearance (f, perfusion) of label from the parenchyma after a short delay or "tissue transit time", τ_2, and the decay of the label's longitudinal magnetization in the parenchyma. As an illustration of the kinetics of arterial and tissue signals, Figure 4.1 shows numerical simulation of the wash-in and wash-out of the label into the arteries and tissue relative to a tagging function (details of this simulation will be presented later in the Methods section of this article). We are interested in the value of M_a relative to the total magnetization in the voxel.

The "ASL signal" consists of the subtraction of a tagged image from a control image. The contribution of each compartment on the ASL signal depends on the pulse sequence's timing parameters along with each subject's arterial arrival time, τ_1, and local arterial delay or transit time, τ_2. In CBF ASL experiments, the arterial contribution to the ASL signal is eliminated using a long post inversion delay (Figure 4.1,a) or by using flow crusher gradients [30, 31]. Without a post inversion delay (Figure 4.1,b), the ASL signal will be a mixture of arterial and tissue signal. Changing the tagging time with no post inversion delay modulates the arterial and tissue contribution of the ASL signal (Figure 4.1,b, c and d). As can be seen in (Figure 4.1,c), by choosing the proper tagging time in this regime it is possible to have the same contribution from tissue in control and tagged images. In this case the tissue signal gets cancel out in the ASL signal and the signal will be from arterial compartment and as the result related to aCBV.

Figure 4.2 shows a simulation of the contribution of each compartment in ASL signal as a function of tagging duration. Note that for each subject, there exist combinations of acquisition parameters (tagging duration and TR) such that the tissue contribution, S_t, is minimal and the bulk of signal is arterial (S_a) (Highlighted with the red rectangle in Figure 4.2) and therefore related to aCBV. Consequently, the fractional ASL signal change using these parameters upon activation during a functional study is related to the local changes in the arterial blood volume.

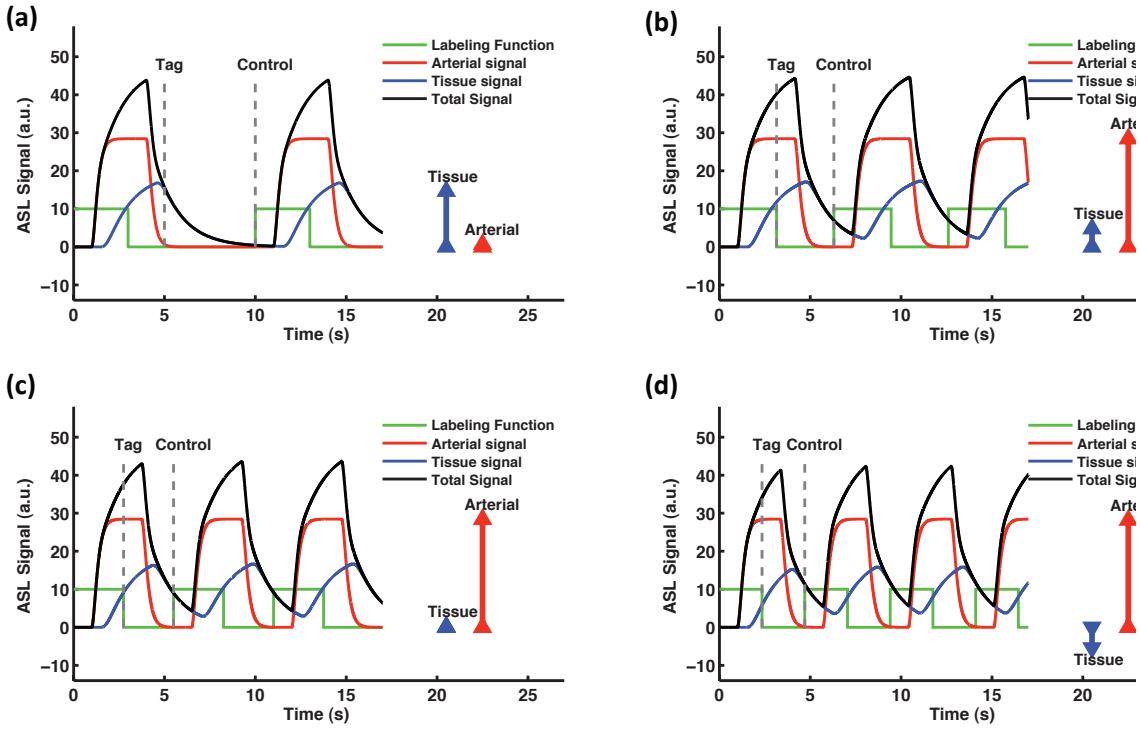

Figure 4.1. Simulation of the inversion label's passage through a voxel's arterial and tissue compartments using different timing parameters. The labeling function, arterial and tissue compartments and total signal time course are shown using green, red, blue and black curves. The timing of the acquisition of control and tag image are shown using dotted vertical lines. Tissue contribution and arterial contribution of the ASL signal (subtraction of tag from control image) are also indicated on the right side of each curve by blue and red arrows, respectively: **(a)** ASL signal in the standard perfusion measurement experiment with long post inversion delay (large tissue signal, no arterial signal); **(b)** ASL signal without using a post inversion delay (large tissue signal, large arterial signal); **(c)** ASL signal without using a post inversion delay with optimal labeling duration for aCBV signal (no tissue signal, large arterial signal); (**d)** ASL signal without using a post inversion delay with shorter labeling duration (negative tissue signal, large arterial signal)

4.3.2. Simulation

In order to explore the effect of the labeling timing with respect to label transit time, we simulated the general kinetics of the ASL signal at different TRs and tagging durations using equations 4.1 and 4.2. In this simulation, we assumed that image acquisition happens instantly after the tagging period (i.e. no post-inversion delays). The following

constants were used in the model (f = 0.015 ml/g/s, M_{0a} = 3000, $aCBV$ = 0.02 ml/ml, T_{1a} = 1.4 s, T_{1t} t= 1.6 s, α = 0.8, λ = 0.9 ml/g). M_{0a} is an arbitrary signal intensity, tagging pulse was assumed to be 80% efficient [32], and T_{1a} and T_{1t} at the static magnetic field strength of 3T were obtained from the literature [33, 34]. To account for the dispersion of tagged blood, we convolved the input function with input function with a Gamma kernel using the parameters suggested in [29]. τ_1 and τ_2 were 1000ms and 500ms [35]. Using this simulation we compare the kinetics of ASL signal in arteries and tissue and identify the range of tagging times and TRs for which the net signal is mostly arterial with small tissue contribution to the signal. Figure 4.1 shows the wash-in and wash-out kinetics of the arterial and tissue compartments of the signal in a given voxel using different labeling timing parameters. The contributions of the arterial and tissue signal to the subtraction ASL signal obtained from control and tag images are also shown using red and blue arrows on the right side of each curve. Figure 4.1.a shows the kinetic of the signal using a typical perfusion measurement timing parameters. Note that in this case the arterial signal is eliminated using a long post inversion delay. Without a post labeling delay, (Figure 4.1.b) there is a large contribution from the arterial compartment in addition to tissue contribution of the signal. By reducing the tagging duration in this regime it is possible to have the same amount of tissue signal contribution in the tag and control images, and consequently, it gets subtracted out in the ASL signal (Figure 4.1.c). In this case, the ASL signal will arise from the arterial compartment alone and related to aCBV rather than perfusion. Further reduction in the tagging duration in this regime produces a negative signal contributed from the tissue compartment (Figure 4.1.d).

The contribution of the arterial and tissue compartments to the ASL signal as function of labeling duration is shown in Figure 4.2, assuming that the image acquisition happens at the end of labeling period. The highlighted points (red crosses) on the curve in Figure 4.2 correspond to the timing parameters shown in Figure 4.1.b,c, and d. As can be seen in Figure 4.2, there are several tagging durations for which the tissue contribution to the arterial signal is zero. At these "zero-crossings" of the tissue contribution curve (blue), there is still plenty of arterial contribution to the ASL signal. The location indicated in the Figure 4.2 by a red rectangle suggests a very stable range of tagging for which the net

signal is mostly arterial with less than 5% tissue contribution to the signal. We dub this point "aCBV point" and use it to collect aCBV-weighted images. Thus, for each subject, our first task is to identify the timing parameters of aCBV point by testing a range of tagging durations with and without arterial suppression gradients, in order to separate the two signal contributions.

4.3.3. Sensitivity to timing error

The location of the aCBV point is determined by the subject's specific arterial and tissue transit times relative to the image acquisition parameters. Therefore, the best selection of

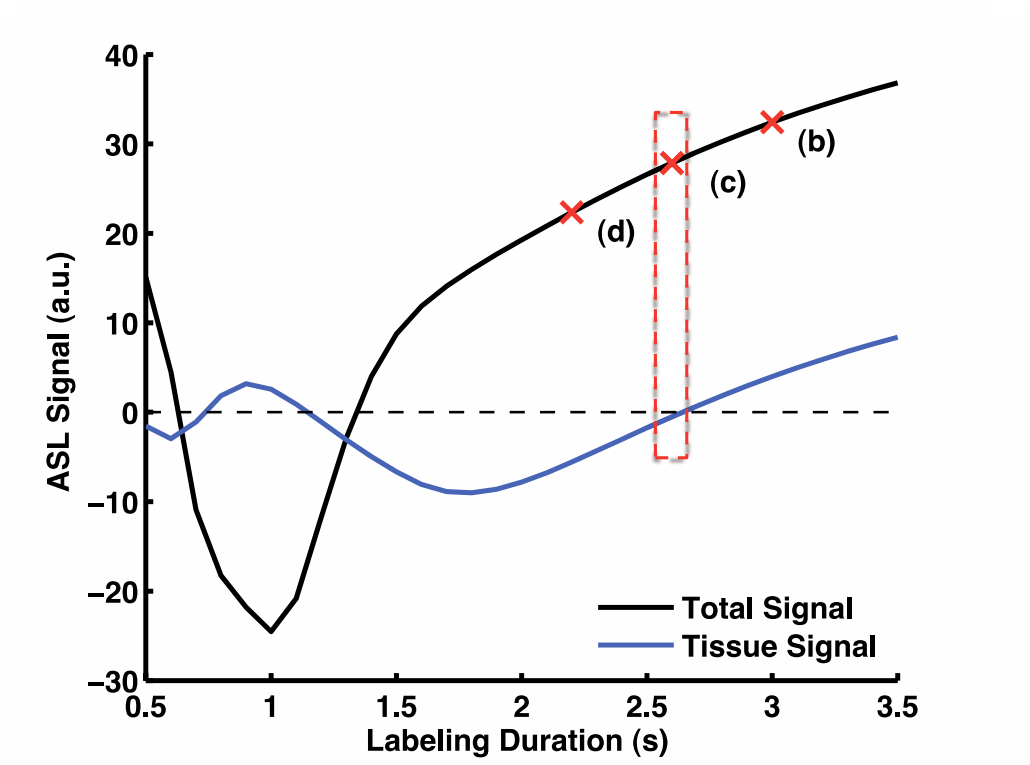

Figure 4.2. Simulated ASL signal (control minus tagged images) as a function of labeling duration. Arterial transit delay assumed to be 1s. TR was adjusted dynamically to accommodate the increasing tagging time. Points highlighted with red crosses corresponds to the kinetic curves shown in Figure 4.1.b, c and d.

parameters will vary from subject to subject and over brain regions. In Figure 4.3 we show a simulation of the ASL signal in which the aCBV sequence is calibrated for a specific region with a given set of physiological parameters, arterial arrival time of 1 sec and transit time of 0.5 sec [35]. Keeping the acquisition parameters the same, we calculated what happens to the signals when the voxels' arrival and transit times differ up to 0.5 second from the original calibration in order to illustrates the amount of tissue contamination that can be potentially found using this method. We see that the contribution from the parenchymal-labeled spins to the aCBV signal is quite small in this regime. If we are wrong by 50% in the arrival time there is only a 10 % contamination from tissue compartment. The technique is even less sensitive to the tissue transit time variation, as it takes 100% change in order to cause a 10% signal contamination.

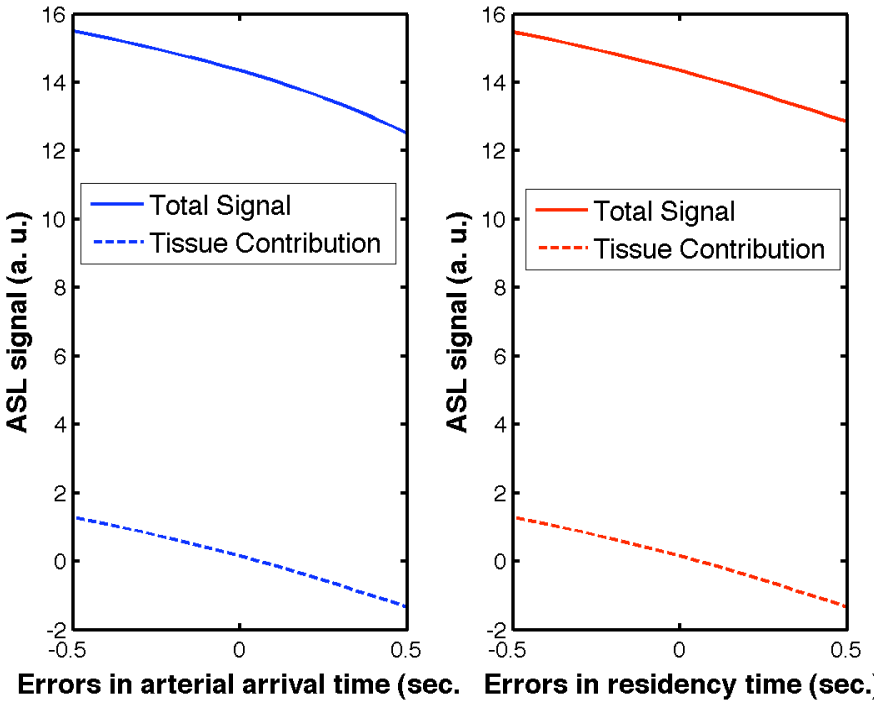

Figure 4.3. Arterial and Tissue ASL signals in aCBV acquisition optimized for a voxel where the arrival time is 1 sec. and the transit time 0.5. These plots show the signal in voxels whose arrival and transit times differ from the original voxel by a broad range.

4.3.4. In Vivo Experiments

4.3.4.1. 3D image acquisition

The image acquisition consists of a segmented 3D acquisition (3D "stack of spirals") implemented using RF-spoiling. The rationale for using 3D imaging techniques is to increase SNR and to eliminate differences in sensitivity to transit times across slices. If we were to use sequential 2D imaging, each slice would be acquired at a different post-inversion delay and consequently, the optimality of the aCBV acquisition would be slice-dependent. We used a cubic flip-angle schedule from 15 to 90 degrees as we traverse k-space along the slab-select direction in to reduce blurring along the slab encoding dimension [26].

4.3.4.2. Finding the aCBV point parameters

The above simulations suggest that the timing parameters producing the aCBV images is determined by each subject's specific arterial and tissue transit times relative to the image acquisition parameters. Therefore, the best selection of parameters will vary from subject to subject, although our simulations indicate that the technique is not very sensitive to errors in transit time. To this end, we identified the timing parameters of the aCBV point producing aCBV images with minimal contribution from the parenchyma by running a calibration sequence before the functional experiment. The calibration sequence tests the ASL signal over a range of TRs in the presence of arterial suppression gradients (similar to the blue curve in Figure. 4.2). Arterial signals were suppressed by using a pair of bipolar crusher gradients (b = 4 s/mm2). Guided by the simulation result and by previous experience [25, 36, 37], TR was varied from 1500 to 2500 ms, steps of 100 ms, while keeping the tagging time 500 ms shorter than TR to allow the acquisition of 11 slices using for the calibration sequence.

The images were reconstructed, pairwise subtracted and averaged (8 pairs for each TR). The TR and tagging that yielded the lowest ASL contrast in the presence of flow crushers (dashed box in Figure 4.2), was selected as optimal for aCBV.

4.3.5. Quantification

Using equation 4.1 it is possible to quantify the aCBV signal obtained using the proposed method. To this end, it is necessary to estimate the arterial arrival time from the tagging plane at the neck to the imaging plane. We estimated the arterial arrival time by varying the tagging time and TR and following the changes in the ASL signal [36, 37]. The signal can then be quantified using the following equations:

$$aCBV = \frac{\Delta M(TR)}{2\alpha . M_{a0}\, c(TR)} \tag{4.3}$$

$$M_{a0} = \frac{M_a(TR)}{(\sin\theta . e^{-TR/T_{1a}})}$$

in which θ is the flip angle of 3D imaging pulse and M_a is the equilibrium magnetization of the arterial blood measured in the sagittal sinus measured from mean of the control images.

4.3.6. Functional experiments

Using the obtained aCBV parameters, we carried out an aCBV based functional MRI experiment and compared it to the result of CBF based and BOLD functional experiments. Ten subjects were scanned using a 3.0 T Signa Excite scanner (General Electric, Waukesha, WI). We employed pseudo-continuous tagging pulses [23, 24] for CBF and aCBV based fMRI experiments. The labeling efficiency of the pCASL pulse sequence was optimized by correcting for the field off-resonance using the method

proposed in chapter 2. Image acquisition was carried out employing the above-mentioned segmented 3D spiral acquisition pulse.

Subjects performed a simultaneous motor (sequential finger opposition) and visual (8Hz flashing checkerboard) activation task while being scanned. The activation paradigm consisted of five cycles of alternating rest (30 seconds) and activation (30 seconds).

The first activation map was collected using a functional aCBV labeling scheme (i.e. TR/tagging time obtained from the calibration scan, no post inversion delay). The second one was collected using a standard CBF weighted pCASL scheme (TR = 4000 ms, tagging duration = 2000ms, post-tagging delay = 1500 ms). A BOLD fMRI study was also conducted (TE=30 ms, TR = 2 s) for comparison purposes. To compare the reproducibility of each method, we repeated the functional experiments one more time using each method for all subjects. All datasets were reconstructed, surround subtracted and analyzed by estimation of standard general linear model (GLM) using home written software FASL01 (http://fmri.research.umich.edu/resources/software/shared_code.php).

4.4. Results

4.4.1. aCBV Calibration

Figure 4.4 shows an example ASL signal acquired at different TRs in an ROI containing 50 voxels of grey matter with and without the flow crusher gradients in one of the subjects. By incrementing the labeling time and TR together, we were able to isolate the arterial contribution to the ASL signal. The black curve corresponds the ASL signal without the flow crusher gradients and contains both arterial and tissue signals. The blue curve corresponds to the ASL signal with the flow crusher gradients. It represents the tissue signal (CBF), which we used to estimate the optimal aCBV parameters by finding the aCBV point (pointed to by the red arrow). Note the later arrival of the tag bolus in the

crushed ASL series. This is to be expected since these spins must traverse the branching arteries and arterioles before they reach the capillary bed where they can exchange.

4.4.2. Functional Study Results

All experiments produced activation in visual cortex, motor cortex and supplementary motor area (SMA). Figure 4.5 shows the activation maps in one of the subjects obtained using CBF-based fMRI, the proposed aCBV-based fMRI and BOLD fMRI. Similar to this subject, in all other subjects, active areas in the aCBV map were more focal than BOLD but aCBV produced wider activated areas compared to CBF.

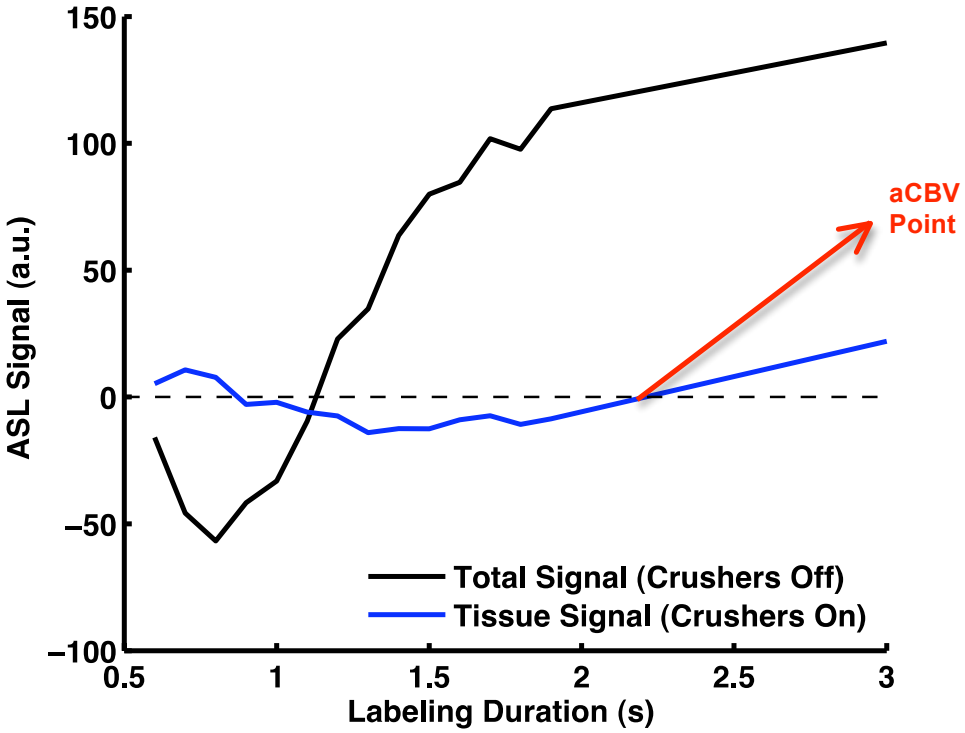

Figure 4.4. Mean ASL signal measured at different TRs with (Red) and without (blue) flow crusher gradients.

There are areas in the activation map obtained using BOLD fMRI that are not present in aCBV and CBF fMRI maps. This is due to diferences in the sensitivity and contrast to noise ratio of these methods relative to the Z threshold chosen for displaying the results.

We compared the hemodynamic response of these methods by averaging the time course of the top 1% of activated voxels for each technique across the 5 cycles and subjects (N=10). Since TR for aCBV experiments are not the same for different subjects, all aCBV datasets were first linearly interpolated to TR=2s before averaging. It can be seen in Figure 4.6 that the aCBV response has an initial overshoot, while the CBF and BOLD response has a delayed time to peak and longer return to baseline than aCBV. The relative signal change due to activation is also higher for aCBV-weighted signal compared to that of CBF weighted signal.

To compare the sensitivity of each method we sorted the voxels of each activation map based on their Z score and calculated the mean Z score of the top 1% of voxels for perfusion-based fMRI, aCBV-based fMRI and BOLD. Figure 4.7 shows the calculated mean Z scores for all ten subjects. Average Z-score for all the subjects were 4.25, 5.52 and 7.87 for CBF-based fMRI, aCBV-based fMRI and BOLD respectively indicating the superior detection sensitivity of the proposed method compared to CBF-based technique.

In order to understand the relationship between activation maps obtained with these methods in terms of locus of activation, we examined the overlap of the top 1% of the activated voxels between aCBV-BOLD , CBF-aCBV and CBF-BOLD. Figure 4.8.a shows the calculated number of overlapping voxels for all ten subjects. The average overlaps over all subjects were 54%, 36% and 46% respectively, which was expected considering the different physiological origin of each signal. We also calculated the number of overlapping voxels of the top 1% of the activated voxels between two runs for each method (Figure 4.8.b) in order to compare the reproducibility of each technique. The results indicate that aCBV method has superior reproducibility compared to CBF but still is outperformed by BOLD.

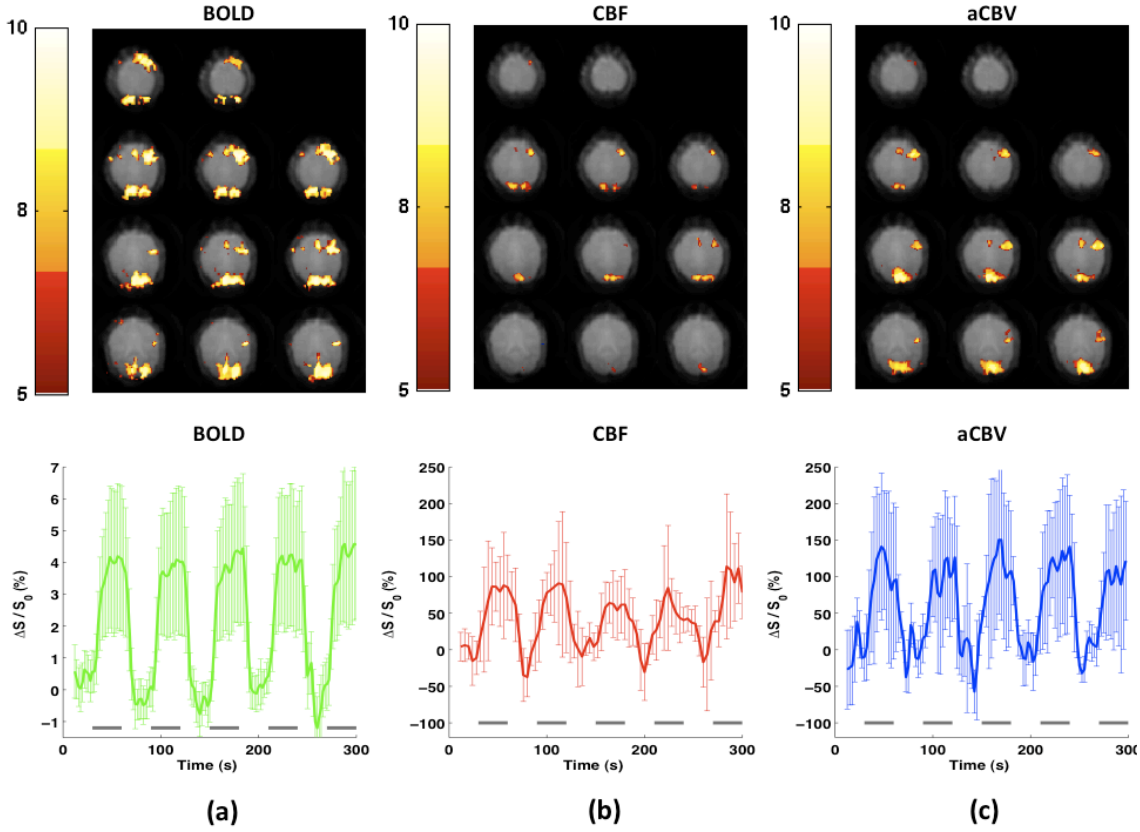

Figure 4.5. Activation maps (Z>5) and their corresponding signal time course for a single representative subject obtained using: **(a)** aCBV weighted imaging, **(b)** standard ASL imaging and **(c)** BOLD contrast fMRI during visual and unilateral motor stimulation. The color bars show the Z value of the activated area. Time courses are averaged over the top 1% of the activated voxels with the highest Z scores for each technique. Error bars indicate the SD across top 1% activated voxels. Dark lines under the time courses show periods of stimulation.

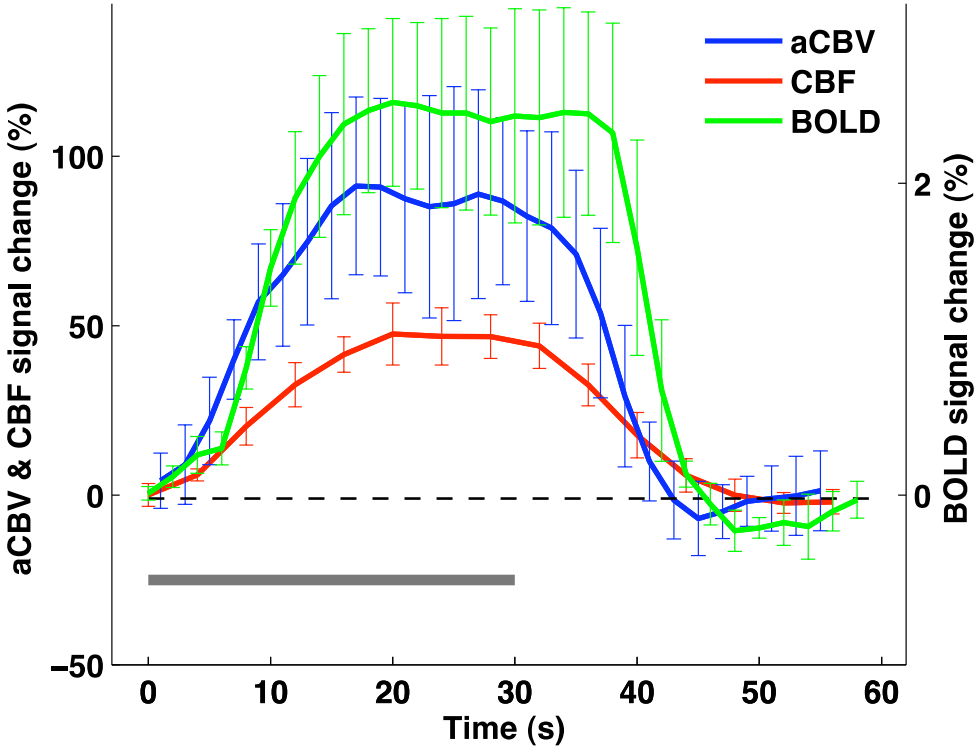

Figure 4.6. Average hemodynamic response averaged across 5 cycles for all subjects (N=10) for aCBV, CBF and BOLD techniques. Error bars indicate the SD across subjects. Dark lines show the period of stimulation.

4.4.3. aCBV Quantification

Figure 4.9.a shows an example of aCBV maps estimated in the resting state. There is a range of values with a mean at 1.1 mL/100 mL. Figure 4.9.b shows the histogram of the obtained values. The obtained values are consistent with excepted values from literature [8, 15]. The large spread in GM aCBV is likely related to different partial volume effects with vessels, white matter and CSF.

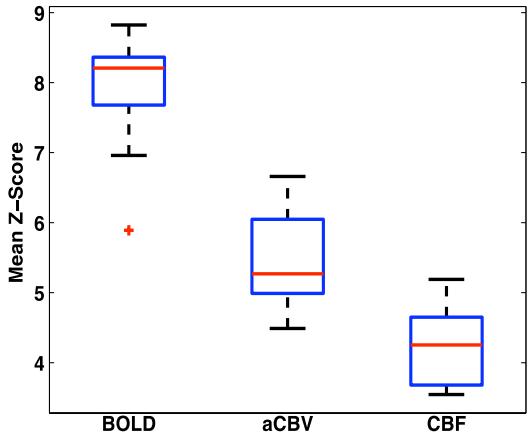

Figure 4.7. Mean Z score value averaged over the top 1% voxels for BOLD, aCBV-based and CBF-based fMRI for all subjects.

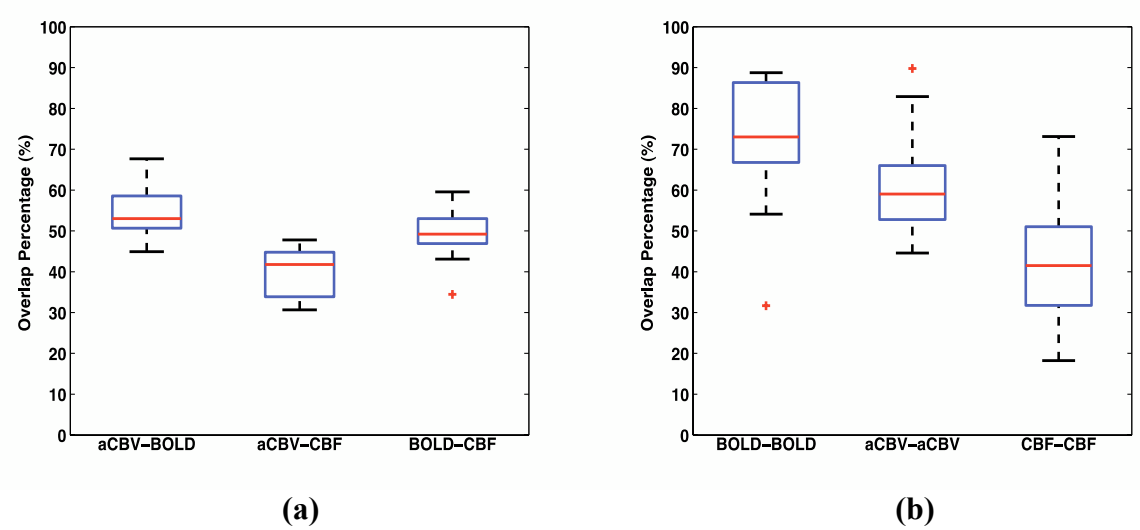

(a) **(b)**

Figure 4.8. Number of overlapping activated voxels detected using the three methods, aBV based, CBF based and BOLD fMRI: **(a)** between two runs of different methods **(b)** between two runs of the same method

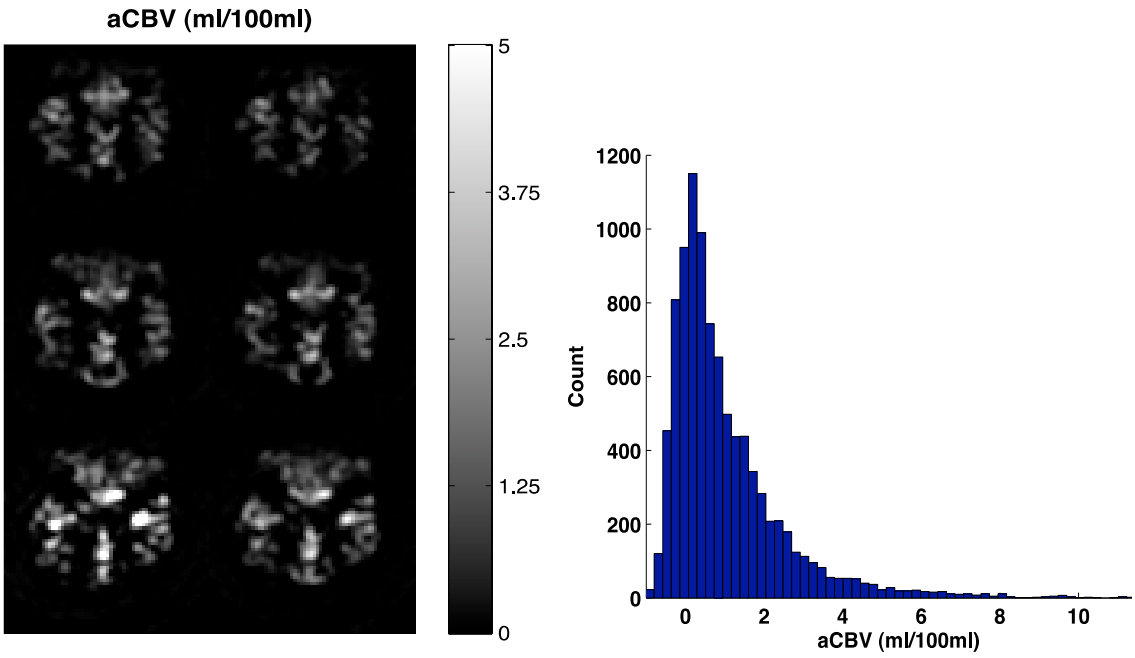

Figure 4.9. Representative aCBV map estimated using the proposed method **(a)** and its corresponding histogram **(b)** for one of the subjects.

4.5. Discussion

While BOLD contributions to the aCBV signal were assumed to be negligible at our choice of TE, they may contribute to the noise of the measurement. If they are severe, they could be included in the general linear model during the analysis, as in [38, 39]. In this case, we have chosen to keep preprocessing to a minimum in order to show a fair comparison among techniques.

As we indicated in our simulations above, changes in transit time will not introduce much parenchymal contamination into the aCBV signal. However, a reduction in the local transit time due to activation can muddle quantification of aCBV signal during activation periods because it exaggerates the observed signal change. While this can be detrimental for the quantification process, it benefits the detection of active regions. This effect is similar to our previous observations in the CBF-based Turbo-CASL technique [37] and a

correction scheme is under development. Because of this dependence of the aCBV signal on transit time, we employed 3D imaging techniques in order to eliminate differences in sensitivity to transit times across slices. In other words, the acquisition delay should be the same for all voxels within the 3D imaging volume, regardless of slice. We used center-out kz-space ordering, in order to maximize the aCBV signal across the whole volume because the bulk of the observed signal is concentrated near the center of kz. This scheme however produces a modest blurring effect in the ASL difference images, which is negligible in this application.

Other challenges to the aCBV technique, as currently implemented, are limited slice coverage (compared to BOLD) and the need to acquire a resting-state calibration curve to determine the optimal sequence timing parameters.

4.6. Conclusion

We have presented a novel method using pseudo-continuous arterial spin labeling technique providing an arterial cerebral blood volume weighted signal suitable for functional imaging experiments. Our initial results, presented in this article, suggest that the proposed aCBV-based fMRI method provides superior sensitivity and temporal resolution over the conventional CBF-based fMRI methods, closer to those of the BOLD technique, while retaining the more desirable properties of arterial spin labeling techniques. Namely, it yields a readily quantifiable physiological parameter, and because it is a subtraction technique, its noise is mostly white and not auto-regressive. Furthermore, minimal echo times can be employed in this scheme, resulting in images that are less sensitive to susceptibility artifact compared to BOLD weighted imaging.

4.7. References:

[1] J. Rother, F. Guckel, W. Neff, A. Schwartz, and M. Hennerici, "Assessment of regional cerebral blood volume in acute human stroke by use of single-slice dynamic susceptibility contrast-enhanced magnetic resonance imaging," *Stroke,* vol. 27, no. 6, pp. 1088-93, Jun, 1996.

[2] C. P. Derdeyn, T. O. Videen, K. D. Yundt, S. M. Fritsch, D. A. Carpenter, R. L. Grubb, and W. J. Powers, "Variability of cerebral blood volume and oxygen extraction: stages of cerebral haemodynamic impairment revisited," *Brain,* vol. 125, no. Pt 3, pp. 595-607, Mar, 2002.

[3] R. H. Wu, R. Bruening, C. Berchtenbreiter, J. Weber, H. J. Steiger, M. Peller, H. Penzkofer, and M. Reiser, "MRI assessment of cerebral blood volume in patients with brain infarcts," *Neuroradiology,* vol. 40, no. 8, pp. 496-502, Aug, 1998.

[4] D. C. Alsop, J. A. Detre, and M. Grossman, "Assessment of cerebral blood flow in Alzheimer's disease by spin-labeled magnetic resonance imaging," *Ann Neurol,* vol. 47, no. 1, pp. 93-100, Jan, 2000.

[5] H. J. Aronen, I. E. Gazit, D. N. Louis, B. R. Buchbinder, F. S. Pardo, R. M. Weisskoff, G. R. Harsh, G. R. Cosgrove, E. F. Halpern, F. H. Hochberg, and et al., "Cerebral blood volume maps of gliomas: comparison with tumor grade and histologic findings," *Radiology,* vol. 191, no. 1, pp. 41-51, Apr, 1994.

[6] D. van Westen, E. T. Petersen, R. Wirestam, R. Siemund, K. M. Bloch, F. Stahlberg, I. M. Bjorkman-Burtscher, and L. Knutsson, "Correlation between arterial blood volume obtained by arterial spin labelling and cerebral blood volume in intracranial tumours," *MAGMA,* vol. 24, no. 4, pp. 211-23, Aug, 2011.

[7] M. Kavec, J. P. Usenius, P. I. Tuunanen, A. Rissanen, and R. A. Kauppinen, "Assessment of cerebral hemodynamics and oxygen extraction using dynamic susceptibility contrast and spin echo blood oxygenation level-dependent magnetic resonance imaging: applications to carotid stenosis patients," *Neuroimage,* vol. 22, no. 1, pp. 258-67, May, 2004.

[8] M. J. Donahue, E. Sideso, B. J. MacIntosh, J. Kennedy, A. Handa, and P. Jezzard, "Absolute arterial cerebral blood volume quantification using inflow vascular-space-occupancy with dynamic subtraction magnetic resonance imaging," *Journal of Cerebral Blood Flow & Metabolism,* vol. 30, no. 7, pp. 1329-1342, 2010.

[9] J. Hua, Q. Qin, J. J. Pekar, and P. C. M. Zijl, "Measurement of absolute arterial cerebral blood volume in human brain without using a contrast agent," *NMR in Biomedicine,* vol. 24, no. 10, pp. 1313-1325, 2011.

[10] T. Kim, K. S. Hendrich, K. Masamoto, and S. G. Kim, "Arterial versus total blood volume changes during neural activity-induced cerebral blood flow change: implication for BOLD fMRI," *J Cereb Blood Flow Metab,* vol. 27, no. 6, pp. 1235-47, Jun, 2007.

[11] T. Kim, and S. G. Kim, "Cortical layer-dependent arterial blood volume changes: improved spatial specificity relative to BOLD fMRI," *Neuroimage,* vol. 49, no. 2, pp. 1340-9, Jan 15, 2010.

[12] T. Jin, and S.-G. Kim, "Improved cortical-layer specificity of vascular space occupancy fMRI with slab inversion relative to spin-echo BOLD at 9.4 T," *Neuroimage,* vol. 40, no. 1, pp. 59-67, 2008.

[13] T. Duong, E. Yacoub, G. Adriany, X. Hu, K. Ugurbil, J. Vaughan, H. Merkle, and S. Kim, "High-resolution, spin-echo BOLD, and CBF fMRI at 4 and 7 T.," *Magn Reson Med,* vol. 48, no. 4, pp. 589-93, Oct, 2002.

[14] P. A. Bandettini, E. C. Wong, R. S. Hinks, R. S. Tikofsky, and J. S. Hyde, "Time course EPI of human brain function during task activation," *Magn Reson Med,* vol. 25, no. 2, pp. 390-7, Jun, 1992.

[15] T. Kim, and S.-G. Kim, "Quantification of cerebral arterial blood volume and cerebral blood flow using MRI with modulation of tissue and vessel (MOTIVE) signals," *Magnetic Resonance in Medicine,* vol. 54, no. 2, pp. 333-342, 2005.

[16] E. T. Petersen, T. Lim, and X. Golay, "Model-free arterial spin labeling quantification approach for perfusion MRI," *Magn Reson Med,* vol. 55, no. 2, pp. 219-32, Feb, 2006.

[17] M. J. Brookes, P. G. Morris, P. A. Gowland, and S. T. Francis, "Noninvasive measurement of arterial cerebral blood volume using Look-Locker EPI and arterial spin labeling," *Magn Reson Med,* vol. 58, no. 1, pp. 41-54, Jul, 2007.

[18] L. Yan, C. Li, E. Kilroy, F. W. Wehrli, and D. J. Wang, "Quantification of arterial cerebral blood volume using multiphase-balanced SSFP-based ASL," *Magn Reson Med*, Nov 29, 2011.

[19] J. Hua, Q. Qin, M. J. Donahue, J. Zhou, J. J. Pekar, and P. C. M. van Zijl, "Inflow-based vascular-space-occupancy (iVASO) MRI," *Magnetic Resonance in Medicine,* vol. 66, no. 1, pp. 40-56, 2011.

[20] J. Wang, D. C. Alsop, H. K. Song, J. A. Maldjian, K. Tang, A. E. Salvucci, and J. A. Detre, "Arterial transit time imaging with flow encoding arterial spin tagging (FEAST)," *Magnetic Resonance in Medicine,* vol. 50, no. 3, pp. 599-607, 2003.

[21] E. L. Barbier, A. C. Silva, S. G. Kim, and A. P. Koretsky, "Perfusion imaging using dynamic arterial spin labeling (DASL)," *Magn Reson Med,* vol. 45, no. 6, pp. 1021-9, Jun, 2001.

[22] T. Kim, and S.-G. Kim, "Quantification of cerebral arterial blood volume using arterial spin labeling with intravoxel incoherent motion-sensitive gradients," *Magnetic Resonance in Medicine,* vol. 55, no. 5, pp. 1047-1057, 2006.

[23] W. Dai, D. Garcia, C. de Bazelaire, and D. C. Alsop, "Continuous flow-driven inversion for arterial spin labeling using pulsed radio frequency and gradient fields," *Magn Reson Med,* vol. 60, no. 6, pp. 1488-97, Dec, 2008.

[24] W. C. Wu, M. Fernandez-Seara, J. A. Detre, F. W. Wehrli, and J. Wang, "A theoretical and experimental investigation of the tagging efficiency of pseudocontinuous arterial spin labeling," *Magn Reson Med,* vol. 58, no. 5, pp. 1020-7, Nov, 2007.

[25] A. L. Vazquez, G. R. Lee, L. Hernandez-Garcia, and D. C. Noll, "Application of selective saturation to image the dynamics of arterial blood flow during brain activation using magnetic resonance imaging," *Magnetic Resonance in Medicine,* vol. 55, no. 4, pp. 816-825, 2006.

[26] J.-F. Nielsen, and L. Hernandez-Garcia, "Functional perfusion imaging using pseudocontinuous arterial spin labeling with low-flip-angle segmented 3D spiral readouts," *Magnetic Resonance in Medicine*, pp. n/a-n/a, 2012.

[27] R. B. Buxton, L. R. Frank, E. C. Wong, B. Siewert, S. Warach, and R. R. Edelman, "A general kinetic model for quantitative perfusion imaging with arterial spin labeling," *Magn Reson Med,* vol. 40, no. 3, pp. 383-96, Sep, 1998.

[28] M. A. Chappell, B. J. MacIntosh, M. W. Woolrich, P. Jezzard, and S. J. Payne, "Modelling dispersion in Arterial Spin Labelling with Validation from ASL Dynamic Angiography." p. 298.

[29] M. A. Chappell, M. W. Woolrich, S. Kazan, P. Jezzard, S. J. Payne, and B. J. MacIntosh, "Modeling dispersion in arterial spin labeling: Validation using dynamic angiographic measurements," *Magnetic Resonance in Medicine*, pp. n/a-n/a, 2012.

[30] F. Q. Ye, V. S. Mattay, P. Jezzard, J. A. Frank, D. R. Weinberger, and A. C. McLaughlin, "Correction for vascular artifacts in cerebral blood flow values measured by using arterial spin tagging techniques," *Magn Reson Med,* vol. 37, no. 2, pp. 226-35, Feb, 1997.

[31] F. Q. Ye, J. J. Pekar, P. Jezzard, J. Duyn, J. A. Frank, and A. C. McLaughlin, "Perfusion imaging of the human brain at 1.5 T using a single-shot EPI spin tagging approach," *Magn Reson Med,* vol. 36, no. 2, pp. 217-24, Aug, 1996.

[32] H. Jahanian, D. C. Noll, and L. Hernandez-Garcia, "B0 field inhomogeneity considerations in pseudo-continuous arterial spin labeling (pCASL): effects on tagging efficiency and correction strategy," *NMR in Biomedicine,* vol. 24, no. 10, pp. 1202-1209, 2011.

[33] H. Lu, X. Golay, J. J. Pekar, and P. C. M. van Zijl, "Functional magnetic resonance imaging based on changes in vascular space occupancy," *Magnetic Resonance in Medicine,* vol. 50, no. 2, pp. 263-274, 2003.

[34] P. Herscovitch, and M. E. Raichle, "What is the correct value for the brain--blood partition coefficient for water?," *J Cereb Blood Flow Metab,* vol. 5, no. 1, pp. 65-9, Mar, 1985.

[35] J. B. Gonzalez-At, D. C. Alsop, and J. A. Detre, "Cerebral perfusion and arterial transit time changes during task activation determined with continuous arterial spin labeling," *Magn Reson Med,* vol. 43, no. 5, pp. 739-46, May, 2000.

[36] L. Hernandez-Garcia, G. R. Lee, A. L. Vazquez, and D. C. Noll, "Fast, pseudo-continuous arterial spin labeling for functional imaging using a two-coil system," *Magnetic Resonance in Medicine,* vol. 51, no. 3, pp. 577-585, 2004.

[37] L. Hernandez-Garcia, G. R. Lee, A. L. Vazquez, C.-Y. Yip, and D. C. Noll, "Quantification of perfusion fMRI using a numerical model of arterial spin labeling that accounts for dynamic transit time effects," *Magnetic Resonance in Medicine,* vol. 54, no. 4, pp. 955-964, 2005.

[38] J. A. Mumford, and T. Nichols, "Simple group fMRI modeling and inference," *Neuroimage,* vol. 47, no. 4, pp. 1469-1475, 2009.

[39] T. Liu, and E. Wong, "A signal processing model for arterial spin labeling functional MRI.," *Neuroimage,* vol. 24, no. 1, pp. 207-15, Jan 1, 2005.

Chapter 5

Conclusion and future directions

5.1. Conclusions

Functional arterial spin labeling has some potential advantages over BOLD fMRI that were discussed in detail in chapter 1. Arterial spin labeling offers quantitative measures of physiological parameters (cerebral blood flow and cerebral blood volume) at rest and activation. Arterial spin labeling is particularly well suited for longitudinal studies and studies with long blocks of activation [1-6]. The widespread use of arterial spin labeling for functional studies however, has been limited by low signal to noise ration and poor temporal resolution of the technique.

The principal objective of the work presented in this dissertation was focused on improvement of the signal to noise ratio and temporal resolution of arterial spin labeling measurements so that it could take a more central role in functional magnetic resonance imaging studies.

Among different arterial spin techniques, pseudo-continuous arterial spin labeling (pCASL) provides the highest signal to noise ratio and also circumvents problems affecting other continuous arterial spin labeling schemes such as magnetization transfer and duty cycle. The caveat is that pCASL is sensitive to magnetic field inhomogeneity at the inversion plane. This effect can severely affect the efficiency of the labeling process, crippling the technique, especially at higher magnetic fields. Loss in labeling efficiency leads to lower signal to noise measurements and also can cause considerable quantification errors if unaccounted. In chapter 2 we investigated and modeled the effect of magnetic field inhomogeneity on pCASL pulse sequence and proposed a method to

recover the loss of inversion efficiency and to optimize the signal to noise ratio of the technique. The proposed method adjusts the phase of the inversion pulses and introduces compensation gradients into the sequence in order to reduce the magnetic field inhomogeneity. As shown in chapter 2, the proposed method can effectively recover the compromised labeling efficiency.

The optimized and robust inversion efficiency of the proposed technique allows the use of pCASL in a wider range of conditions and applications where it may have otherwise been impractical. Two examples of such applications were presented in Chapter 3. First we demonstrated the first implementation of real-time acquisition and analysis of ASL-based fMRI time series. In this implementation, all calculations, including image reconstruction, were executed within a single TR (4 s). Our pulse sequence allows the user to adjust acquisition and labeling parameters while observing their effect on the image within two successive TRs. We were able to achieve the reconstruction and analysis on a laptop computer interfaced with the MRI scanner. By tracking individual time courses and by interactively selecting an ROI as a nuisance covariate, we were able to improve signal detection in real time.

Second, we presented a reduced SAR version of pCASL pulse sequence in Chapter 3. The high specific absorption rate of the original pCASL pulse sequence is an important challenge at ultra high field MRI ($\geq$ 7T) that limits the labeling duration and/or increases the repetition time of the pulse sequence resulting in lower signal to noise time per unit time. Limiting the flip angle of the RF pulses reduces the SAR level but at the same time compromises the labeling efficiency and signal to noise ratio of the technique. Employing the optimized pCASL technique, presented in chapter 2, a reduced specific absorption rate (SAR) version of pCASL pulse sequence is proposed that allows the reduction of the flip angle of RF pulses without compromising the signal to noise ratio of the measurements.

In chapter 4, we developed a new framework for non-invasive, dynamic, quantitative imaging of arterial blood volume using pseudo-continuous arterial spin labeling technique. The approach introduced in chapter 4 takes advantage of the kinetics of

arterial spin labeling techniques however the observed signal is primarily determined by arterial blood volume, with little or no contributions from the parenchyma. The new approach has several important advantages over existing functional ASL techniques in terms of SNR and temporal resolution. We also developed the modeling framework and estimation techniques necessary to quantify arterial blood volume through the arterial network from the observed MR signals.

5.2. Future Directions

5.2.1 Further SNR improvement: Background suppression

Additional gain in the SNR can also be achieved by adding background suppression pulses [7-10] to the optimized pCASL technique presented in chapter 2. Signal from blood is only 1-4% compared with the background tissue signal in the brain and subtraction of tag and control images in ASL measurements often could not achieve complete cancellation of the background static tissue signal as a result of physiological noise that fluctuates across time [10]. Incomplete subtraction of tissue signal leads to an increase in the ASL signal noise. Background suppression works by attenuating the signal from background static tissue in control and tag images and dramatically reduces the noise contribution from stationary tissue. Employing background suppression, substantial improvements in the SNR of ASL measurements have been reported [9, 10]. These background suppression pulses, however, interfere with the ability to quantify perfusion, so they limit the measurement to relative CBF measures [11].

5.2.2. Automating the pCASL calibration process

The method proposed in chapter 2 is very effective in terms of improving the signal to noise ratio. The calibration part of the method however is time-consuming, and frequent user interventions are required. Therefore, the current implementation of the optimized

pCASL might not be ideal in the real clinical environment. The method can benefit from improving the implementation that addresses the limitations of the original version by automating the calibration step and eliminating the user interventions as much as possible.

An alternative approach to solve this implementation problem could be having a calibrating pulse sequence that examines different phase correction and mean gradient values and empirically finds the parameters providing the maximum signal. For this purpose, the optimum range of mean gradients values for the search algorithm needs to be determined by investigating the typical range of gradient errors and their contribution to the final phase error in a large group of subjects.

5.2.3. Quantification improvement

Errors in measurement of inversion efficiency and steady state magnetization of arterial blood can strongly affect CBF and CBV estimates of arterial spin labeling measurements. Measuring the inversion efficiency directly for each artery using method proposed in chapter 2 is time-consuming and requires user interventions and therefore may not be practical in clinical environments. Employing phase-contrast velocity MRI [12-14] may provide faster and more straightforward method for measuring the inversion efficiency on a per-subject basis.

In addition to the flow increase, neuronal activation is also accompanied by a local reduction in the arterial transit time of approximately 10–20% [15-17]. This reduction in the local transit time can muddle quantification of aCBV signal during activation periods because it exaggerates the observed signal change as the result of less T1 decay. This introduces the need for a modification scheme (e.g. approach used in [17]) to correct for the overestimation of aCBV signal change during activation.

One issue that is not completely addressed in quantification of aCBV in this study is the issue of spatial dispersion of the tag during transit to the imaging region. In this study we modeled the tag dispersion using Gamma kernel as suggested in [18], but the sensitivity

of quantification results to the parameters of the dispersion model needs to be further investigated. More accurate dispersion models and estimation methods should be developed if needed.

5.2.4. Velocity Selective Arterial Spin Labeling

The strong dependence of the ASL signal on delayed arterial transit times between the tagging and imaging planes is a major source of error in CBF quantification using ASL. This is a fundamental issue because the labeled spins that arrive late, perhaps through collateral pathways, may be incorrectly interpreted as absence of flow. This could be a critical distinction in some cases such as acute ischematic stroke, in which collateral flow has been shown to be a key factor in patient outcome [19]. This problem has limited clinical enthusiasm for the use of ASL in pathologies with long arterial transit time delays. Recently, a new technique known as velocity-selective ASL (VSASL) has been proposed, which labels blood spins based on velocity rather than by spatial location [20, 21]. This technique is theoretically insensitive to arterial arrival time, and has been postulated to mitigate this problem. Several artifacts such as B_0 and B_1 inhomogeneities and eddy current artifacts, however, hinder accurate quantification of VSASL [22]. Developing B_0 and B_1 labeling pulses or modeling the effects of these fieldimhomogeneities and correcting for them can improve the quality and reliability of VSASL measurements in future studies.

5.2.5. Validation Methods

Several ASL techniques have been proposed for quantitative CBF measurements. One way to investigate the accuracy of these ASL techniques is to compare CBF values determined using these methods with CBF values determined using a gold standard technique. Radioactive microsphere method [23] has been regarded as a gold standard technique and has been employed for validation purposes. The use of radioactive tracer, however, limits the widespread use of this technique. Xenon-enhanced computed

tomography (Xe-CT) is a promising non-radioactive method that recently has been used for CBF measurements. Xe-CT is an imaging technique in which the subject inhales xenon gas while CT images are collected. Xe-CT is considered a gold standard for CBF measurement, as inhaled xenon gas is a freely diffusible, stable tracer [24].

Positron emission tomography (PET), employing ^{15}O-labeled water as a tracer, has been used for estimating CBV [25] and can be employed for validating the CBV measurements determined using MRI techniques. Using PET it is also possible to measure the arterial fraction of CBV by investigating the changes in regional CBV during hypercapnia and hypocapnia [25, 26].

5.2.6. ASL studies other than on the brain

Several recent studies have explored arterial spin labeling methods for blood flow measurements in some organs outside the brain such as lung [27], eye [28, 29], prostate [30], heart [31] and kidney [32-34]. Results of these studies indicate that arterial spin will likely provide unique insights into the physiology and pathophysiology of the hemodynamic state of different organs in patients and normal subjects.

The optimized pCASL pulse, presented in chapter 2 has been evaluated and tested using CBF studies in the human brain. The developed framework, however, can be used for blood flow measurements on organs other than the brain as well. In fact, these studies may greatly benefit from the improved inversion efficiency of this technique. Due to the difference in the blood velocity of the feeding arteries between the brain and other organs, additional optimization of the labeling parameters may provide additional gains in the signal to noise ratio. The effects of different patterns of motion and other instabilities on the ASL signal in different organs also need to be explored and corrected for accordingly.

5.3. References

[1] I. R. Olson, H. Rao, K. S. Moore, J. Wang, J. A. Detre, and G. K. Aguirre, "Using perfusion fMRI to measure continuous changes in neural activity with learning," *Brain Cogn,* vol. 60, no. 3, pp. 262-71, Apr, 2006.

[2] J. Kim, J. Whyte, J. Wang, H. Rao, K. Z. Tang, and J. A. Detre, "Continuous ASL perfusion fMRI investigation of higher cognition: quantification of tonic CBF changes during sustained attention and working memory tasks," *Neuroimage,* vol. 31, no. 1, pp. 376-85, May 15, 2006.

[3] H. Rao, J. Wang, K. Tang, W. Pan, and J. A. Detre, "Imaging brain activity during natural vision using CASL perfusion fMRI," *Hum Brain Mapp,* vol. 28, no. 7, pp. 593-601, Jul, 2007.

[4] J. Wang, H. Rao, G. S. Wetmore, P. M. Furlan, M. Korczykowski, D. F. Dinges, and J. A. Detre, "Perfusion functional MRI reveals cerebral blood flow pattern under psychological stress," *Proc Natl Acad Sci U S A,* vol. 102, no. 49, pp. 17804-9, Dec 6, 2005.

[5] R. G. Wise, and I. Tracey, "The role of fMRI in drug discovery," *J Magn Reson Imaging,* vol. 23, no. 6, pp. 862-76, Jun, 2006.

[6] R. L. Gollub, H. C. Breiter, H. Kantor, D. Kennedy, D. Gastfriend, R. T. Mathew, N. Makris, A. Guimaraes, J. Riorden, T. Campbell, M. Foley, S. E. Hyman, B. Rosen, and R. Weisskoff, "Cocaine decreases cortical cerebral blood flow but does not obscure regional activation in functional magnetic resonance imaging in human subjects," *J Cereb Blood Flow Metab,* vol. 18, no. 7, pp. 724-34, Jul, 1998.

[7] D. M. Garcia, G. Duhamel, and D. C. Alsop, "Efficiency of inversion pulses for background suppressed arterial spin labeling," *Magn Reson Med,* vol. 54, no. 2, pp. 366-72, Aug, 2005.

[8] S. Mani, J. Pauly, S. Conolly, C. Meyer, and D. Nishimura, "Background suppression with multiple inversion recovery nulling: applications to projective angiography," *Magn Reson Med,* vol. 37, no. 6, pp. 898-905, Jun, 1997.

[9] F. Q. Ye, J. A. Frank, D. R. Weinberger, and A. C. McLaughlin, "Noise reduction in 3D perfusion imaging by attenuating the static signal in arterial spin tagging (ASSIST)," *Magn Reson Med,* vol. 44, no. 1, pp. 92-100, Jul, 2000.

[10] Q. Shen, and T. Q. Duong, "Background suppression in arterial spin labeling MRI with a separate neck labeling coil," *NMR Biomed,* vol. 24, no. 9, pp. 1111-8, Nov, 2011.

[11] D. D. Shin, H.-L. Liu, E. C. Wong, and T. T. Liu, "Effect of background suppression on CBF quantitation in pseudo continuous arterial spin labeling," *Proceedings of International Society for Magnetic Resonance in Medicine* pp. 2101, 2011.

[12] M. O'Donnell, "NMR blood flow imaging using multiecho, phase contrast sequences," *Med Phys,* vol. 12, no. 1, pp. 59-64, Jan-Feb, 1985.

[13] V. J. Wedeen, R. A. Meuli, R. R. Edelman, S. C. Geller, L. R. Frank, T. J. Brady, and B. R. Rosen, "Projective imaging of pulsatile flow with magnetic resonance," *Science,* vol. 230, no. 4728, pp. 946-8, Nov 22, 1985.

[14] M. F. Walker, S. P. Souza, and C. L. Dumoulin, "Quantitative flow measurement in phase contrast MR angiography," *J Comput Assist Tomogr,* vol. 12, no. 2, pp. 304-13, Mar-Apr, 1988.

[15] J. Gonzalez-At, D. Alsop, and J. Detre, "Cerebral perfusion and arterial transit time changes during task activation determined with continuous arterial spin labeling.," *Magn Reson Med,* vol. 43, no. 5, pp. 739-46, May, 2000.

[16] Y. Yang, W. Engelien, S. Xu, H. Gu, D. Silbersweig, and E. Stern, "Transit time, trailing time, and cerebral blood flow during brain activation: measurement using multislice, pulsed spin-labeling perfusion imaging.," *Magn Reson Med,* vol. 44, no. 5, pp. 680-5, Nov, 2000.

[17] L. Hernandez-Garcia, G. R. Lee, A. L. Vazquez, C.-Y. Yip, and D. C. Noll, "Quantification of perfusion fMRI using a numerical model of arterial spin labeling that accounts for dynamic transit time effects," *Magnetic Resonance in Medicine,* vol. 54, no. 4, pp. 955-964, 2005.

[18] M. A. Chappell, M. W. Woolrich, S. Kazan, P. Jezzard, S. J. Payne, and B. J. MacIntosh, "Modeling dispersion in arterial spin labeling: Validation using dynamic angiographic measurements," *Magnetic Resonance in Medicine*, pp. n/a-n/a, 2012.

[19] G. Zaharchuk, "Better Late than Never: The Long Journey for Noncontrast Arterial Spin Labeling Perfusion Imaging in Acute Stroke," *Stroke*, 2012.

[20] D. Qiu, M. Straka, Z. Zun, R. Bammer, M. E. Moseley, and G. Zaharchuk, "CBF measurements using multidelay pseudocontinuous and velocity-selective arterial spin labeling in patients with long arterial transit delays: Comparison with xenon CT CBF," *Journal of Magnetic Resonance Imaging*, pp. n/a-n/a, 2012.

[21] E. C. Wong, M. Cronin, W. C. Wu, B. Inglis, L. R. Frank, and T. T. Liu, "Velocity-selective arterial spin labeling," *Magn Reson Med,* vol. 55, no. 6, pp. 1334-41, Jun, 2006.

[22] J. A. Meakin, and P. Jezzard, "An optimized velocity selective arterial spin labeling module with reduced eddy current sensitivity for improved perfusion quantification," *Magnetic Resonance in Medicine*, pp. n/a-n/a, 2012.

[23] B. I. Hoffbrand, and R. P. Forsyth, "Validity studies of the radioactive microsphere method for the study of the distribution of cardiac output, orn blood flow, and resistance in the conscious rhesus monkey," *Cardiovasc Res,* vol. 3, no. 4, pp. 426-32, Oct, 1969.

[24] D. S. DeWitt, P. P. Fatouros, A. O. Wist, L. M. Stewart, H. A. Kontos, J. A. Hall, P. R. Kishore, R. L. Keenan, and A. Marmarou, "Stable xenon versus radiolabeled microsphere cerebral blood flow measurements in baboons," *Stroke,* vol. 20, no. 12, pp. 1716-23, Dec, 1989.

[25] H. Ito, M. Ibaraki, I. Kanno, H. Fukuda, and S. Miura, "Changes in the arterial fraction of human cerebral blood volume during hypercapnia and hypocapnia measured by positron emission tomography," *J Cereb Blood Flow Metab,* vol. 25, no. 7, pp. 852-7, Jul, 2005.

[26] H. Ito, I. Kanno, M. Ibaraki, J. Hatazawa, and S. Miura, "Changes in human cerebral blood flow and cerebral blood volume during hypercapnia and hypocapnia measured by positron emission tomography," *J Cereb Blood Flow Metab,* vol. 23, no. 6, pp. 665-70, Jun, 2003.

[27] K. S. Burrowes, R. B. Buxton, and G. K. Prisk, "Assessing potential errors of MRI-based measurements of pulmonary blood flow using a detailed network flow model," *J Appl Physiol,* vol. 113, no. 1, pp. 130-41, Jul, 2012.

[28] N. Maleki, W. Dai, and D. C. Alsop, "Optimization of background suppression for arterial spin labeling perfusion imaging," *MAGMA,* vol. 25, no. 2, pp. 127-33, Apr, 2012.

[29] N. Maleki, W. Dai, and D. C. Alsop, "Blood flow quantification of the human retina with MRI," *NMR Biomed,* vol. 24, no. 1, pp. 104-11, Jan, 2011.

[30] X. Li, and G. J. Metzger, "Feasibility of measuring prostate perfusion with arterial spin labeling," *NMR Biomed*, Jun 7, 2012.

[31] A. E. Campbell-Washburn, A. N. Price, J. A. Wells, D. L. Thomas, R. J. Ordidge, and M. F. Lythgoe, "Cardiac arterial spin labeling using segmented ECG-gated Look-Locker FAIR: Variability and repeatability in preclinical studies," *Magn Reson Med*, Mar 12, 2012.

[32] M. Cutajar, D. L. Thomas, T. Banks, C. A. Clark, X. Golay, and I. Gordon, "Repeatability of renal arterial spin labelling MRI in healthy subjects," *MAGMA,* vol. 25, no. 2, pp. 145-53, Apr, 2012.

[33] I. Pedrosa, K. Rafatzand, P. Robson, A. A. Wagner, M. B. Atkins, N. M. Rofsky, and D. C. Alsop, "Arterial spin labeling MR imaging for characterisation of renal masses in patients with impaired renal function: initial experience," *Eur Radiol,* vol. 22, no. 2, pp. 484-92, Feb, 2012.

[34] L. Mannelli, J. H. Maki, S. F. Osman, H. Chandarana, D. J. Lomas, W. P. Shuman, K. F. Linnau, D. E. Green, G. Laffi, and M. Moshiri, "Noncontrast functional MRI of the kidneys," *Curr Urol Rep,* vol. 13, no. 1, pp. 99-107, Feb, 2012.